

Diffraction Optics Applied to Eyepiece Design

by

Michael David Missig

Submitted in Partial Fulfillment

of the

Requirements for the Degree

Master of Science

19961125 063

Supervised by

Professor G. Michael Morris

Institute of Optics

The College

School of Engineering and Applied Sciences

The University of Rochester
Rochester, New York

1994

DTIC QUALITY INSPECTED 3

DISTRIBUTION STATEMENT A

Approved for public release;
Distribution Unlimited

Dedication

To my parents, for always helping me keep the faith.

Acknowledgments

I would like to thank my advisor G. Michael Morris for his support and instruction. I would also like to thank my friends and colleagues at the Institute for many fascinating research discussions, including Al Heaney, Juan Carlos Barreiro, Don Miller, Scott Norton, Song Peng, and Tasso Sales.

I also express thanks to many people who have helped me in my research. Thanks to Jim Cornell (and the testing facilities at Melles Griot Rochester) for his assistance in measuring the lens prescription data of the Bausch and Lomb binoculars. Thanks to Bill Cross and Bausch and Lomb for providing the all-refractive binoculars for this thesis. Thanks to Rochester Photonics Corporation for supplying the fabrication of the diffractive elements for the hybrid eyepiece; thanks also to the employees at RPC, including John Bowen, Dean Faklis, Michael Hoppe, and Dan Raguin.

I would also like to especially thank Professor Greg Forbes for sparking my initial interest in optics and for offering guidance and advice throughout both my undergraduate and graduate education, which have been a great help.

Special thanks to my parents for their love, faith, and support which have helped me to become who I am today, and will help guide me for the rest of my life. I would also like to thank my brothers and sisters for their support. Thanks to Dusty Tinsley for making all the times special and many more to come.

I would also like to acknowledge the support provided by the U. S. Army Research Office.

Abstract

In many visual instruments the eyepiece limits the overall optical performance of the system. Furthermore, inherent features of eyepieces make the design task quite difficult, thus conventional eyepieces often take complex forms. However, diffractive optics offers new design variables and thus greater degrees of freedom for the designer. In addition diffractive optics can be quite effective in reducing the weight and size of the system while also improving optical performance. The objective of this thesis is to present the role of diffractive optics in eyepiece design.

A general description of eyepiece design is presented with special considerations to those areas in which diffractive lenses can be most beneficial. Several wide field-of-view, hybrid diffractive-refractive eyepiece designs are presented. These are contrasted with examples of conventional wide field-of-view eyepieces, which are composed of several refractive elements and therefore can limit their usefulness in applications where size and weight are critical. The hybrid, three-refractive-element designs presented in this thesis offer wide-field performance at least equivalent to the well-known 5-element Erfle eyepiece. In one design, the hybrid eyepiece weighs 70% less than the Erfle eyepiece, while having enhanced optical performance such as a 50% decrease in pupil spherical aberration and a 25% reduction in distortion. In addition, the hybrid eyepiece is comprised of a single, common glass type (BK-7) which is less expensive than the glass types found in the Erfle design.

Application of one of the hybrid wide-angle eyepieces for use in a pair of binoculars is demonstrated to make a qualitative assessment of its performance in a visual instrument. The diffractive-element fabrication and alignment processes are explained including a tolerance analysis of the lens. Opto-mechanical eyepiece mounts

designed to fit a set of Bausch and Lomb Legacy 8X40 binoculars are detailed through drawings, specifications, and tolerances.

Experimental results are presented for the hybrid wide-FOV eyepiece. Experimental tests included an MTF evaluation, and two visual imaging experiments. Experimental MTF results are in excellent agreement with the theoretical predictions. The imaging tests show qualitative measurements of the performance of the hybrid eyepiece in two applications, as a magnifier and in a set of binoculars.

Table of Contents

Curriculum Vitae.....	iii
Acknowledgments.....	iv
Abstract.....	v
List of Tables.....	x
List of Figures.....	xii
Chapter 1. Introduction.....	1
1.1. Brief History of Visual Instruments using Diffractive Lenses....	1
1.1.1. Preface.....	1
1.1.2. Previous Research.....	1
1.2. The Eyepiece Design Problem - Wide-Field Example.....	5
1.3. Overview of Thesis.....	7
1.4. References for Chapter 1.....	9
Chapter 2. Diffractive Lenses.....	10
2.1. Introduction.....	10
2.2. Surface Relief Diffractive Lenses.....	12
2.2.1. Surface Relief Structure.....	12
2.2.2. Diffraction Efficiency.....	15
2.3. Modeling Diffractive Lenses in Lens Design Programs.....	21
2.3.1. Lens Design Models.....	21
2.3.2. Third Order Aberrations of Diffractive Lenses.....	23
2.3.3. Converting the Ultra-High Index Lens to Fabrication Specifications.....	26
2.4. References for Chapter 2.....	29

Chapter 3. Diffractive-Refractive Eyepiece Design.....	31
3.1. Introduction.....	31
3.1.1. Overview of Chapter 3.....	31
3.1.2. General Eyepiece Design.....	31
3.2. Eyepiece Design.....	34
3.2.1. Conventional Eyepiece Design.....	34
3.2.2. Conventional Eyepiece Examples.....	41
3.3. Hybrid Diffractive-Refractive Eyepiece Design.....	44
3.3.1. Diffractive Optics In Eyepieces - Benefits.....	44
3.3.2. Previous Work And Design Objectives.....	45
3.3.3. Hybrid Diffractive-Refractive Eyepiece Designs.....	46
3.3.4. Comparisons and Results.....	61
3.4. Summary of Chapter 3.....	69
3.5. References for Chapter 3.....	71
Chapter 4. Hybrid Diffractive-Refractive Binoculars.....	72
4.1. Introduction.....	72
4.2. Design and Analysis of Hybrid Binoculars.....	74
4.2.1. Bausch and Lomb Legacy Binoculars.....	74
4.2.2. Binocular Eyepiece.....	76
4.2.3. Diffractive-Refractive Eyepiece Design For The Binoculars.....	81
4.2.4. Diffraction Efficiency of the Hybrid Binoculars.....	84
4.3. Fabrication.....	87
4.3.1. Fabrication Tolerances.....	87
4.3.2. Fabrication and Replication of the Diffractive Element	91
4.3.3. Eyepiece Mount.....	97
4.4. References for Chapter 4.....	100

Chapter 5. Experimental Results.....	102
5.1. Introduction.....	102
5.2. Modulation Transfer Function.....	103
5.2.1. Theory and Experiment.....	103
5.2.2. Diffraction Efficiency – Experimental.....	106
5.2.3. Experimental MTF Results.....	112
5.3. Imaging Experiment - Eyepiece as a Magnifier.....	122
5.4. Binoculars - Imaging Experiment.....	125
5.5. References for Chapter 5.....	127
Chapter 6. Summary and Conclusions.....	128
6.1. Review of Thesis.....	128
6.2. The Role of Diffractive Optics in Eyepiece Design.....	129
6.3. Future Work.....	132

List of Tables

<u>Table</u>	<u>Title</u>	<u>Page</u>
Table 3.3.1.	Lens description of the Erfle eyepiece based upon data from U.S. Patent number 1,478,704.....	48
Table 3.3.2.	Lens prescription data for hybrid eyepiece depicted in Fig. 3.3.2.	60
Table 3.3.3.	Lens prescription data for hybrid eyepiece depicted in Fig. 3.3.5.	60
Table 3.3.4.	Characteristics and performance features for four eyepieces, the Erfle eyepiece, Wide-angle Hybrid Diffractive-Refractive Eyepiece No. 1 in Fig. 3.3.1, Wide-angle Hybrid Diffractive-Refractive Eyepiece No. 2 in Fig. 3.3.2, Wide-angle Hybrid Diffractive-Refractive Eyepiece No. 3 in Fig.3.3.5. The ratio of the Petzval field radius to the eyepiece focal length (FL), the ratio of the overall length –first physical surface to last surface–(OAL) to the eyepiece focal length, the ratio of eye relief (ER) to the eyepiece focal length, and the ratio of the back focal length (BFL) to the eyepiece focal length are shown.....	61
Table 3.3.5.	Comparison of weights of three of the hybrid, wide-angle eyepieces with the Erfle eyepiece. Values are normalized to the weight of one Erfle eyepiece.....	61
Table 4.2.1.	Specification data for the Bausch and Lomb 8X40 Legacy Binoculars.....	74
Table 4.2.2.	Vignetting data for the eyepiece modeled from the measured quantities of the Bausch and Lomb 8X40 Legacy Binoculars.....	78
Table 4.2.3.	Optical performance data for the eyepiece modeled from the measured quantities of the Bausch and Lomb 8X40 Legacy Binoculars with comparisons to a standard Kellner eyepiece. Overall length is measured from the first physical surface to the last; F is the total eyepiece focal length. For comparison, the first order constructional parameters of the Kellner were scaled appropriately, i.e. focal length = 19.28mm, f -number = 3.73, FOV=30°.....	79
Table 4.2.4.	Vignetting data for the wide-angle, hybrid diffractive-refractive eyepiece implemented into the binoculars.....	83
Table 4.2.5.	Data for the locations of images produced by the zeroth and second diffracted orders of the diffractive lens in the binoculars.....	85

Table 4.3.1. The tolerance budget for the hybrid diffractive-refractive eyepiece for use in the binoculars. Listed also are the percent deviations from nominal for the various errors in the design. The optical merit used to describe the deviation from the nominal performance is the root mean square spot size for the on-axis case (the fringe wavelength is 546.1 nm).....	89
Table 4.3.2. Comparison of diffraction efficiency versus photopic visual sensitivity for blaze height fabrication errors of $\pm 5\%$ in a diffractive lens with a nominal peak diffraction efficiency at 555 nm.....	91
Table 5.2.1. Measured diffraction efficiency for specific radial positions of the diffractive lens for $\lambda = 543.5$ nm.....	107
Table 5.2.2. Measured diffraction efficiency for specific radial positions of the diffractive lens for $\lambda = 488.0$ nm.....	107
Table 5.2.3. Measured diffraction efficiency for specific radial positions of the diffractive lens for $\lambda = 632.8$ nm.....	108

List of Figures

<u>Figure</u>	<u>Title</u>	<u>Page</u>
Fig. 2.2.1.	A surface-relief diffractive lens with full-period (2π) zones.....	13
Fig. 2.2.2.	Scalar diffraction efficiency for a quadratic-blaze, diffractive lens....	17
Fig. 2.2.3.	Four-level diffractive lens superimposed with equivalent quadratic-blaze profile lens.....	17
Fig. 2.2.4.	Phase profile for a discrete-step profile diffractive lens after a change of variables.....	18
Fig. 2.2.5.	Scalar diffraction efficiencies of diffractive lenses fabricated as multi-level profile elements, 16-level, 8-level, 4-level, and 2-level with peak efficiencies occurring at $\lambda = 555$ nm.....	19
Fig. 3.2.1.	A Bundle of Chief Rays through a Telescope.....	37
Fig. 3.2.2.	Pupil Spherical Aberration of a singlet lens eyepiece.....	38
Fig. 3.2.3.	Ramsden Eyepiece, ⁷ 30° FOV. Performance: 25.4 mm FL, Spot Size = 0.075 mm, 2% distortion, ER/FL = 0.47.....	41
Fig. 3.2.4.	Kellner Eyepiece, ⁷ 40° FOV. Performance: 25.4 mm FL, Spot Size = 0.16 mm, 2.5 % distortion, ER/FL = 0.03.....	42
Fig. 3.2.5.	Symmetrical (Plossl) Eyepiece, ⁷ 50° FOV. Performance: 25.4 mm FL, Spot Size = 0.2 mm, 6% distortion, ER/FL = 0.84.....	42
Fig. 3.2.6.	Erfle Eyepiece, ⁷ 60° FOV. Performance: 25.4 mm FL, Spot Size = 0.39 mm, 8% distortion, ER/FL = 0.83.....	43
Fig. 3.2.7.	Wild Eyepiece, ⁷ 70° FOV. Performance: 25.4 mm FL, Spot Size = 0.24 mm, 12.5 % distortion, ER/FL = 0.75.....	43
Fig. 3.3.1.	Wide-angle, hybrid diffractive-refractive eyepiece. The eyepiece consists of two diffractive elements and three refractive elements. The aperture stop is indicated to the left of the lens by a broken line crossing the axis; the image plane is indicated to the right of the lens by a solid hatch mark across the axis.....	50
Fig. 3.3.2.	Wide-angle, hybrid diffractive-refractive eyepiece. The eyepiece consists of two diffractive elements and three refractive elements. The aperture stop is indicated to the left of the lens by a broken line crossing the axis; the image plane is indicated to the right of the lens by a solid hatch mark across the axis.....	51

- Fig. 3.3.3. Wide-angle, hybrid diffractive-refractive eyepiece. The eyepiece consists of two diffractive elements and three refractive elements. The aperture stop is indicated to the left of the lens by a broken line crossing the axis; the image plane is indicated to the right of the lens by a solid hatch mark across the axis..... 52
- Fig. 3.3.4. Wide-angle, hybrid diffractive-refractive eyepiece. The eyepiece consists of one diffractive element and three refractive elements. The aperture stop is indicated to the left of the lens by a broken line crossing the axis; the image plane is indicated to the right of the lens by a solid hatch mark across the axis..... 57
- Fig. 3.3.5. Wide-angle, hybrid diffractive-refractive eyepiece. The eyepiece consists of one diffractive element and three refractive elements. The aperture stop is indicated to the left of the lens by a broken line crossing the axis; the image plane is indicated to the right of the lens by a solid hatch mark across the axis..... 58
- Fig. 3.3.6. Percent distortion plots for four eyepieces. (a)The 5-element Erfle eyepiece, (b) wide-angle hybrid diffractive-refractive eyepiece 1 (Fig. 3.3.1), (c) wide-angle hybrid diffractive-refractive eyepiece 2 (Fig. 3.3.2), (d) wide-angle hybrid diffractive-refractive eyepiece 3 (Fig. 3.3.5) All four eyepiece designs have a focal length of unity, have an entrance pupil diameter of $0.40F$, and a 60° FOV..... 63
- Fig. 3.3.7. Field sags plots for four eyepieces. (a)The 5-element Erfle eyepiece, (b) wide-angle hybrid diffractive-refractive eyepiece 1 (Fig. 3.3.1), (c) wide-angle hybrid diffractive-refractive eyepiece 2 (Fig. 3.3.2), (d) wide-angle hybrid diffractive-refractive eyepiece 3 (Fig. 3.3.5) All four eyepiece designs have a focal length of unity, have an entrance pupil diameter of $0.40F$, and a 60° FOV. 64
- Fig. 3.3.8. Primary and secondary lateral color plots for four eyepieces. (a)The 5-element Erfle eyepiece, (b) wide-angle hybrid diffractive-refractive eyepiece 1 (Fig. 3.3.1), (c) wide-angle hybrid diffractive-refractive eyepiece 2 (Fig. 3.3.2), (d) wide-angle hybrid diffractive-refractive eyepiece 3 (Fig. 3.3.5) All four eyepiece designs have a focal length of unity, have an entrance pupil diameter of $0.40F$, and a 60° FOV..... 65
- Fig. 3.3.9. Longitudinal spherical aberration of the pupil (for three wavelengths) plots for four eyepieces. (a)The 5-element Erfle eyepiece, (b) wide-angle hybrid diffractive-refractive eyepiece 1 (Fig. 3.3.1), (c) wide-angle hybrid diffractive-refractive eyepiece 2 (Fig. 3.3.2), (d) wide-angle hybrid diffractive-refractive eyepiece 3 (Fig. 3.3.5) All four eyepiece designs have a focal length of unity, have an entrance pupil diameter of $0.40F$, and a 60° FOV..... 66
- Fig. 3.3.10. Transverse ray aberration plots for two eyepieces. (a)The five-element Erfle eyepiece, (b) wide-angle hybrid diffractive-refractive eyepiece 1 (Fig. 3.3.1) Both eyepiece designs have a focal length of unity, have an entrance pupil diameter of $0.40F$, and a 60° FOV..... 67

Fig. 3.3.11. Transverse ray aberration plots for two eyepieces. (a) Wide-angle hybrid diffractive-refractive eyepiece 2 (Fig. 3.3.2), (b) wide-angle hybrid diffractive-refractive eyepiece 3 (Fig. 3.3.5) Both eyepiece designs have a focal length of unity, have an entrance pupil diameter of $0.40F$, and a 60° FOV.....	68
Fig. 4.2.1. The optical layout of the Bausch and Lomb 8X40 Legacy Binoculars.....	75
Fig. 4.2.2. The optical layout and performance evaluation curves for the eyepiece modeled from the measured quantities of the Bausch and Lomb 8X40 Legacy Binoculars. Included are transverse ray plots for three field positions, 0.0, 0.7, and 1.0 (where 1.0 refers to 27° hFOV); percent distortion; field curves; and lateral color.....	77
Fig. 4.2.3. Longitudinal pupil spherical aberration of the eyepiece modeled from the measured quantities of the Bausch and Lomb 8X40 Legacy Binoculars. The edge of the field corresponds to 27° hFOV.....	77
Fig. 4.2.4. On-axis transverse ray plots for the tangential and sagittal fields of the eyepiece from the Bausch and Lomb 8X40 Legacy Binoculars.....	80
Fig. 4.2.5. The optical layout of the hybrid eyepiece implemented into the Bausch and Lomb Legacy Binoculars.....	82
Fig. 4.2.6. The phase function of the diffractive lens in the eyepiece for the hybrid binoculars.....	83
Fig. 4.2.7. The diffraction efficiency of a diffractive lens with a quadratic-blaze profile with $\lambda_0 = 0.555 \mu\text{m}$ and the relative spectral response of the human eye for photopic conditions.....	86
Fig. 4.3.1. Refractive element with tilt. The optical axis of the lens is defined by the line containing the centers of curvature of the two elements; the mechanical axis is defined by the edge of the lens.....	87
Fig. 4.3.2. Decenter between the axes of the refractive element and the diffractive element.....	88
Fig. 4.3.3. Error in the blaze height of a diffractive lens.....	88
Fig. 4.3.4. Fabrication process for diffractive elements. a.) Writing the diffractive pattern into photoresist to create master, b.) making the tool from the master, c.) casting the pattern into UV resin on a plano-convex refractive element, d.) the resulting hybrid diffractive-refractive doublet after the UV curing step.....	93

Fig. 4.3.5. Alignment and replication assembly for fabricating diffractive-refractive doublet lenses. (a) Cylinder stage with x- and y-translation and θ rotation for centering the diffractive lens, and the V-block assembly for aligning the diffractive and refractive elements, (b) refractive lens mount with spring-loaded rod for pressure against V-block.....	94
Fig. 4.3.6. Edge mounting a lens. (a) A perfect lens in a perfect cell, (b) a tilted lens in a perfect cell, (c) a decentered lens in a perfect cell.....	98
Fig. 4.3.7. Mounting a lens by contacting the lens on a polished, optical spherical surface; errors in edging the lens do not result in mounting errors. (a) a tilted lens in a cell, (b) a decentered lens in a cell.....	98
Fig. 4.3.8. Mount for hybrid diffractive-refractive eyepiece.....	99
Fig. 5.2.1. MTF bench used to test the eyepieces described in this section.....	106
Fig. 5.2.2. Surface profilometer measurement of diffractive lens. The blaze height of the lens is measured to be 0.885 μm	110
Fig. 5.2.3. Theoretical scalar diffraction efficiencies for a diffractive lens designed with a peak wavelength at $\lambda_0 = 555 \text{ nm}$ and for a diffractive lens fabricated with a blaze height error such that the peak wavelength occurs at $\lambda_0 = 530 \text{ nm}$; individual points plotted for measured on-axis diffraction efficiency of fabricated lens.....	112
Fig. 5.2.4. Experimental and theoretical on-axis MTF data for hybrid eyepiece with $\lambda = 555 \text{ nm}$	114
Fig. 5.2.5. Experimental on-axis MTF data for six-element Erfle eyepiece and hybrid eyepiece with $\lambda = 555 \text{ nm}$	114
Fig. 5.2.6. Experimental and theoretical 30° full field-of-view (FOV) MTF data for hybrid eyepiece with $\lambda = 555 \text{ nm}$	115
Fig. 5.2.7. Experimental 30° FOV MTF for six-element Erfle eyepiece and hybrid eyepiece with $\lambda = 555 \text{ nm}$	115
Fig. 5.2.8. Experimental and theoretical on-axis MTF for hybrid eyepiece with $\lambda = 486 \text{ nm}$	117
Fig. 5.2.9. Experimental on-axis MTF data for six-element Erfle eyepiece and hybrid eyepiece with $\lambda = 486 \text{ nm}$	117
Fig. 5.2.10. Experimental and theoretical 30° FOV MTF for hybrid eyepiece with $\lambda = 486 \text{ nm}$	118
Fig. 5.2.11. Experimental 30° FOV MTF for six-element Erfle eyepiece and hybrid eyepiece with $\lambda = 486 \text{ nm}$	118

Fig. 5.2.12. Experimental and theoretical on-axis MTF for hybrid eyepiece with $\lambda = 656 \text{ nm}$	119
Fig. 5.2.13. Experimental on-axis MTF data for six-element Erfle eyepiece and hybrid eyepiece with $\lambda = 656 \text{ nm}$	119
Fig. 5.2.14. Experimental and theoretical 30° FOV MTF for hybrid eyepiece with $\lambda = 656 \text{ nm}$	120
Fig. 5.2.15. Experimental 30° FOV MTF for six-element Erfle eyepiece and hybrid eyepiece with $\lambda = 656 \text{ nm}$	120
Fig. 5.3.1. Imaging experiment using an eyepiece as a magnifier.....	123
Fig. 5.3.2. On-axis imaging performance of (a) a 6-element Erfle eyepiece and (b) the hybrid eyepiece.....	124
Fig. 5.3.3. Off-axis (20° hFOV) imaging performance of (a) a 6-element Erfle eyepiece and (b) the hybrid eyepiece.....	124
Fig. 5.4.1. Imaging experiment capturing an image through binoculars.....	125
Fig. 5.4.2. Image captured via video camera through the Bausch and Lomb binoculars equipped with (a) the standard all-refractive eyepiece and (b) the hybrid diffractive-refractive eyepiece.....	126

1. Introduction

1.1. Brief History of Visual Instruments using Diffractive Lenses

1.1.1. Preface

The purpose of this thesis is to investigate the role of diffractive optics – in conjunction with refractive elements – in eyepiece design. There are many areas of optics to which diffractive lenses have been applied, but the area of visual, broadband instruments is one which has not seen many applications of diffractive lenses. This section provides a brief history of designs of visual instruments which are comprised of at least one diffractive lens.

1.1.2. Previous Research

The earliest work in visual instruments with the use of diffractive lenses was done by Wood in 1898.¹ He built two telescopes employing the first surface-relief diffractive elements. In the first telescope, he replaced a five-inch refractive objective with a phase-reversal zone plate. He used a low-power, refractive eyepiece to view the internal image. In another telescope, one which he referred to as a diffraction-telescope, he used phase-reversal zone-plates for both the objective and the eyepiece. Although Wood had noted some of the unique spectral properties of the phased-zone-plates, neither telescope was constructed to benefit from the unique chromatic properties of diffractive lenses. In both telescopes, both the objectives and the eyepieces were unachromatized.

More recently, telescopes utilizing the color-correcting features of diffractive lenses have been designed.^{2,3} In one design, the color correction of the objective and eyepiece are independent; in the other, the diffractive eyepiece compensates for the longitudinal chromatic aberration in the refractive objective.

Bennett showed the design of a Galilean telescope incorporating a two-element, holographic eyepiece, which is corrected for longitudinal chromatic aberration.² In that design the objective and eyepiece are independently corrected for color. The powers of the two holographic elements of the eyepiece are opposite in sign to each other.

In another telescope design, a refractive objective is combined with an all-diffractive eyepiece to allow for larger aperture telescopes.³ By utilizing the dispersive properties of diffractive elements in the eyepiece to correct for the color in an unachromatized objective, a simple singlet can be used as the objective. In one design, the diffractive eyepiece corrects for chromatic variation of magnifying power using a classical Huygens' eyepiece configuration in which the real, internal image of the telescope is located "inside" the eyepiece. The well-known advantage that this design exploits is the correction of paraxial lateral color without the use of a negative element. This type of eyepiece is not corrected for longitudinal chromatic aberration, since although the focal length of the eyepiece is wavelength independent, the principal planes for different wavelengths will not be coincident. This result has two consequences. The first is that a reticle cannot be used with this eyepiece, and second, that the eyepiece exhibits severe chromatic variation of exit pupil location. The reason that a reticle cannot be used with this eyepiece is actually twofold. Since the focal plane is internal to the eyepiece system it is inconvenient to use a reticle at that location,⁴ but more importantly, the internal image plane is viewed with only the single eyelens. Since the image of an object in that plane is not well-corrected for either chromatic or

monochromatic aberrations, it is unsuitable for a reticle,⁵ except in special circumstances.⁶

Bennett showed that two holograms, producing a real image, must have powers of opposite sign in order to correct for axial color.² This is not the case for the Huygens'-style diffractive eyepiece where both elements are positive. In conjunction with the objective, the *overall* telescope is corrected for longitudinal chromatic aberration, but separately the eyepiece exhibits longitudinal chromatic aberration.³ As a consequence, there is a strong dependence of exit pupil location with wavelength. A bundle of chief rays, i.e. rays which have zero height at the entrance pupil and various heights at the object, traced through a telescope, can be treated as axial rays limited only by the apertures of the eyepiece.⁷ Just as when evaluating pupil spherical aberration, the intersection of these rays with the optical axis indicates the severity of the shift of exit pupil location with field, here the longitudinal chromatic aberration effects a shift of exit pupil location with wavelength. Therefore the result is chromatic variation of the exit pupil. The chromatic variation of the exit pupil was noted to be 12 mm in one design, and the author speculated that this aberration could limit the telescope in high magnifications. Furthermore, the design is not corrected for monochromatic aberrations and few degrees of freedom remain to correct the monochromatic field aberrations for a wide-field scope.

Recently there has been work done in the area of hybrid diffractive-refractive magnifiers.^{8,9} Often eyepieces and magnifiers are placed in the same group of instruments, but to be more precise, they belong to two different classes of visual instruments, namely, coherently coupled and incoherently coupled.¹⁰ Instruments such as telescopes, binoculars, and microscopes belong to the coherently coupled class. These are instruments in which light emanating from the object passes through the device and enters the eye. Incoherently coupled systems are those in which an

objective forms a real, intermediate image, just as in the prior group, but the image is then stored, converted, or processed before the eye views the final image. In other words, the light path from the object to the eye is not continuous. Examples of this type of system are image-intensifying systems and thermal imagers. In many cases the image is then placed on a small screen. A back-end subsystem then views the screen and projects an image for the eye. These back-end subsystems are sometimes referred to as eyepieces. Unfortunately the terms "eyepiece", "ocular", and "magnifier" are used interchangeably. (Monocular magnifier is used when one eye views the image, biocular magnifier is used in the case where both eyes use the same system.⁵) A more clear distinction is to use the term eyepiece when referring to coherently coupled devices, and to use the term magnifier when referring to those used in incoherently coupled systems. There is a clear distinction between the two systems. For instance, in incoherently coupled systems, the internal image is re-imaged at a comfortable distance for the eye and is magnified, but the key difference is that there is no pupil imaging. This important feature clearly separates the two groups. While in magnifier designs, an exit pupil is referred to, this is merely a construction indicating the most likely axial position of the viewer's eye. Furthermore, in magnifiers there is no optical correction for the pupil aberrations; also there is no requirement for telecentricity as there is in eyepiece design. Additionally, magnifiers are often used in systems in which the screen illumination covers a relatively small wavelength band, therefore the system need not be corrected for chromatic aberrations as well as a device operating in broadband illumination. For example, certain cathode ray tubes (CRT) display greenish images which have a spectral distribution of approximately 50 nm. As an application, an eyepiece can be used as a monocular magnifier; but the opposite is not necessarily the case. For example, the Erfle eyepiece has commonly been used as a magnifier in these types of instruments.

A recent example of an incoherently coupled visual device employing diffractive optical elements is a hybrid biocular magnifier.⁸ A biocular magnifier is a system which is very different from a typical eyepiece in that the exit pupil is the viewing location for both eyes, thus the designer must carefully consider the variation of the aberrations with pupil coordinate. In this hybrid biocular magnifier, diffractive lenses are used to improve the performance of the magnifier over a quasi-monochromatic wavelength band of 50 nm.

A diffractive-refractive doublet was designed for use as an eyepiece-magnifier. In that design one refractive surface was aspheric, and the diffractive element was to be placed on a curved substrate. The design goal in this case was to minimize weight not necessarily to reduce complexity. The operable wavelength band also was limited to 50 nm. The author's conclusion was that due to the complexity of the fabrication, diffractive optics was unsuitable for eyepieces/magnifiers.⁹

1.2. The Eyepiece Design Problem - Wide-Field Example

In visual instruments, such as telescopes or binoculars, an objective forms a real, internal image of an object being viewed, and the eyepiece magnifies it and places the final image at a comfortable viewing distance for the eye, usually infinity for the unaccommodated eye. The eyepiece is often the limiting factor in the overall optical performance of the instrument and, due to the requirements for wide field-of-view (FOV) and high performance, it presents a difficult design problem. Improvement of existing eyepiece designs is limited using conventional design variables.

Wide-field eyepiece design is considered a difficult task due to particular features of the device.⁶ Typical features that are necessary in this type of eyepiece include a sufficient eye relief (10 to 20 mm), a wide field-of-view such that the user

does not experience tunnel vision, and a well defined exit-pupil location to avoid vignetting. The combination of these features makes it difficult to design a good eyepiece. In particular, the external aperture stop and pupils eliminate the symmetry of the chief ray, which would help to reduce -- among the third order aberrations -- distortion, coma, and lateral color. The well-defined exit pupil location and the wide field-of-view require that the system be well-corrected for spherical aberration of the pupil and off-axis aberrations.¹¹ Since the correction of all the aberrations is quite difficult, often in wide-field eyepieces some aberrations are tolerated, ignored, or are corrected by another part of the entire (overall) visual instrument. For example, a certain amount of distortion at the edge of the field is acceptable due to the fact that the instrument user does not use this area other than to orient himself/herself,⁵ and often the lateral color is corrected with a dispersive prism.⁵

As a result of these design limitations, solutions for these eyepieces often result in multi-element or exotic configurations, which are extremely heavy and bulky; this significantly reduces their desirability in a number of situations. In such cases, optical performance is often sacrificed to satisfy weight or cost requirements. It is shown in this thesis that diffractive optics technology offers new and unique solutions to the area of eyepiece design, which exhibit comparable or better performance than all-refractive designs, while significantly reducing the size, weight, and potentially the cost of the eyepieces.

1.3. Overview of Thesis

In Chapter Two an overview of the theory and design of diffractive lenses is presented. The characterization of a diffractive lens is discussed along with the use of diffractive elements in optical design. Using optical design software to model and optimize diffractive lenses is presented. Issues of diffraction efficiency and its effects on imaging are covered.

Eyepiece design is presented in Chapter Three. An overview of general eyepiece design issues is discussed in the first section. In Section 3.2, a discussion of all-refractive eyepiece design is presented. There are inherent disadvantages or limitations of all-refractive optical design that have limited the performance of conventional eyepieces. Examples of several conventional eyepieces are presented showing the increase in complexity with increases in the field-of-view. Hybrid diffractive-refractive eyepiece design is presented in Section 3.3. Diffractive lenses are used in combination with refractive elements to provide achromatization and to aid in monochromatic aberration correction. Wide-field hybrid eyepiece examples are given. Comparisons to an all-refractive, high-performance eyepiece are presented.

In Chapter Four, an experimental application for the hybrid eyepieces is presented. A set of binoculars provides a good application of wide-field eyepieces. Implementation of a wide-field, hybrid eyepiece into an existing all-refractive set of binoculars is shown. This process involved "reverse-engineering" an off-the-shelf set of binoculars to characterize the all-refractive design and designing and fabricating a hybrid eyepiece specifically for that set of binoculars. Theoretical comparisons with the original refractive binoculars are shown. A tolerance analysis of fabrication errors is presented. A diffraction analysis of the binoculars is presented along with a

comparison of the diffraction efficiency of the lens to the relative sensitivity of the human eye. It is shown that the spectral characteristics of the diffractive lens match well with the visual performance of the human eye.

In Chapter Five experimental results are presented. Several experimental measurements were performed to test the hybrid eyepiece. These tests included modulation transfer function (MTF) experiments at several wavelengths and field positions and two imaging experiments. One imaging experiment tests the eyepiece as a magnifier in white light. The other imaging experiment tests the eyepiece within the binoculars. In two of the three tests, comparison data of a six-element Erfle eyepiece is also presented.

1.4. References for Chapter 1

1. R. W. Wood, "Phase-reversal zone-plates, and diffraction-telescopes," *Philos. Mag. [Series 5]* **45**, pp. 511-522 (1898).
2. S. J. Bennett, "Achromatic Combinations of hologram optical elements," *Appl. Opt.* **15**, 542-545 (1976).
3. T. W. Stone, "Hybrid diffractive-refractive telescope," in *Practical Holography IV*, Stephen A. Benton, ed. *Proc. SPIE*, **1212**, 257-266 (1990).
4. R. Kingslake, *Optical System Design* (Academic Press, Inc., Orlando, 1983) pp. 208-210.
5. W. J. Smith, *Modern Optical Engineering Second Ed.* (McGraw-Hill, Inc., New York, 1990), pp. 403-408.
6. *Optical Design-Military Standardization Handbook MIL-HDBK-141* (Defense Supply Agency, Washington, D.C., 1962), pp. 14-2 – 14-3 and 23-9 – 23-10.
7. S. Rosin, *Applied Optics and Optical Engineering, Vol. III Optical Components*, R. Kingslake, ed. (Academic Press, Inc., New York, 1965), ch. 9, pp. 337-344.
8. C. W. Chen, U.S. Patent no. 5,151,823 (29 September 1992).
9. R. E. Aldrich, "Ultra Lightweight Diffractive Eyepiece," in *Diffractive Optics: Design, Fabrication, and Applications, Technical Digest, 1992* (Optical Society of America, Washington, D.C., 1992), Vol. 9, p. 129.
10. D. Williamson, "The eye in optical systems," in *Geometrical Optics*, Robert E. Fischer, ed. *Proc. SPIE*, **531**, 136-147 (1985).
11. R. Kingslake, *Lens Design Fundamentals* (Academic Press, New York, 1978), pp.335-343.

2. Diffractive Lenses

2.1. Introduction

Lens design with diffractive lenses is quite unique compared to refractive or reflective design. Due to many of these unique features, diffractive optics opens new areas of applications and possibilities when one considers hybrid designs employing both refractive and diffractive optics or reflective and diffractive optics. Diffractive lenses can also be reproduced as replicated structures which occupy considerably less mass and volume than their refractive or reflective counterparts.¹⁻⁶ Diffractive lenses can reduce the size of a system, since they can be mounted on an existing surface already contained within a design; often a planar surface is used to ease the fabrication process. This chapter deals with the theory used to design and analyze diffractive lenses and also a method to convert a designed diffractive lens to a manufacturable structure. The calculation and analysis of diffraction efficiency are also presented.

There are several features of diffractive lenses that make the use of optical design with them quite unique compared to conventional optics. For example, since a diffractive lens is a type of diffraction grating, the lens has an effective dispersion that is opposite in sign to that of glass;⁷ red light being diffracted at stronger angles than blue light. The dispersion is also many times stronger than that of ordinary glass. For these reasons, combinations of refractive and diffractive elements can significantly reduce the amount of glass in conventional systems that are corrected for chromatic aberrations. Additionally, an aspheric or general conic profile can be included in the phase function of the diffractive lens without usually increasing the difficulty level of

the fabrication process. This feature can be especially useful in correcting the aberrations of an optical system.

In Section 2.2 the theory of diffractive lenses is presented along with calculations of diffraction efficiency. Unlike with refractive or reflective surfaces, diffractive lenses have many orders of diffraction, which can be used as a design parameter in some cases or can hinder a system's performance in others. In either situation, a designer must account for the light diffracted into other orders. The blaze height of a diffractive lens can be adjusted to shift the wavelength location of the peak efficiency.

In Section 2.3 models used to implement diffractive lenses into existing lens design software packages are presented. Three models for designing and optimizing diffractive lenses in optical design software are discussed. Aberrations of a diffractive lens are also presented. A simple method for converting a diffractive lens modeled in optical software to a physical prescription from which the lens is to be manufactured is important for the success of diffractive lens' usefulness. A method for performing this operation is presented in Section 2.3.

2.2. Surface Relief Diffractive Lenses

2.2.1. Surface Relief Structure

In 1898 R. W. Wood produced the first phase-reversal zone plates, which had previously been described by Raleigh.⁸ Before Wood's first phase plates, zone plates that blocked alternate Huygens' zones on a transmitted wavefront had been produced by photographically reducing drawings of blackened concentric circles with radii proportional to the square roots of the natural numbers. By replacing the alternate blocked zones with a surface relief element yielding a π phase reversal, a focusing lens could be produced with an increase of light in the desired diffracted order. Wood noted that if a principle mentioned by Rayleigh to introduce an arbitrary phase retardation at every part of an aperture were applied to zone-plates, then an efficiency of 100% could be achieved in a specific diffracted order (at a specific wavelength). He suggested possible methods, similar to those used to create his phase-reversal plates, to fabricate such an element, such as shading the element or using wedge shaped strips of tinted glass or gelatin in the fabrication process.

In the case of a diffractive surface that could impart a continual phase profile across the aperture in concentric, 2π zones, light from infinity incident upon each zone would constructively interfere at the focal plane. A surface relief structure as shown in Fig. 2.2.1. has the proper phase function to constructively interfere all of the incident light of a certain wavelength at a common focus. The radius of the zone spacings are given by :

$$r_j^2 + f^2 = (f + j\lambda)^2 \quad (2.2.1)$$

and

$$r_j = \sqrt{(j\lambda)^2 + 2j\lambda f}. \quad (2.2.2)$$

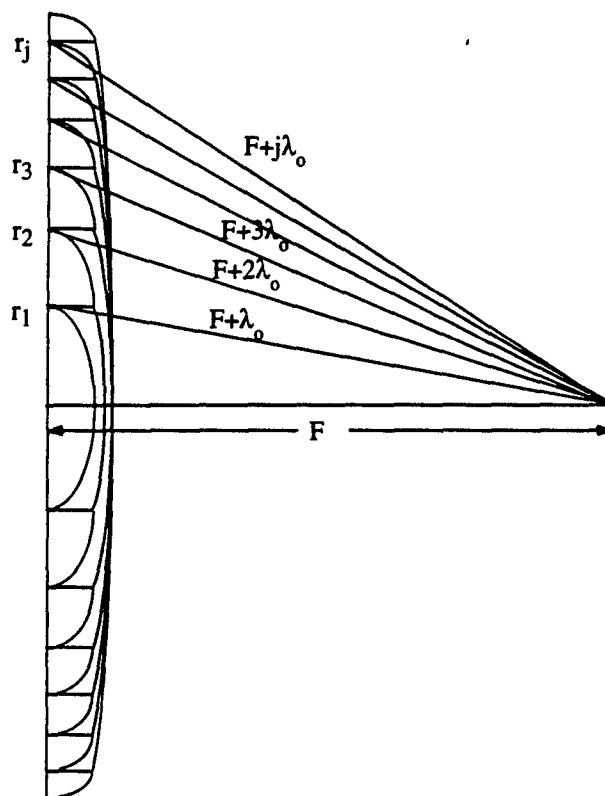


Fig. 2.2.1. A surface-relief diffractive lens with full-period (2π) zones.

In the paraxial approximation $f \gg j\lambda$, the radii of the zones are

$$r_j \equiv \sqrt{2j\lambda f}. \quad (2.2.3)$$

In general, the phase function can be written as

$$\varphi(r) = 2\pi\alpha(m + Ar^2 + Dr^4 + Er^6 + \dots) \quad (2.2.4)$$

$$\text{for } r_{m-1} < r < r_m; m = \pm 1, \pm 2, \pm 3, \dots$$

For paraxial zone spacings, the phase function can be expressed as⁹

$$\varphi(r) = 2\pi\alpha\left(m - \frac{r^2}{2\lambda_0 f}\right). \quad (2.2.4.b)$$

The term α is a factor that allows for detuning from the center wavelength. Recall that the phase of a lens is given by

$$\varphi(r) = \frac{2\pi}{\lambda} \text{OPD}(r). \quad (2.2.5)$$

The optical path difference (OPD) of a lens is

$$\text{OPD}(r) = [n(\lambda) - 1]d(r) \quad (2.2.6)$$

where $n(\lambda)$ is the index of refraction as a function of the incident wavelength for the diffractive lens material and $d(r)$ is the thickness of the element as a function of r , the radial distance from the axis. By combining Eqs. (2.2.5) and (2.2.6) and assuming that the diffractive lens imparts a phase difference of 2π at $\lambda = \lambda_0$, the maximum height of the surface relief element is equal to d_{\max} .

$$\varphi_{\max}(\lambda = \lambda_0) = \frac{2\pi}{\lambda_0} [n(\lambda) - 1]d_{\max} = 2\pi, \quad (2.2.7)$$

therefore

$$d_{\max} = \frac{\lambda_0}{n(\lambda_0) - 1}. \quad (2.2.8)$$

To solve for the term α , one examines the value of the imparted phase in Eq. (2.2.4) at d_{\max} for wavelengths other than the design wavelength λ_0 . By substituting the value

of d_{\max} from Eq. (2.2.8) into Eqs. (2.2.6) and (2.2.5), the detuning factor α in Eqs. (2.2.4a) and (2.2.4b) is found to be

$$\alpha = \left(\frac{\lambda_o}{\lambda} \right) \left(\frac{n(\lambda) - 1}{n(\lambda_o) - 1} \right). \quad (2.2.9)$$

2.2.2. Diffraction Efficiency

The phase function φ in Eq. (2.2.4.b) can be represented as a periodic function by making the appropriate change of variables, as shown by Dammann,⁹

$$\xi = \frac{r^2}{2\lambda_o f}. \quad (2.2.10)$$

The phase function then becomes

$$\varphi(\xi) = 2\pi\alpha(m - \xi). \quad (2.2.11)$$

The transmission function, $t(\xi)$ can be represented as a Fourier series,

$$t(\xi) = e^{i\varphi(\xi)} = \sum_{m=-\infty}^{m=\infty} C_m e^{+i2\pi m \xi}, \quad (2.2.12)$$

where C_m is given by

$$C_m = \frac{e^{-i\pi(\alpha+m)}}{\pi(\alpha+m)} \sin[\pi(\alpha+m)]. \quad (2.2.12b)$$

For positive values of m to correspond to positive, converging diffracted orders, a change of variables from $+m$ to $-m$ is performed, and the order of summation is reversed. Changing back from the substitution of variables in Eq. (2.2.11), the diffractive lens then has the following transmission function:

$$t(r) = \sum_{m=-\infty}^{m=\infty} e^{-i\pi(\alpha-m)} \text{sinc}(\alpha-m) e^{\frac{-i\pi r^2}{\lambda_0(f/m)}}, \quad (2.2.13)$$

where

$$\text{sinc}(x) \equiv \frac{\sin(\pi x)}{(\pi x)}. \quad (2.2.14)$$

Comparing this expression to the transmission function for a conventional thin lens, with a paraxial approximation Eq. (2.2.15),¹⁰ one can find the effective focal length of the diffractive lens.

$$T_{\text{thin lens}}(r) = e^{\frac{-i\pi r^2}{\lambda f}} \quad (2.2.15)$$

and

$$e^{\frac{-i\pi r^2}{\lambda_0(f/m)}} = e^{\frac{-i\pi r^2}{\lambda f_{\text{DOE}}}}, \quad (2.2.16)$$

therefore,

$$f_{\text{DOE}} = \left(\frac{f}{m} \right) \frac{\lambda_0}{\lambda}. \quad (2.2.17)$$

The diffraction efficiency of the diffractive lens in the m^{th} order is given by¹¹

$$\eta_m = C_m C_m^* = \text{sinc}^2(\alpha - m), \quad (2.2.18)$$

where C_m is given in Eq. (2.2.12b). For the first diffracted order ($m=1$) when $\alpha=1$ ($\lambda=\lambda_0$), $\eta=1.0$; in other words it has 100% efficiency in this case. The diffraction efficiency versus wavelength for a diffractive lens with a quadratic blaze profile as described above in Eq. (2.2.18), is plotted in Fig. 2.2.2.

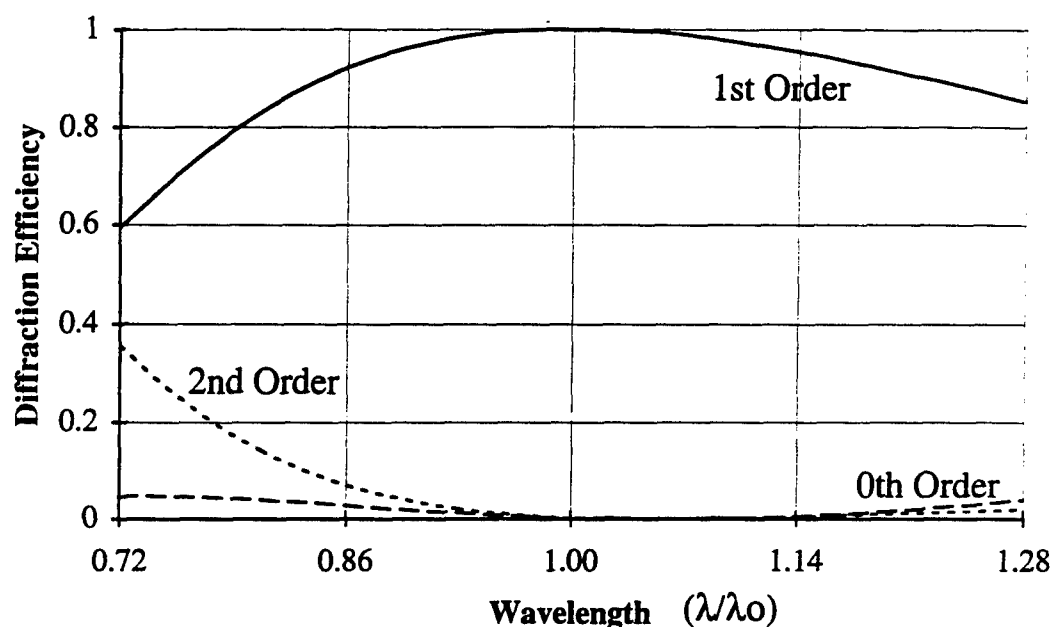


Fig. 2.2.2. Scalar diffraction efficiency for a quadratic-blaze, diffractive lens.

Diffractive lenses have been fabricated using lithographic technologies in which the phase profile is approximated by discrete steps,¹² as shown in Fig. 2.2.3. In the case of discrete step profiles, optical properties such as power, dispersion, and aberration correction are unchanged, but diffraction efficiency is affected.



Fig. 2.2.3. Four-level diffractive lens superimposed with equivalent quadratic-blaze profile lens.

The phase function for a discrete step profile diffractive lens is calculated in a similar manner as that for the quadratic blaze profile described above. The first step is to start with a quadratic profile and make the same change of variables as in Eq. (2.2.10).⁹

The linear phase profile is then approximated by the appropriate number of phase levels, and the phase of the k^{th} step is given by

$$\phi(\xi) = \frac{2\pi\alpha}{p}(p-k), \quad (2.2.19)$$

$$\text{for : } \frac{kd}{p} \leq \xi < \frac{(k+1)d}{p}$$

where $k = 0, 1, 2, \dots, (p-1)$ and p is the number of phase steps.

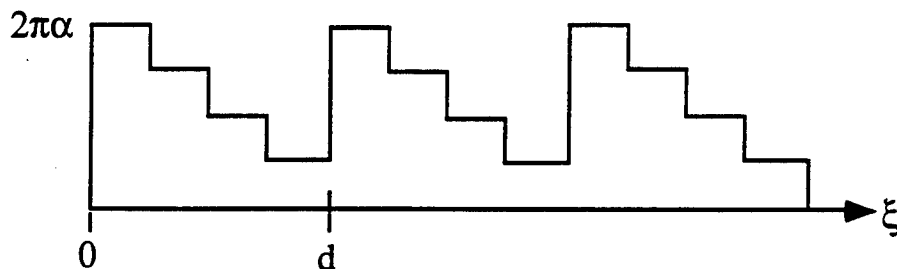


Fig. 2.2.4. Phase profile for a discrete-step profile diffractive lens after a change of variables.

Since the transmission function for the diffractive lens is periodic in ξ , it can be represented as a Fourier series :

$$t(\xi) = e^{i\phi(\xi)} = \sum_{m=-\infty}^{\infty} C_m e^{i2\pi m \frac{\xi}{d}}, \quad (2.2.20)$$

where

$$C_m = \frac{1}{d} \int_0^d t(\xi) e^{-i2\pi m \frac{\xi}{d}} d\xi. \quad (2.2.21)$$

C_m is given by

$$C_m = e^{-i\pi(m+\alpha-\frac{1}{p})} \frac{\sin[\pi(m+\alpha)]}{\sin[(\pi(m+\alpha)/p)]} \frac{\sin(\pi m/p)}{\pi m}. \quad (2.2.22)$$

The efficiency is again equal to the square of the complex Fourier coefficient,

$$\eta_m = |C_m|^2 = \frac{\sin^2[\pi(\alpha-m)]}{\sin^2[(\pi(\alpha-m)/p)]} \frac{\sin^2(\pi m/p)}{(\pi m)^2}. \quad (2.2.23)$$

For $\alpha = 1$, the diffraction efficiency of the first diffracted order is given by

$$\eta_1 = \text{sinc}^2(1/p). \quad (2.2.24)$$

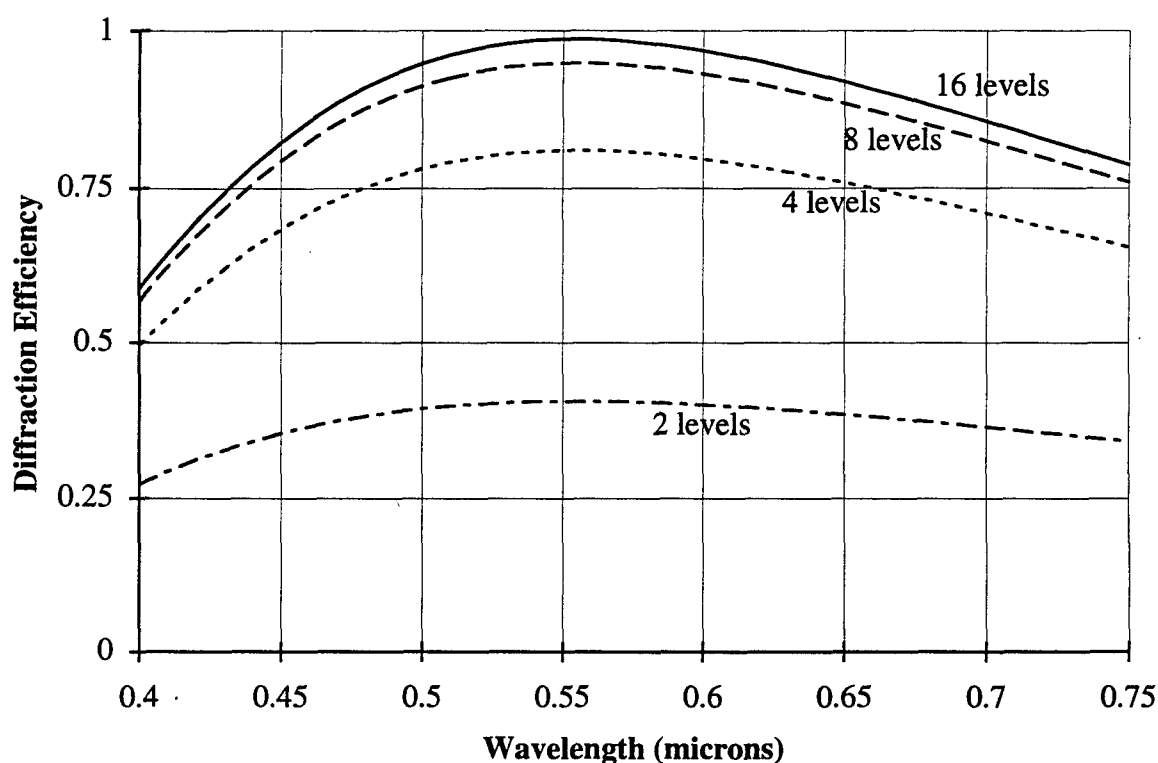


Fig. 2.2.5. Scalar diffraction efficiencies of diffractive lenses fabricated as multi-level profile elements, 16-level, 8-level, 4-level, and 2-level with peak efficiencies occurring at $\lambda = 555$ nm.

Since the zone spacings of a diffractive lens vary across the aperture, the diffraction efficiency can vary as the zone-spacing to wavelength ratio changes across the aperture. As this ratio decreases below a certain limit, the scalar model for diffraction efficiency is no longer valid, and efficiencies of less than 100% can be expected. For diffractive lenses operating in the visible spectral band at an $f/\#$ of approximately $f/1$ or $f/2$ or less, the Fourier model begins to fail to accurately predict efficiency with errors in efficiency of 10 to 20 percent.¹³ The integrated efficiency is a

figure of merit for the diffraction efficiency over the area of the entire aperture, and is given by¹¹

$$\eta_{\text{int}} = \frac{1}{A_{\text{pupil}}} \int_{-\infty}^{\infty} \int_{-\infty}^{\infty} \eta_{\text{local}}(u, v) du dv, \quad (2.2.25)$$

where A_{pupil} is the pupil area and η_{local} is the local efficiency of the diffractive lens for a given aperture coordinate. It has been shown that the integrated efficiency is useful in evaluating optical systems employing diffractive lenses, in that it provides a scaling factor for the optical transfer function. For diffractive lenses operating over a finite spectral band the diffraction efficiency is a function of aperture position and wavelength. The polychromatic integrated efficiency gives a measure of diffraction efficiency accounting for the light diffracted into other orders as result of a wavelength change from the nominal wavelength. The polychromatic integrated efficiency is defined as^{11,14}

$$\eta_{\text{int,poly}} = \frac{\int_{\lambda_{\text{min}}}^{\lambda_{\text{max}}} \eta_{\text{int}}(\lambda) d\lambda}{\lambda_{\text{max}} - \lambda_{\text{min}}}. \quad (2.2.26)$$

An approximate formula the polychromatic, integrated efficiency of diffractive lenses with efficiencies that are accurately predicted by scalar theory is¹⁴

$$\eta_{\text{int,poly}} \cong 1 - \left(\frac{\pi \Delta\lambda}{6 \lambda_o} \right)^2 \quad (2.2.27)$$

2.3. Modeling Diffractive Lenses in Lens Design Programs

2.3.1. Lens Design Models

If diffractive lenses are to be implemented into many systems, it is important that methods or models for analyzing the lenses in optical design software be commonly available and be easy to use. There are various methods of modeling diffractive lenses in lens design programs. In this section, three models are discussed. They are the "Two-point source" method, the phase polynomial description, and the Sweatt model.

Some design programs such as CODEV,¹⁵ allow a diffractive lens to be modeled as an optically recorded holographic lens with a phase term representing the interference between a "reference beam" and an "object beam". Each of these is a point source, placed at the proper conjugates for the designed application. The terms defining the phase function can be used to optimize the lens. The phase function of the lens is then given by:

$$\varphi_{\text{DOE}} = \varphi_{2\text{-pt_sources}} + \varphi_{\text{poly}}, \quad (2.3.1)$$

where φ_{poly} is a term including higher order terms :

$$\varphi_{\text{poly}} = \sum a_{mn} x^m y^n. \quad (2.3.2)$$

Alternatively, a rotationally symmetric phase function of the radial coordinate ρ can be used to represent the diffractive lens:

$$\phi_{\text{DOE}} = \frac{2\pi}{\lambda_o} (s_1 \rho^2 + s_2 \rho^4 + s_3 \rho^6 + s_4 \rho^8 + s_5 \rho^{10}), \quad (2.3.3)$$

where
$$s_1 = -\frac{1}{2F}. \quad (2.3.4)$$

A drawback of the use of either of the above two methods is that paraxial first and third order data are not available. The models typically are only accurately used for real raytracing. The equations for conventional paraxial optics do not include the two types of "special surfaces" described above.

Sweatt¹⁶ and Kleinhans¹⁷ independently showed that a diffractive lens is mathematically equivalent to a zero-thickness lens with an equivalent index of refraction equal to infinity. Using this model, paraxial first order data and third order aberration data are available and are accurate. Since using an infinite refractive index value in lens design programs is not feasible, a very large number is substituted; usually 10,001 works well as the index at the center wavelength. For wavelengths other than the design wavelength, the index of refraction is given by:¹⁶

$$n_{\text{Sweatt}}(\lambda, m) = \frac{m}{m_o} \frac{\lambda}{\lambda_o} [n_{\text{Sweatt}}(\lambda_o, m_o) - 1] + 1, \quad (2.3.5)$$

where λ_o and m_o are the design wavelength and the design diffracted order, respectively. By substituting the 'Sweatt' indices of refraction for the short, middle, and long wavelengths into the Abbe v-number equation, which is

$$v = \frac{n(\lambda_m) - 1}{n(\lambda_s) - n(\lambda_l)}, \quad (2.3.6)$$

the effective v-number for a diffractive lens is given by

$$v_{\text{DOE}} = \frac{\lambda_{\text{middle}}}{\lambda_{\text{short}} - \lambda_{\text{long}}}. \quad (2.3.7)$$

For the visible spectrum, using the C, d, and F lines, v_{DOE} is equal to -3.45. The curvatures of the model Sweatt lens are given as :

$$c_{1,2} = c_s \pm \frac{\varphi(\lambda_o, m_o)}{2[n_{\text{Sweatt}}(\lambda_o, m_o) - 1]}, \quad (2.3.8)$$

where $\varphi(\lambda_o, m_o)$ is the power of the diffractive lens at the design wavelength for the design diffracted order. With the use of this model, higher order aspheric terms can also be used as design variables to optimize the performance of the lens.

2.3.2. Third Order Aberrations of Diffractive Lenses

The third order aberrations of a diffractive lens have been determined by examining the third order aberration expressions for a thin lens with an aperture stop in contact, and taking the limits as the index of refraction approaches infinity ($n \rightarrow \infty$, $c_{1,2} \rightarrow c_s$) and as the two curvatures of the diffractive model lens approach the substrate curvature.^{16,17,18}

The wavefront aberration polynomial to third order is given by:¹⁹

$$\begin{aligned} W(h, \rho, \cos \phi) = & \frac{1}{8} S_I \rho^4 + \frac{1}{2} S_{II} h \rho^2 \cos \phi + \frac{1}{2} h^2 \rho^2 \cos^2 \phi \\ & + \frac{1}{4} (S_{IV} + S_{III}) h^2 \rho^2 + \frac{1}{2} S_V h^3 \rho \cos \phi. \end{aligned} \quad (2.3.9)$$

The aberration coefficients for a thin lens in air with the aperture stop in contact are :

S_I – Spherical aberration

$$S_I = \frac{y^4 \phi^3}{4} \left[\left(\frac{n}{n-1} \right)^2 + \frac{n+2}{n(n-1)^2} B^2 + \frac{4(n+1)}{n(n-1)} BT + \frac{3n+2}{n} T^2 \right] + 8Gy^4(\Delta n), \quad (2.3.10)$$

S_{II} – Coma

$$S_{II} = \frac{-y^2 \phi^2 H}{2} \left[\frac{n+1}{n(n-1)} B + \frac{2n+1}{n} T \right], \quad (2.3.11)$$

S_{III} – Astigmatism

$$S_{III} = H^2 \phi, \quad (2.3.12)$$

S_{IV} – Petzval field curvature

$$S_{IV} = \frac{H^2 \phi}{n}, \quad (2.3.13)$$

and

S_V – Distortion

$$S_V = 0. \quad (2.3.14)$$

In Eqs. (2.3.10)-(2.3.14), n is the lens refractive index, y is the paraxial marginal ray height at the surface, $\phi = (c_1 - c_2)(n-1)$ is the power of the lens ($c_{1,2}$ are the curvatures of the lens), $H = y\bar{u} - \bar{y}u$ is the Lagrange invariant of the lens, G is the fourth-order aspheric term of a surface (either or both surfaces may not be spherical), Δn is the change in refractive index across the aspheric surface, B is the bending parameter of the lens (a dimensionless quantity), which is defined as:

$$B = \frac{c_1 + c_2}{c_1 - c_2}, \quad (2.3.15)$$

and T is the conjugate parameter (a dimensionless quantity), which is defined as:

$$T = \frac{u + u'}{u - u'}. \quad (2.3.16)$$

By taking the limits as described above, the third order aberrations of a diffractive lens with the stop in contact are:¹⁸

$$S_I = \frac{y^4}{f^3} \left(\frac{\lambda}{\lambda_o} \right)^3, \quad (2.3.17)$$

$$S_{II} = \frac{-y^3 \bar{u}}{f^2} \left(\frac{\lambda}{\lambda_o} \right)^2, \quad (2.3.18)$$

$$S_{III} = \frac{-y^2 \bar{u}^2}{f} \left(\frac{\lambda}{\lambda_o} \right), \quad (2.3.19)$$

$$S_{IV} = 0, \quad (2.3.20)$$

and

$$S_V = 0. \quad (2.3.21)$$

In Eqs. (2.3.17)-(2.3.21), the power of the diffractive lens in the first diffracted order is given by Eq. (2.2.17), where $m=1$.

When the stop is not in contact with the diffractive lens, the stop shift formulae can be applied to calculate the aberration coefficients as follows:²⁰

$$S_I^* = S_I, \quad (2.3.22)$$

$$S_{II}^* = S_{II} + \left(\frac{\bar{y}}{y} \right) S_I, \quad (2.3.23)$$

$$S_{III}^* = S_{III} + 2\left(\frac{\bar{y}}{y}\right)S_{II} + \left(\frac{\bar{y}}{y}\right)^2 S_I, \quad (2.3.24)$$

$$S_{IV}^* = S_{IV}, \quad (2.3.25)$$

and

$$S_V^* = S_V + \left(\frac{\bar{y}}{y}\right)(3S_{III} + S_{IV}) + 3\left(\frac{\bar{y}}{y}\right)^2 S_{II} + \left(\frac{\bar{y}}{y}\right)^3 S_I. \quad (2.3.26)$$

In Eqs. (2.3.22)-(2.3.26), the starred (*) quantities refer to the aberration after the stop has been shifted.

2.3.3. Converting the Ultra-High Index Lens to Fabrication Specifications

To fabricate the diffractive lens, one needs to convert the modeled diffractive lens to specifications that can be manufactured. In short, one needs to solve for the zone spacings given the refractive index of the diffractive lens material, the surface radii, and the higher order aspheric terms from the design (Sweatt) model.

The first step in doing this process is to convert the thin lens model to a phase function. Once this is achieved, the phase function can then be numerically solved for multiples of 2π .

The terms in the equation for the sag of a rotationally symmetric, curved surface can be equated with terms in the phase function of a diffractive lens by following the appropriate steps. The sag of a surface, to tenth order, can be described by a function of the radial coordinate r as :

$$z(r) = \frac{cr^2}{1 + \sqrt{1 - (\kappa + 1)(cr)^2}} + dr^4 + er^6 + fr^8 + gr^{10}. \quad (2.3.27)$$

The optical path introduced by the surface is $-(\Delta n)\{z(r)\}$, where Δn is defined as $\pm(n_s - 1)$, where the + (plus sign) is for the surface on the front of the lens (1st surface), the - (minus sign) is for the back surface of the lens (2nd surface). A Taylor series expansion to the tenth order of the surface sag equation is given by:

$$z(r) = \frac{c}{2}r^2 + \left(\frac{c^3}{8} + d\right)r^4 + \left(\frac{c^5}{16} + e\right)r^6 + \left(\frac{5c^7}{128} + f\right)r^8 + \left(\frac{7c^9}{256} + g\right)r^{10}. \quad (2.3.28)$$

The additional optical path introduced by the diffractive lens phase function described in Eq. (2.3.3) is given by:

$$\text{OPL}_{\text{DOE}} = \frac{\lambda_o}{2\pi} \varphi(r) = s_1\rho^2 + s_2\rho^4 + s_3\rho^6 + s_4\rho^8 + s_5\rho^{10}. \quad (2.3.29)$$

By equating terms in Eq. (2.3.29) with the appropriate optical path terms introduced by the surface sag terms in Eq. (2.3.27), the following conversions can be made:

$$s_1 = -\Delta n \frac{c}{2}, \quad (2.3.30)$$

$$s_2 = -\Delta n \left(\frac{c^3}{8} + d \right), \quad (2.3.31)$$

$$s_3 = -\Delta n \left(\frac{c^5}{16} + e \right), \quad (2.3.32)$$

$$s_4 = -\Delta n \left(\frac{5c^7}{128} + f \right), \quad (2.3.33)$$

and

$$s_5 = -\Delta n \left(\frac{7c^9}{256} + g \right). \quad (2.3.34)$$

2.4. References for Chapter 2

1. M. Tanigami, S. Ogata, T. Yamashita, K. Imanaka "Low-wavefront aberration and high-temperature stability molded micro fresnel lens," *IEEE Photonics Technology Letters*, **1**, 384-385 (1989).
2. H. W. Deckman, J. H. Dunsmuir, "Replication lithography," in *Plasma Synthesis and Etching of Electronic Materials*, R.P.H. Chang and B. Abeles, eds. Symposia Proc.Mater. Res. Soc., **38**, 267-273 (1985).
3. M. T. Gale, M. Rossi, H. Schütz, "Fabrication and replication of continuous-relief DOEs," in *Fourth International Conference on Holographic Systems, Components and Applications*, IEE Conf. Publ., **379**, 66-70 (1993).
4. M. T. Gale, M. Rossi, H. Schütz, P. Ehbets, H.P.Herzig, D. Prongué, "Continuous-relief diffractive optical elements for two-dimensional array generation," *Appl. Opt.* **32**, 2526- 2533 (1993).
5. C. Budzinski, B. Kleemann, "Fabrication and replication of radiation-resistant diffractive optical elements," in *Holographics International 1992*, Y.N. Denisyuk, F. Wyrowski, eds. Proc. SPIE, **1732**, 641-645 (1992).
6. J. Jahns, K. H. Brenner, W. Däschner, C. Doubrava, T. Merklein, "Replication of diffractive microoptical elements using a PMMA molding technique," *Optik* **89**, 98-100 (1992).
7. T. Stone, N. George, "Hybrid diffractive-refractive lenses and achromats," *Appl. Opt.* **27**, 2960-2971 (1988).
8. R. W. Wood, "Phase-reversal zone-plates, and diffraction-telescopes," *Philos. Mag. [Series 5]* **45**, pp. 511-522 (1898).
9. H. Dammann, "Blazed synthetic phase-only holograms," *Optik* **31**, 95-104 (1970).
10. J. W. Goodman, *Introduction to Fourier Optics* (McGraw-Hill, New York, 1968) p.80.
11. D. A. Buralli, G. M. Morris, "Effects of diffraction efficiency on the modulation transfer function of diffractive lenses," *Appl. Opt.* **31**, 4389-4396 (1992).
12. See for example, L. d'Auria, J. P. Huignard, A. M. Roy, E. Spitz, "Photolithographic fabrication of thin film lenses," *Opt. Commun.* **5**, 232-235 (1972); G. J. Swanson, W. B. Veldkamp, "Diffractive Optical Elements for Use in Infrared Systems," *Opt. Eng.* **28**, 605-608 (1989).

13. J. A. Cox, T. Werner, J. Lee, S. Nelson, B. Fritz, J. Bergstrom, "Diffraction efficiency of binary optical elements," in *Computer and Optically Formed Holographic Optics*, Sing H. Lee, ed. Proc. SPIE, **1211**, 116-124 (1990).
14. G. J. Swanson, "Binary Optics Technology : The Theory and Design of Multi-Level Diffractive Optical Elements," Tech. Rep. 854 (Lincoln Laboratory, MIT, Lexington, Mass., 1989).
15. CODEV is a registered trademark of Optical Research Associates, 550 North Rosemead Blvd., Pasadena, CA 91107.
16. W. C. Sweatt, "Describing Holographic Optical Elements as Lenses," J. Opt. Soc. Am. **67**, 803-808 (1977).
17. W. A. Kleinhans, "Aberrations of curved zone plates and Fresnel lenses," Appl. Opt. **16**, 1701-1704 (1977).
18. D. A. Buralli, G.M. Morris, "Design of a wide field diffractive landscape lens," Appl. Opt. **28**, 3950-3959 (1989).
19. W. T. Welford, *Aberrations of Optical Systems* (Adam Hilger, Boston, 1986), pp.130-140.
20. Ref. 19, pp.148-152.

3. Diffractive-Refractive Eyepiece Design

3.1. Introduction

3.1.1. Overview of Chapter 3

This chapter deals with eyepiece design. Section 3.2 discusses conventional methods of eyepiece design. There are features and characteristics of all-refractive eyepiece designs that contribute to certain difficulties in correcting their aberrations. Furthermore, due to the function of eyepieces, there are design constraints, such as the external aperture stop and large element apertures, which make eyepiece design difficult. These design issues become magnified in wide-angle eyepieces. Examples of several all-refractive eyepieces covering various fields-of-view are shown. In Section 3.3 hybrid, diffractive-refractive eyepiece design is presented. The fundamentals of optical design with diffractive lenses discussed in Chapter 2 are utilized in eyepiece designs that employ both diffractive and refractive elements. Several hybrid designs are shown. Theoretical optical performance comparisons of hybrid, wide-angle eyepieces with the well-known Erfle eyepiece are presented. In Section 3.4 the results of the comparisons are presented and discussed.

3.1.2. General Eyepiece Design

Eyepiece design is a unique lens design problem in that several features and characteristic requirements make eyepieces very different from typical photographic imaging systems or relay lens systems.¹ In a visual instrument, an eyepiece is used to

view an internal, real image by placing the final image at or near infinity with an increased angular subtense. Along with acting as a magnifying device, an eyepiece is required to image the entrance pupil of the visual instrument at the external exit pupil location with acceptable performance. Therefore in eyepiece design one needs to be concerned with not only the standard, third order, Seidel imaging aberrations but also pupil aberrations, particularly spherical aberration of the pupil.¹ Aberrations in the eyepiece are often so difficult to correct that certain aberrations are left uncorrected, tolerated, or are corrected by other components in the system. For example, lateral color is often left undercorrected in the eyepiece and balanced with dispersive prisms.²

The first order requirements and third order characteristics of eyepieces are unique. First order characteristics that are unique to eyepieces are the following : an external aperture stop, particularly large aperture elements relative to the system aperture, and a required minimum distance from the last surface to the exit pupil (eye relief). Also, as the eye relief is increased relative to the focal length, while the field angle is kept the same, the diameters of the elements increase. (The element diameters also increase with a fixed constant eye relief, while the field angle is increased.) As the diameters of the elements increase, the off-axis monochromatic aberrations and lateral color are severely aggravated. Consequently it is difficult to design a well-corrected eyepiece with both a long eye relief and a wide field of view.

Third order characteristics which are typical in eyepieces are the following : a large amount of distortion relative to the field angle, uncorrected lateral color at the edge of the field, strongly curved tangential image field due to the lack of Petzval field correction, and spherical aberration of the exit pupil . With these first order requirements and third order issues, eyepieces take on forms with increasing complexity as the field angle increases and as the f -number decreases. Particularly, as the field angle increases, the curvatures of the elements tend to get stronger, elements

tend to get thicker, more exotic glasses are used, and the number of elements increases. In the following section (Section 3.2) examples and descriptions of conventional, all-refractive eyepieces are shown and are accompanied by figures of merit describing their performance.

The results of these wide-field design constraints have been multi-element, bulky eyepieces, which may limit their usage in certain applications where weight, cost, and size are critical. Due to the severe chromatic aberrations in eyepieces, it has been necessary to include highly dispersive, negative elements into their designs to balance the undercorrected, residual chromatic aberrations of the positive elements. In several wide-field eyepieces, including many variations of the original Erfle eyepiece, the lateral color is so severe that each positive element is achromatized with a negative element.² As a result of these limitations imposed by refractive optics and conventional design variables, improvements of existing eyepiece designs has been limited.

By incorporating a new technology - diffractive optics - added degrees of freedom can be included into the eyepiece design problem to arrive at new solutions. Benefits of diffractive optics such as wavefront shaping to correct the monochromatic aberrations and the dispersion being opposite in sign to that of glass to correct chromatic aberrations can be used to improve upon existing eyepiece designs. Fabricated as surface-relief structures, significant reductions in eyepiece weight and size can be achieved with the inclusion of diffractive lenses. The hybrid designs presented in this thesis offer equivalent – or better – performance than multi-element, refractive eyepieces, while reducing their size, weight, and possibly cost. By reducing the surface curvatures of the elements and the overall material in the system, significant cost reduction can be achieved in eyepiece systems with the inclusion of diffractive lenses.

3.2. Eyepiece Design

3.2.1. Conventional Eyepiece Design

There are two inherent features of eyepieces that limit their performance in visual instruments. These are the lack of chief ray symmetry about an aperture stop or pupil, due to the fact that the stop is *outside* the eyepiece, and the large diameters of the elements, which is due to the large chief ray angular field. For these reasons, field aberrations are the most difficult to correct in the eyepiece.¹ Spherical aberration and paraxial axial chromatic aberration in the eyepiece are generally small in comparison to the contributions of these aberrations from the objective lens (in a visual instrument) due to the small size of the eyepiece aperture and the comparatively shorter eyepiece focal length.² The marginal ray heights in the eyepiece are small compared to the marginal ray heights in the objective lens. Therefore, in terms of the primary aberrations the most difficult to correct are Petzval field curvature, astigmatism, lateral color, distortion, and pupil spherical aberration or spherical aberration of the chief ray. The aberrations of the eyepiece are typically calculated by tracing rays from the exit pupil, through the eyepiece, and are evaluated at the focal plane, i.e. the location of the real, internal image; to evaluate spherical aberration of the pupil a bundle of chief rays are traced traveling in the opposite direction.³

Since an eyepiece acts as a relay lens for the system pupils, the eyepiece is comprised mainly of strong, positive elements. This closely grouped set of positively-powered elements therefore tends to have a strong, inward-curving Petzval field curvature.³ Some conventional eyepiece designs employ a thick, meniscus lens near the internal image which aids in flattening the image field and in extending the eye

relief.⁴ This option quickly leads to an increase in number of elements and overall weight. Note that when assessing image field curvature, astigmatism and Petzval field curvature must be evaluated together as a unit.³

Due to the relatively short focal lengths of eyepieces, there is little one can do to reduce the Petzval field curvature of an eyepiece.¹ Therefore, most eyepieces are designed such that the Petzval field curvature is left essentially uncorrected, and over-corrected astigmatism is introduced into the design in order to flatten the curvature at the edge of the field.³ The designer typically aims to achieve a flat sagittal field. As a consequence, the tangential field becomes slightly backward curving.¹ The designer is then forced to make a compromise. Since the amount of field curvature in eyepieces is significant, it is more desirable to have the image field curved toward the eye than to have it curve away from the eye. The reason for this is that typically with visual instruments the on-axis, final image (to the eye) is placed at infinity, and the off-axis image lies along a curved field. If the curved image field were backward-curving away from the eye, the light from the off-axis image would focus in front of the eye, or in other words, light from the off-axis image would be converging at the eye. Only a hyperopic eye can comfortably focus light from beyond infinity, i.e. light that is converging at the eye.⁵ To achieve a flat sagittal field in an eyepiece optical system, astigmatism opposite in sign to that of the amount of Petzval field curvature must be introduced.³ In conventional wide-angle eyepieces, this is commonly achieved by optimizing the index change across the boundary of one or more achromats in the system.^{1,3,6} Surfaces which are responsible for undercorrected spherical aberration will also contribute undercorrected astigmatism.³

An aberration that strongly suffers from the complete lack of stop symmetry in eyepieces is distortion. The distortion found in eyepieces is the "pincushion" or positive type.² Values of distortion typical in wide-field eyepieces, i.e. 60° to 70° full

field-of-view, are 8-12%.² The amount of this aberration would be unacceptable in standard photographic lenses, yet is tolerated in eyepieces in part due to its difficulty to correct and also due to the fact that the eye is a forgiving detector. For example, it is not uncommon in visual instruments that the edge of the field is used to orient the user and to locate objects;² objects seen at the edge of the field are then brought to the center of the field to view with better detail. Aspheric surfaces are used in some cases to correct the distortion in wide-field eyepieces.² This is often an expensive, undesirable option to improve the quality of the optical device, since aspheric glass surfaces can be expensive to fabricate. Consequently, distortion is often left uncorrected in many eyepieces.³

Eyepieces of long focal length and/or large field angle often suffer from pupil spherical aberration or spherical aberration of the principal ray.³ While image-affecting aberrations are calculated by tracing rays from exit pupil to focal plane, spherical aberration of the chief ray must be calculated by tracing chief rays as they travel through the eyepiece in actual usage; if the aberration is calculated in reverse it is assumed then that the chief rays are originating from the center of the exit pupil.

To calculate the amount of pupil spherical aberration, a bundle of chief rays are traced from the center of the entrance pupil, typically at the system objective, through the eyepiece, and the longitudinal aberration is evaluated at the exit pupil. [Note: a chief ray is defined as a geometric ray originating from the object and passing through the center of the entrance pupil.] The bundle of chief rays is essentially an axial bundle of rays, with respect to the eyepiece, limited only by the apertures of the eyepiece elements or a field stop. A bundle of chief rays, traced from the system objective and passing through the eyepiece, should all intersect the optical axis at the same location. [Note that this intersection location is known as the exit pupil, and it is important that the spherical aberration of the pupil be minimized since it is the location of the eye's

position. To conserve light through the *total* system – including the observer's eye, the eye must be placed at the exit pupil.] As the eyepiece is usually comprised of a closely gathered group of convergent elements, these chief rays will usually suffer from undercorrected spherical aberration.³

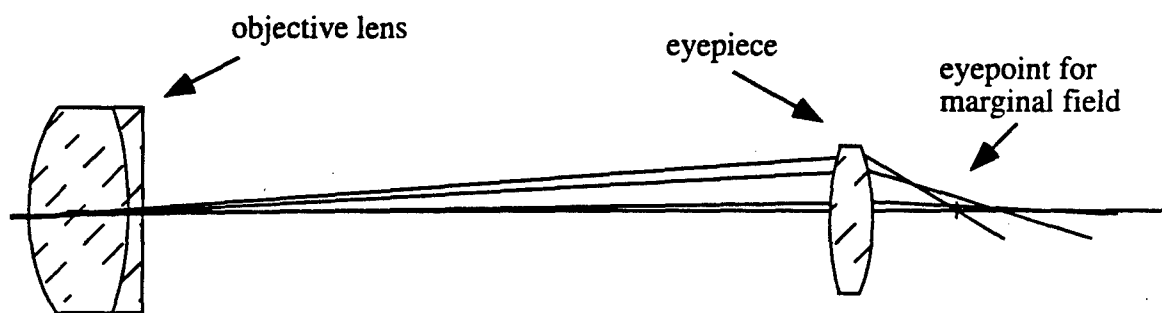


Fig. 3.2.1. A Bundle of Chief Rays through a Telescope.

As the field angle increases, the intersection of the chief ray with the optical axis progresses closer to the last lens, as shown in Fig. 3.2.1. Two situations can result from the case of undercorrected pupil spherical aberration. One problem is that a zonal portion of the visual field is vignetted; another problem is that the eye-position is no longer well defined. In either case, as the eye is moved around, the field appears to "swim" or become shadowed in the shape of a kidney bean. This effect is commonly referred to as the "kidney bean effect".^{1,3}

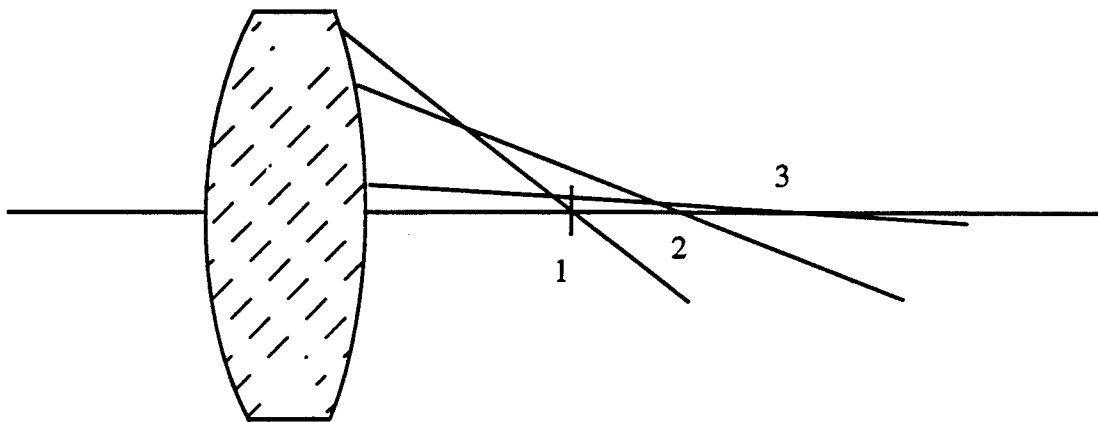


Fig. 3.2.2. Pupil Spherical Aberration of a singlet lens eyepiece.

In Fig. 3.2.2, chief rays for different off-axis beams are drawn for an eyepiece exhibiting a severe amount of pupil spherical aberration. A paraxial chief ray intersects the optical axis at point 3, which is the *design* exit pupil location; an intermediate chief ray intersects the axis at point 2; and a chief ray from the maximum field angle intersects the optical axis at location 1. If an observer using the device desires to view the edge of the field, he or she would place the eye at point 1. At that location, rays from the intermediate field may be vignetted entirely by the eye's pupil while the rays from the center and from the edge of the field will enter the eye. This situation leads to a case where the middle zone of the field is vignetted and a kidney-shaped shadow seems to have replaced it. Since the user typically cannot keep his or her eye stationary or if the user purposefully moves the eye back and forth to capture more of the field-of-view, other parts of the field will be vignetted, while previously shadowed areas return to view. The visual field appears to "swim" in and out of shadowy areas. In less severe cases of pupil spherical aberration, these effects can be seen if the user moves

his or her eye off-axis to view the edge of the field or if the user moves back and forth with respect to the instrument.

Pupil spherical aberration must be kept under reasonable control in eyepieces. Typical methods of correcting this aberration are to distribute the power of the elements by splitting them, replacing a spherical surface with an aspheric or parabolic surface,^{1,6} or using a Schmidt corrector plate at the focal plane.³ All of these options may be unattractive, because they can increase one or more of the following: the number of elements, the weight of the eyepiece, the complexity, and/or the cost of the eyepiece.

Pupil spherical aberration and distortion are closely related in eyepieces.⁴ As was seen in the above description, in the case of undercorrected pupil spherical aberration, the chief ray is bent at progressively steeper angles as the field angle increases. With the steeper chief ray angles, the corresponding part of the image field will be magnified larger than expected. This is known as pincushion distortion, which as mentioned earlier, is the type of distortion found in eyepieces.

Lateral color can be a large problem in eyepieces, especially in wide angle instruments. It is important to account for this aberration at the initial layout of the eyepiece design. In the case of wide-field eyepieces, higher-order lateral color can significantly degrade the image. Paraxial lateral color increases linearly with field angle; a chromatic magnification error varying as the cube of the field angle can also be a problem in eyepieces. This chromatic magnification error is known as chromatic variation of distortion or chromatic distortion.⁶ Therefore a first order correction may be insufficient, and the designer must compromise a third order solution for lateral color correction that extends beyond simply achromatizing a thin lens design. As with other off-axis aberrations, this aberration is difficult to correct or reduce due to the lack of chief ray symmetry in the eyepiece. In some designs, each positive element in the eyepiece is achromatized by an accompanying negative, dispersive element. For

example, the Erfle eyepiece has been modified to have the center element achromatized to better correct for lateral color.^{2,7} These types of eyepiece designs require many elements and therefore may also be relatively heavy and large.

3.2.2. Conventional Eyepiece Examples

In conventional, all-refractive eyepiece designs, complexity increases with field-of-view and performance requirements. Factors such as lateral color, field curvature, distortion, and spherical aberration of the pupil rapidly become more of a problem at larger field angles. In Figs. 3.2.3-3.2.7 some common eyepieces are shown which demonstrate these design issues. Notice that eye relief also is an important factor; as the field angle becomes greater, the element aperture diameters increase due to the external exit pupil, or in other words, due to the requirement for sufficient eye relief. An interesting difference from photographic objectives is that the eyepiece element apertures are virtually independent of the system clear aperture, i.e. the entrance pupil diameter, but are directly related to the field angle. In Figs. 3.2.3-3.2.7 the dashed line crossing the optical axis represents the exit pupil location; the **X** marks the image plane or the field stop location. ER/FL is the ratio of eye relief to focal length. In each of the figure captions, the specified optical merits refer to the optical evaluation when rays are traced from infinity through the aperture stop and the lens to the focal plane. The full-field performance is specified in each case.

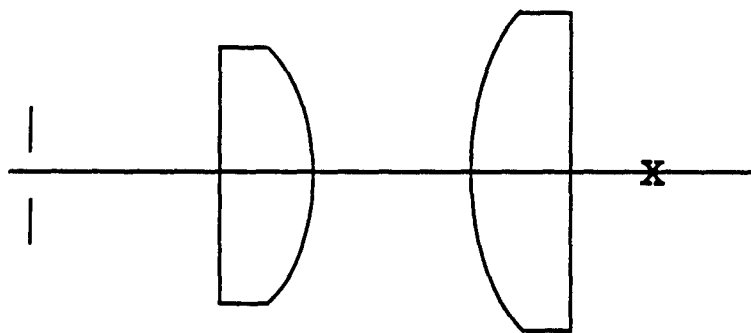


Fig. 3.2.3. Ramsden Eyepiece,⁷ 30° FOV. Performance: 25.4 mm FL, Spot Size = 0.075 mm, 2% distortion, ER/FL = 0.47.

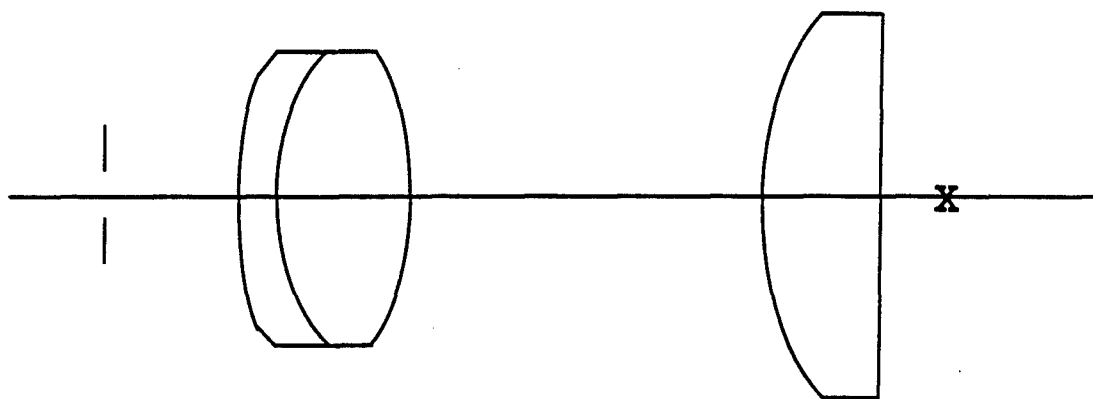


Fig. 3.2.4. Kellner Eyepiece,⁷ 40° FOV. Performance: 25.4 mm FL, Spot Size = 0.16 mm, 2.5 % distortion, ER/FL = 0.03.

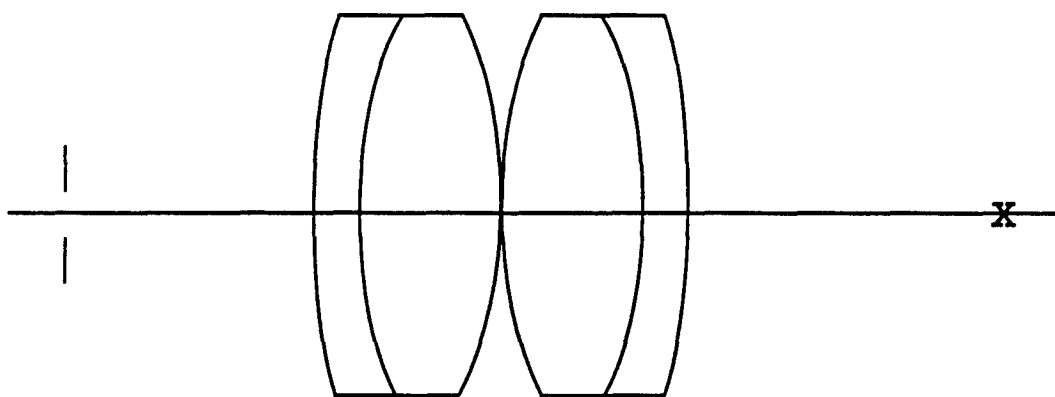


Fig. 3.2.5. Symmetrical (Plossl) Eyepiece,⁷ 50° FOV. Performance: 25.4 mm FL, Spot Size = 0.2 mm, 6% distortion, ER/FL = 0.84.

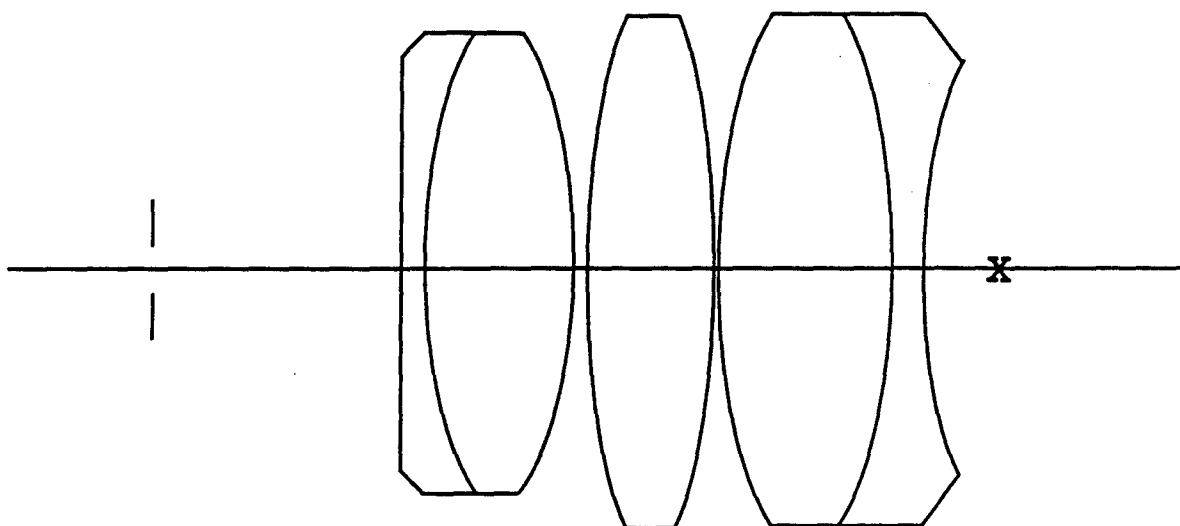


Fig. 3.2.6. Erfle Eyepiece,⁷ 60° FOV. Performance: 25.4 mm FL, Spot Size = 0.39 mm, 8% distortion, ER/FL = 0.83.

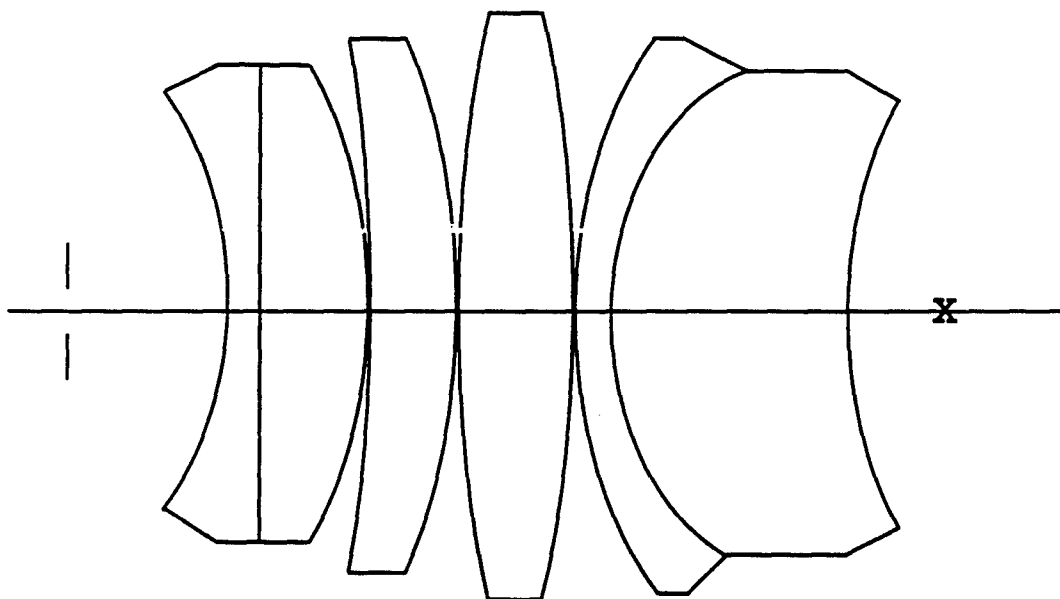


Fig. 3.2.7. Wild Eyepiece,⁷ 70° FOV. Performance: 25.4 mm FL, Spot Size = 0.24 mm, 12.5 % distortion, ER/FL = 0.75.

3.3. Hybrid Diffractive-Refractive Eyepiece Design

3.3.1. Diffractive Optics In Eyepieces - Benefits

There are several important features of diffractive optics which can be beneficial to the field of eyepiece design. By examining the unique design difficulties specific to eyepieces, it seems likely that there are several areas in which a tool such as diffractive optics can offer significant contributions. For example, correcting lateral color is a challenging design issue in eyepieces, and often in wide-angle eyepieces many very strong negative, thick elements are used to correct this aberration. This is due in large part, as is the case with other off-axis aberrations, to the lack of an internal stop or pupil in the eyepiece system. The inherent, strong, negative dispersion characteristics of a diffractive lens⁸ offer lightweight solutions to this problem, which therefore makes it an attractive technology to implement into this area. Furthermore, by employing all positive elements, the curvatures of the individual elements tend to be weaker, which in turn has the benefit of reducing the difficulty of the correction of the monochromatic aberrations. In addition to this feature, weaker curvatures can often ease the refractive lens fabrication tolerances.

Of the monochromatic aberrations, distortion and spherical aberration of the exit pupil are perhaps the most difficult to correct in eyepieces, as discussed in Section 3.2.1. The correction of these aberrations in conventional eyepieces has involved the use of aspheric surfaces. The wavefront shaping ability of diffractive optics offers another possible solution of aberration correction.⁹ Unlike with traditional glass lenses, adding an aspheric profile to a diffractive lens effectively does little to change or

complicate the fabrication process. An additional benefit of diffractive lenses is that they contribute nothing to the Petzval sum.^{8,10}

3.3.2. Previous Work And Design Objectives

As can be seen from Section 3.2.2, narrow field eyepieces (about 15° half FOV) typically consist of two or three elements. In such instances, it is unlikely that employing diffractive elements would significantly reduce the size or weight of the eyepiece. Stone examined the use of all-diffractive eyepieces in telescopes, particularly for narrow field cases.¹¹ The primary usefulness of the telescope designs was the ability to correct for the residual color in the objective with the use of a diffractive eyepiece (discussed in Section 1.1.2). He investigated singlet and doublet eyepiece designs. The two element design configuration was based upon the principle of the Huygens' eyepiece, which is a design that is corrected for lateral color while utilizing only two separated elements made of the same glass type. There are inherent drawbacks and limitations to this all-diffractive design which prohibit such a design from having a large field angle. For example, Bennett shows that for a two-element diffractive lens system where both elements have positive power, with a real object and a real image, longitudinal color cannot be corrected.¹² It seems that this principle plays a significant role in pupil imaging, for as Stone notes that although the overall longitudinal chromatic aberration (of the entire telescope) and the lateral color in the eyepiece are corrected in his design, he observes that the pupil position varied dramatically with wavelength. What was happening was that although the chief rays for various wavelengths exited the eyepiece at the same angle (i.e. lateral color was corrected), the chief ray heights at the last surface were different for different wavelengths, and thus their intersections with the optical axis were substantially

different. The resulting drawback is the severe chromatic variation of exit pupil location. This characteristic is exhibited even at fairly small fields-of-view and limits the design from larger field angles. In this section, the primary concern is on implementing diffractive optics into wide-field eyepieces.

3.3.3. Hybrid Diffractive-Refractive Eyepiece Designs

Among various eyepiece designs (types), the correction of the field aberrations is naturally the most difficult in wide-angle eyepieces. Lateral color, distortion, curvature of the image fields, and spherical aberration of the pupil are aberrations which tend to be very strong as the field angle is increased to - and extended beyond - about thirty degrees half field-of-view. Wide-angle eyepieces appear to be the area of eyepiece design in which diffractive optics can offer the most significant contributions. The most common wide-field eyepiece is the Erfle eyepiece.² It is known to be a rather good compromise of the number of elements, size, weight, and optical performance. An Erfle eyepiece consists of a five-element design, with strong positive and negative elements, covering up to a sixty degree apparent field-of-view.¹³ This design provides a situation where diffractive optics can be applied to reduce the number of elements and overall weight. In many applications the central element of the Erfle design is also achromatized with a negative element to reduce lateral color. The Erfle eyepiece is shown in Fig. 3.2.4. The performance characteristics of the Erfle eyepiece are presented at the end of this chapter (Figs. 3.3.6 - 3.3.10) as a comparison with the hybrid eyepiece designs described herein.

In designing a wide-angle hybrid eyepiece, the objective was to design a three refractive-element eyepiece with one or two diffractive elements having similar or improved optical performance compared to the Erfle. In the design process certain

constraints were applied so as to limit the weight and size of the eyepiece. The design limitations were : to avoid using thick elements, to avoid using negative elements, to mount the diffractive elements on planar surfaces, and if possible, to try to mount the diffractive elements on lens surfaces as opposed to placing them on added planar elements. An additional quasi-restriction was to use inexpensive, common glasses wherever possible. It seemed reasonable that a three element design (counting only glass elements) would yield considerable weight and size reduction compared to conventional wide-angle eyepieces, while offering a good first and third order eyepiece design.

The first step in designing the hybrid eyepiece was to start with the same distribution of powers as is used in the Erfle, replacing the flint elements with diffractive lenses, and allow the center element to remain. (Note that the glasses used in the first of Erfle's designs meet the criterion to use only common glasses.) The process went as follows: create two hybrid diffractive-refractive achromats with overall powers equivalent to the two refractive doublets in the Erfle design. The necessary construction parameters for the Erfle eyepiece (scaled to a unit focal length) are listed below in Table 3.3.1. Lens element 1 refers to the element closest to the eye; the elements are numbered successively, continuing in order to element 5 which refers to the element nearest the internal image.

element no.	index (d-line)	v #	glass type	EFL (mm)
1	1.6200	36.365	F2	-1.93264
2	1.5400	59.710	BAK2	1.23199
3	1.5168	64.166	BK7	2.79060
4	1.5400	59.710	BAK2	1.26047
5	1.6200	36.365	F2	-1.52005

Table 3.3.1. Lens description of the Erfle eyepiece based upon data from U.S. Patent number 1,478,704.

Using the thins lens equations for an achromat,¹⁴ the diffractive-refractive (starting point) doublets were designed. The following equations describe the powers of the first and second elements,

$$\phi_1 = \frac{v_1}{v_1 - v_2} \Phi_T \quad (3.3.1)$$

$$\phi_2 = \frac{v_2}{v_2 - v_1} \Phi_T, \quad (3.3.2)$$

where $\Phi_T \equiv$ total power of doublet, $\phi_1 \equiv$ power of first element, $\phi_2 \equiv$ power of second element, $v_1 \equiv$ Abbe dispersion number of first, element, and $v_2 \equiv$ Abbe dispersion number of second element. Applying the numbers from the Erfle design and using $v_{DOE} = -3.45$, as described in Section 2.3.1, and using BAK-2 (see Table 3.3.1 for data) for the refractive components, the following solution results:

the powers for the first refractive-diffractive doublet are

$$\phi_r = 0.27818 \text{ mm}^{-1}$$

$$\phi_d = 0.01609 \text{ mm}^{-1},$$

and the powers for the second refractive-diffractive doublet are

$$\phi_r = 0.12807 \text{ mm}^{-1}$$

$$\phi_d = 0.00741 \text{ mm}^{-1}.$$

After this initial design was completed, the constructional parameters were adjusted to maintain the correct first order values, such as total focal length and chief-ray exiting angle (telecentric condition). This design became the starting point for further optimizations and other designs.

Since one of the most important benefits of diffractive optics is in color correction and since lateral color is an important issue in eyepiece design, it seemed appropriate to first correct lateral color as best as possible without seriously aggravating other aberrations. Secondly, the refractive surface curvatures were bent to optimally flatten the sagittal field. As was indicated in Section 3.2.1, little can be done to reduce the amount of Petzval field curvature in eyepieces due to their relatively short focal lengths, so lens designers try to flatten the sagittal field curvature and allow the tangential field to curve rearward. This naturally has to be balanced against a strongly backward curved tangential field. By optimizing various configurations of the elements, while maintaining the initial constraints, some designs with reduced field curvature and well-corrected lateral color were found. The aspheric terms in one of the diffractive lenses were used to reduce the amounts of pupil spherical aberration and distortion, and to further flatten the sagittal image field. There were trade-offs involved in which the monochromatic aberration correction was very excellent, but the chromatic aberrations were too strong.

Several different lens configurations were investigated. The result of trying several forms and optimizing upon several variables, such as refractive curvatures, diffractive powers, and airspace thicknesses, is the lens shown in Fig. 3.3.1.

Several features and performance characteristics of this lens are described in Tables 3.3.2 - 3.3.3 and in Figs. 3.3.6 - 3.3.11 at the end of this chapter. In further comparisons this lens will be referred to as Hybrid Wide-Angle Diffractive-Refractive Eyepiece No. 1.

The diffractive element nearest the aperture stop has a focal length equal to $18F$, where F is the focal length of the overall eyepiece. The second diffractive lens has a focal length equal to $37F$. Fourth and sixth order aspheric terms in the first diffractive element are used to control aberrations. Notice that the center element is equi-convex. This element was constrained to have equal curvatures to decrease fabrication costs. It seemed that in designing the lens there were enough degrees of freedom to allow for that.

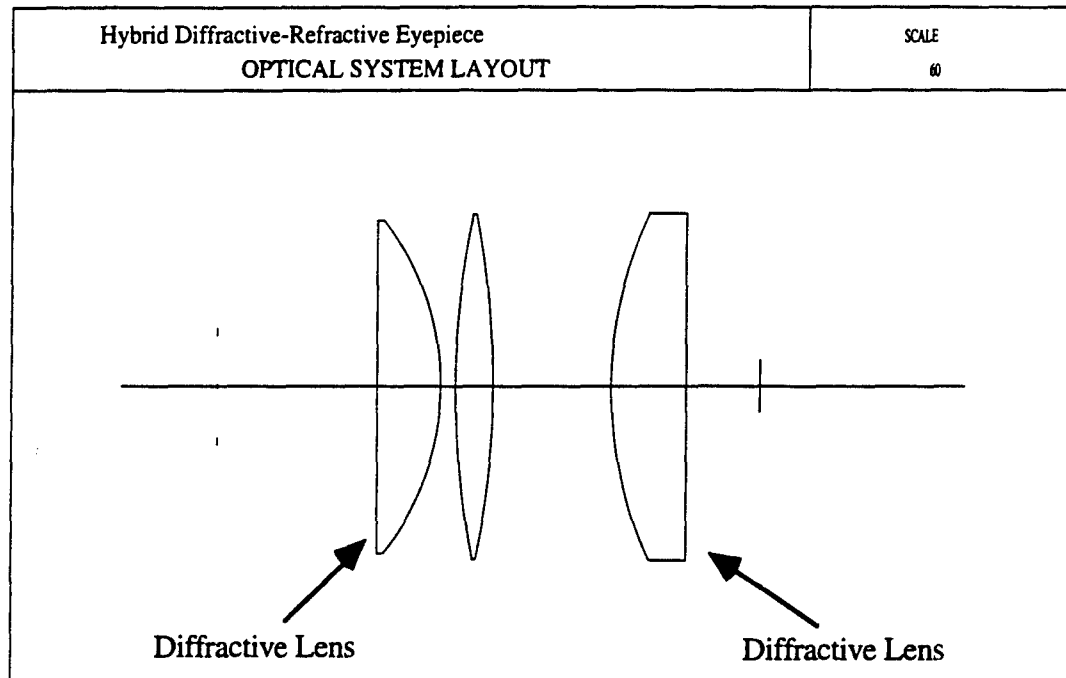


Fig. 3.3.1. Wide-angle, hybrid diffractive-refractive eyepiece. The eyepiece consists of two diffractive elements and three refractive elements. The aperture stop is indicated to the left of the lens by a broken line crossing the axis; the image plane is indicated to the right of the lens by a solid hatch mark across the axis.

By allowing the airspaces to vary and optimizing the lens performance with a computer, a similar design was developed, which is presented below in Fig. 3.3.2. Note that in all the designs, the center thicknesses of the refractive elements are

approximately equal. The center thicknesses of refractive elements typically are not useful variables while the elements still remain thin.

Several features and performance characteristics of this lens are described in Tables 3.3.4 - 3.3.5 and in Figs. 3.3.6 - 3.3.11. In further comparisons this lens will be referred to as Hybrid Diffractive-Refractive Eyepiece No. 2. This design configuration was quite similar to the design in Fig. 3.3.1. The key difference between this lens and the last (Fig. 3.3.1) is that the airspaces between the elements are reduced which allows for a more compact system.

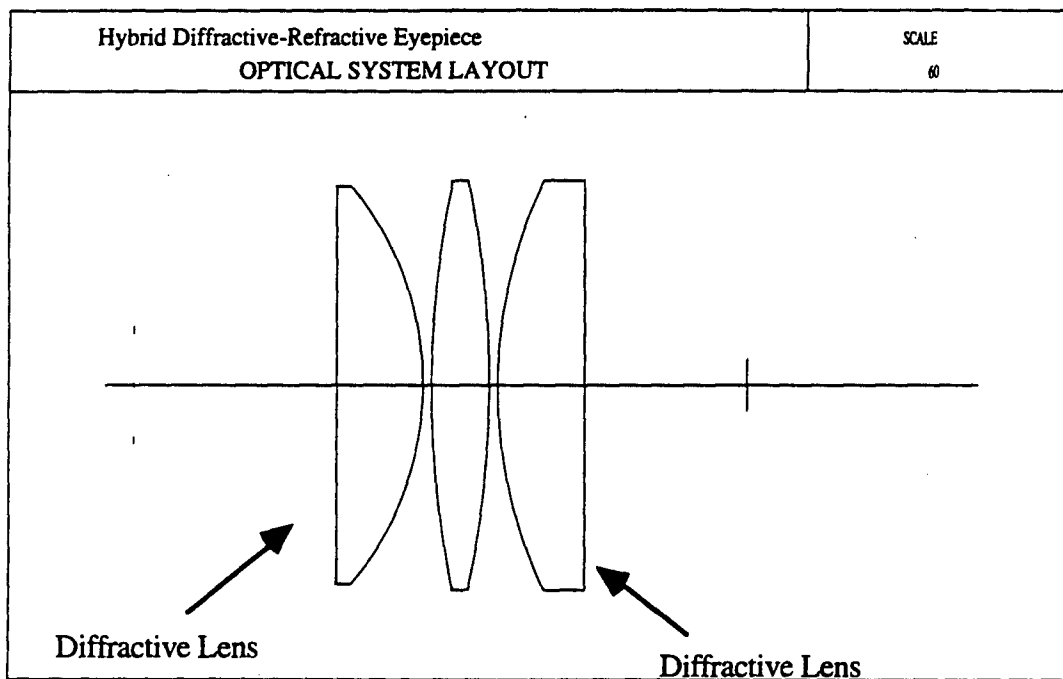


Fig. 3.3.2. Wide-angle, hybrid diffractive-refractive eyepiece. The eyepiece consists of two diffractive elements and three refractive elements. The aperture stop is indicated to the left of the lens by a broken line crossing the axis; the image plane is indicated to the right of the lens by a solid hatch mark across the axis.

Both of the previous designs have exceptional performance and have significant weight and size reductions in comparison to the Erfle, but they each have a potential

drawback. In each of these designs there is a diffractive element that is 'external' to the system. For example if the eyepiece were to be used in a telescope, the diffractive lens near the image plane would be environmentally protected and essentially would be 'internal' to the system. On the other hand the element nearest the eye would be on the outside of the system, and performance degradation may occur as a result of certain environmental conditions. For instance, dust and dirt may get trapped within the groove spacings or the surface may get scratched. These conditions can significantly reduce the performance of the diffractive element. So alternate solutions were investigated in an attempt to avoid this situation.

The next attempted configuration is similar to the design shown in Fig. 3.3.1 with the difference that the first hybrid doublet is flipped back-to-front. This design is depicted in Fig. 3.3.3.

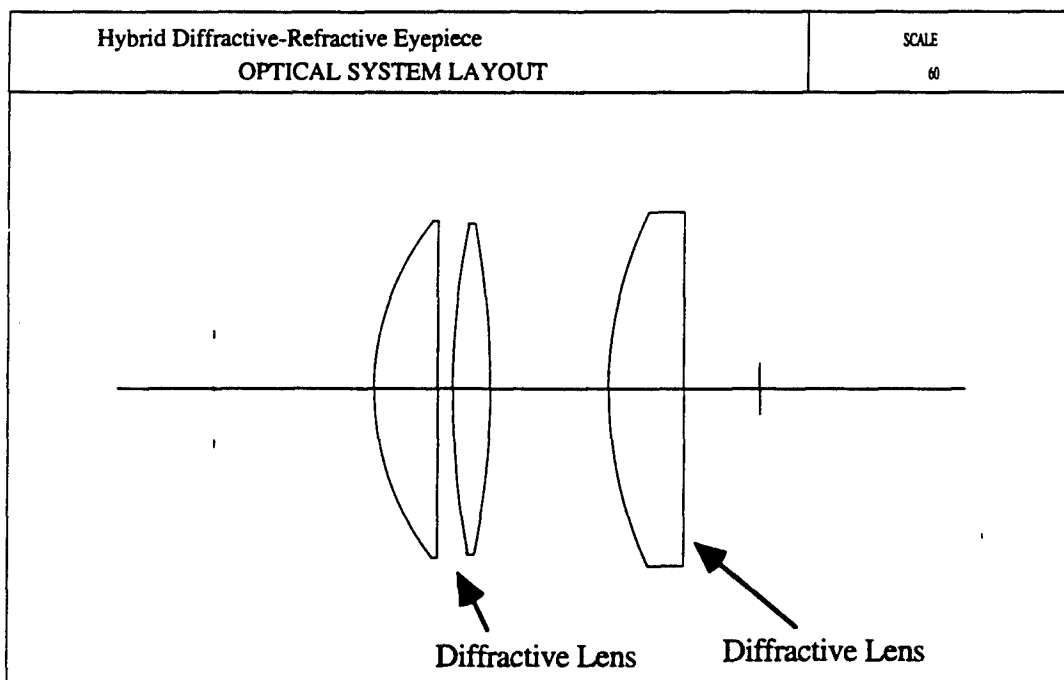


Fig. 3.3.3. Wide-angle, hybrid diffractive-refractive eyepiece. The eyepiece consists of two diffractive elements and three refractive elements. The aperture stop is indicated to the left of the lens by a broken line crossing the axis; the image plane is indicated to the right of the lens by a solid hatch mark across the axis.

The performance of this eyepiece is significantly worse than that of the two previous designs, even after optimizing the curvature of the first refractive element and the power of the diffractive element. This design had reduced performance in terms of distortion, astigmatism, and pupil spherical aberration. Even with the use of the higher order terms in the phase function of the diffractive element, the aberrations induced by this configuration could not be corrected. This discovery was not surprising. In certain systems which exploit symmetry about an internal aperture stop, some of the surfaces are curved concave toward the stop. This symmetrical configuration minimizes the angle of incidence of the chief ray, and thus reduces certain aberrations. In the design shown in Fig. 3.3.3, the converse is occurring, the chief ray angles of incidence are increased at the first surface.

In this type of wide-angle, hybrid eyepiece system not only is there no internal stop, but also there are not many surface curvatures and glass-index boundaries to use as design variables. Therefore every parameter is critical in terms of aberration correction. Assuming the diffractive element is mounted on a plane side of any of the refractive elements, the specific refractive component of a given hybrid doublet has two possible shapes (with respect to the aperture stop location) : plano-convex and convex-plano. The shape of the element can drastically affect the aberration correction. The first shape option – with the planar side facing the aperture stop – naturally minimizes the angle of incidence of the chief ray, whereas the second shape – the convex side facing the aperture stop – increases this angle, and thus aggravates the field aberration correction. It would seem likely that the second option would reduce the axial aberrations, such as spherical aberration and longitudinal color. That was the actual result in this case, but the contributions to the field aberrations of this element were much stronger than the reductions of the axial aberrations. One reason for this is that

the surface intersection heights of the chief ray at this doublet lens are much larger than those of the marginal ray.

With this understanding, a few degrees of freedom in the choice of surface curvatures became essentially fixed or solved (not necessarily exactly, but at least in shape). Based on the description from the previous paragraph, the first curvature, i.e. the surface facing the aperture stop, was fixed to have a radius = ∞ . The second curvature was fixed to be convex; note that a concave surface would lead to a negatively powered lens, thus violating one of the initial criteria. An alternative to placing the diffractive surface on the plano-convex element was to place it on a planar substrate in front of the first lens (like a cover window). This achieved satisfactory results. Of course in this configuration an additional element is essentially introduced, which violates an initial constraint - that is, to limit the design to the number of refractive elements to three. Furthermore this design configuration obviously reduces the eye relief by at least the amount of the planar element.

Examining the shapes of the other two elements, it makes sense that if one surface of the four is to have a curvature = 0, then it ought to be the one nearest the internal image. The reason for this is the same as that for shape and configuration of the first hybrid doublet described above, except that in this case the roles of the marginal and chief rays and the roles of the internal image location and the aperture stop location are interchanged. To minimize the angle of incidence of the marginal ray, the best shape for the third element is convex-plano (plane side facing the internal image). [Lens design note : this configuration is the same as it would be for an objective singlet lens imaging an object at infinity.]

The middle element remains as the only element without a specific shape. By altering the shape from bi-convex to a meniscus shape does little to improve the eyepiece performance without significantly increasing the thickness of the lens element.

Although using a meniscus shape aided in reducing field curvature, the element tended to become weaker and thus distributed more power to the other elements in order to compensate for its weakness.

The last degrees of freedom are the airspaces and element center thicknesses. Airspaces are used in investigating other solution forms, while element center thickness is not an effective variable without largely increasing a given element's size and weight.

In each of the previous designs, the powers of the diffractive elements were relatively weak. The strongest element had an f -number of $F/15$. Therefore, designs with a *single*, stronger diffractive element were attempted; this would have the advantage of eliminating one of the two diffractive elements. Of course there is a limiting factor here. As diffractive optical elements are micro-structures with feature sizes on the order of a few wavelengths, fabrication issues and limitations must be considered throughout the design process. The zone spacing at the edge of a diffractive lens usually tends to be the smallest spacing of the lens. For a diffractive lens with paraxial zone spacings, it can be shown that the zone spacing at the edge is given approximately by

$$r_j - r_{j-1} \cong 2\lambda(F/\#), \quad (3.3.3)$$

where r_j is the radius of the j^{th} zone, λ is the illuminating center wavelength, and $F/\#$ is the focal ratio of the diffractive lens. Zone spacings of less than $10\mu\text{m}$ start to become difficult to fabricate, especially in terms of maintaining reasonable design tolerances. Furthermore the diffraction efficiency at zone spacings around this region can no longer adequately be described by scalar theory, and the diffraction efficiency varies across the aperture.¹⁵ Therefore as discussed in Chapter 2, for visible applications, i.e. center wavelengths of about 500 nm, diffractive lenses with f -numbers of 10 and higher are much more desirable than 'faster' diffractive lenses, both in terms of high diffraction efficiency and of ease in lens fabrication.

In eliminating one diffractive element from the prior design configurations and simultaneously trying to eliminate the 'external' diffractive surface, it seems logical from the above descriptions that a suitable place for the diffractive lens is on the surface nearest the internal image plane. Therefore the refractive element substrate essentially has a fixed shape, convex-plano (planar side facing the internal image location). That being the case the shapes of the other two elements remain as variables.

The initial idea of this type of eyepiece design was to design the front two elements to be positive, meniscus-shaped elements, concave toward the eye. In this configuration the chief ray incident angles would be minimized at the surfaces. It seemed plausible to use these first two elements to adequately correct certain field aberrations, and to use the hybrid doublet to correct color and residual spherical aberration. This design configuration did yield some of the expected results. The Petzval field curvature and spherical aberration of the pupil were significantly reduced from the previous hybrid designs. On the other hand, astigmatism, spherical, coma, and distortion were increased from the amounts in prior designs. With the front two elements having meniscus shapes (concave toward the eye), undercorrected astigmatism was introduced into the design. This design is shown in Fig. 3.3.4.

It appeared that, with this design, the distribution of design variables to correct certain aberrations was not the optimum. It appeared that the hybrid doublet held a larger role in reducing field aberrations than initially anticipated, and that the front meniscus element could be used to maintain the necessary eye relief.

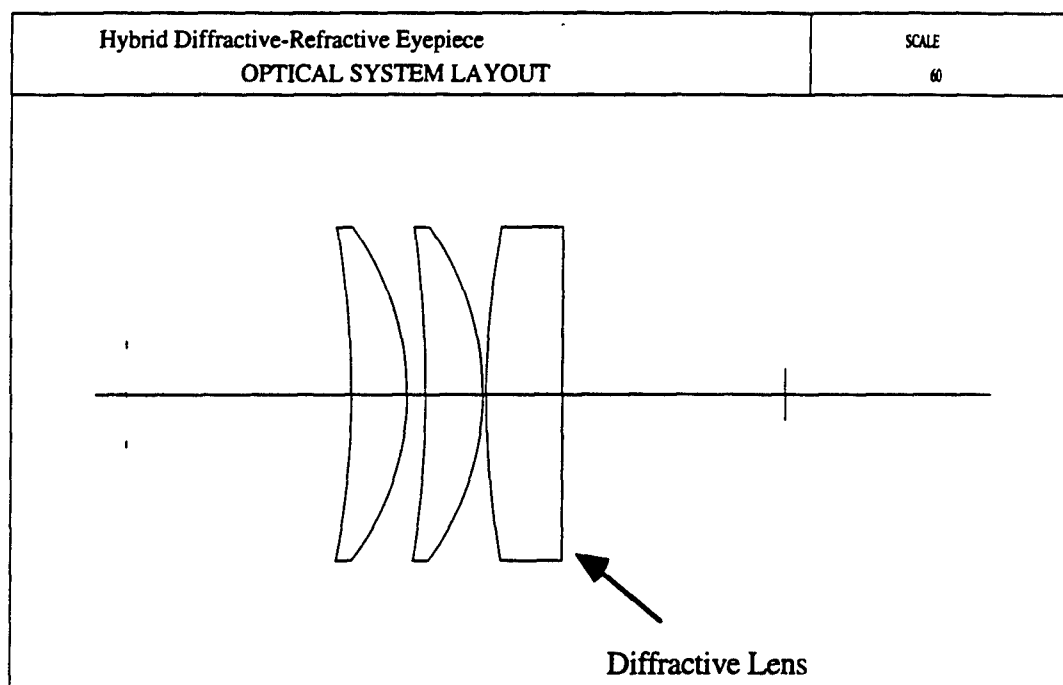


Fig. 3.3.4. Wide-angle, hybrid diffractive-refractive eyepiece. The eyepiece consists of one diffractive element and three refractive elements. The aperture stop is indicated to the left of the lens by a broken line crossing the axis; the image plane is indicated to the right of the lens by a solid hatch mark across the axis.

To control the residual aberrations, an optimum form was found. The first element of the design was a meniscus refractive element, concave toward the eye, and the middle element was bi-convex with the stronger curvature convex toward the internal image plane. The third element maintained the same shape as in the previous design. Reducing the airspaces between the elements also helped to reduce the aberrations. The decreased airspaces also makes the design more compact. By optimizing on various starting points for this design, very similar configurations were found each time. A fourth order aspheric term in the diffractive element was used to add overcorrected astigmatism, to reduce distortion, and to reduce the spherical aberration of the exit pupil. A fragile balance was found between adequately correcting

the monochromatic and chromatic aberrations. As the fourth order aspheric term was used to correct distortion, astigmatism, and pupil spherical aberrations, a change in the term would often quickly throw the lateral color to large values during the optimization process. A compromise was found and the design is shown in Fig. 3.3.5.

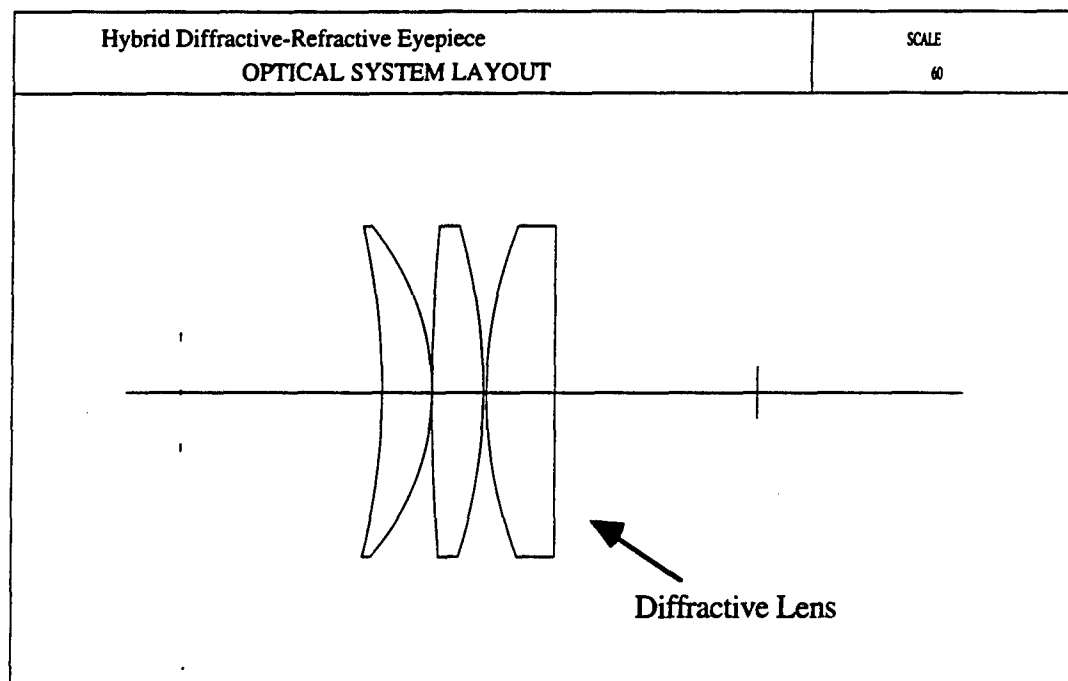


Fig. 3.3.5. Wide-angle, hybrid diffractive-refractive eyepiece. The eyepiece consists of one diffractive element and three refractive elements. The aperture stop is indicated to the left of the lens by a broken line crossing the axis; the image plane is indicated to the right of the lens by a solid hatch mark across the axis.

Several features and performance characteristics of this lens are described in the following section in Tables 3.3.4 - 3.3.5 and in Figs. 3.3.6 - 3.3.11. In further comparisons this lens will be referred to as Hybrid Diffractive-Refractive Eyepiece No. 3. The power of the diffractive element is $13F$, where F is the total focal length of the eyepiece. The f -number is $F/10$.

In many ways, this design was the best eyepiece yet. As is shown in the following section, this eyepiece design exhibits many improvements in comparison to the Erfle eyepiece. Most notably, this hybrid eyepiece is almost 50% more compact than the Erfle eyepiece, while having a longer eye relief, reduced distortion, and reduced pupil spherical aberration, along with having other beneficial features.

The lens design prescription data for the two hybrid eyepieces depicted in Figs. 3.3.2 and 3.3.5 are listed in Tables 3.3.2 and 3.3.3, respectively. (These two eyepieces offer the best performance of the hybrid eyepieces.) The curvatures of the refractive elements of these hybrid designs are significantly less than those of the Erfle eyepiece. Furthermore, with the use of diffractive elements in the design, the necessity for exotic glass use has been eliminated. In the hybrid eyepieces, only common glasses were used. The eyepiece in Fig. 3.3.2 was comprised of BK-7 and BAK-2; the eyepiece shown in Fig. 3.3.5 was comprised entirely of BK-7. The phase coefficients supplied for the diffractive lens correspond to the coefficients in Eq. (2.3.3).

Surface	Radius (mm)	Thickness (mm)	Glass	Semi-diam (mm)
		15.81185		
1*	0	6.77651	BAK2	15.5
2	-24.17843	0.67765		15.5
3	78.01601	4.51767	BK7	16.0
4	-78.01601	0.67765		16.0
5	36.92287	6.83163	BAK2	16.0
6*	0			16.0
*diffractive lens 1 phase coefficients		$s_1 = -0.0011802$	$s_2 = 2.789686e-6$	
*diffractive lens 2 phase coefficients		$s_1 = -5.789915e-4$		

Table 3.3.2. Lens prescription data for hybrid eyepiece depicted in Fig. 3.3.2.

Surface	Radius (mm)	Thickness (mm)	Glass	Semi-diam (mm)
1	-54.09807	3.92929	BK7	12.8
2	-19.42586	0.1		12.8
3	157.28572	4.03694	BK7	13.0
4	-43.01555	0.24401		13.0
5	34.97115	5.38258	BK7	13.0
6*	0			13.0
*diffractive lens phase coefficients		$s_1 = -0.001945$	$s_2 = 4.121263e-6$	

Table 3.3.3. Lens prescription data for hybrid eyepiece depicted in Fig. 3.3.5.

3.3.4. Comparisons and Results

The following tables describe comparisons of the Erfle eyepiece with three of the hybrid diffractive-refractive eyepieces described in Section 3.3.3., namely those in Figs. 3.3.1, 3.3.2, and 3.3.5.

Eyepiece	Petzval radius/FL	OAL/FL	ER/FL	BFL/FL
Erfle Eyepiece	-1.51614	1.480	0.584	0.457
Hybrid Eyepiece 1	-1.35247	1.248	0.643	0.298
Hybrid Eyepiece 2	-1.52800	0.974	0.791	0.638
Hybrid Eyepiece 3	-1.60900	0.680	0.789	0.794

Table 3.3.4. Characteristics and performance features for four eyepieces, the Erfle eyepiece, Wide-angle Hybrid Diffractive-Refractive Eyepiece No. 1 in Fig. 3.3.1, Wide-angle Hybrid Diffractive-Refractive Eyepiece No. 2 in Fig. 3.3.2, Wide-angle Hybrid Diffractive-Refractive Eyepiece No. 3 in Fig. 3.3.5. The ratio of the Petzval field radius to the eyepiece focal length (FL), the ratio of the overall length –first physical surface to last surface– (OAL) to the eyepiece focal length, the ratio of eye relief (ER) to the eyepiece focal length, and the ratio of the back focal length (BFL) to the eyepiece focal length are shown.

Eyepiece	Weight
Erfle eyepiece	1.00
Hybrid Eyepiece 1	0.44
Hybrid Eyepiece 2	0.61
Hybrid Eyepiece 3	0.31

Table 3.3.5. Comparison of weights of three of the hybrid, wide-angle eyepieces with the Erfle eyepiece. Values are normalized to the weight of one Erfle eyepiece.

In Figs. 3.3.6 through 3.3.11, several plots of performance characteristics are shown. These plots include comparisons of percent distortion, field curvature, lateral color, longitudinal pupil spherical aberration, and polychromatic transverse ray error plots for three field points. The plots were generated for all four eyepieces scaled to the same focal length, f -number, and field-of-view. The focal lengths were scaled to unity, the f -number was opened to $F/2.5$, and the full field-of-view was sixty degrees. Note that in Fig. 3.3.6 the sign of distortion flips when rays are traced from long conjugate to short conjugate.

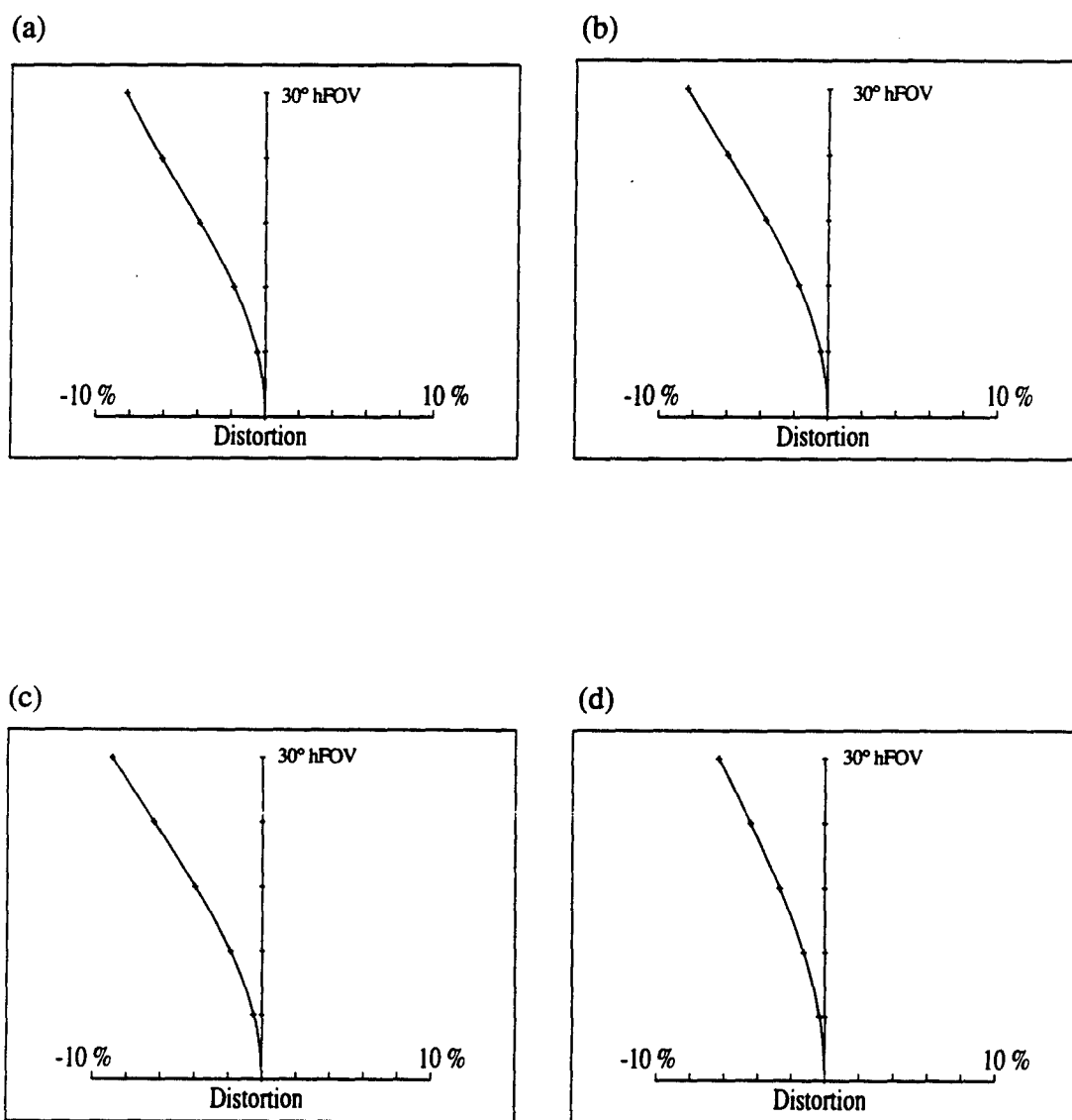


Fig. 3.3.6. Percent distortion plots for four eyepieces. (a) The 5-element Erfle eyepiece, (b) wide-angle hybrid diffractive-refractive eyepiece 1 (Fig. 3.3.1), (c) wide-angle hybrid diffractive-refractive eyepiece 2 (Fig. 3.3.2), (d) wide-angle hybrid diffractive-refractive eyepiece 3 (Fig. 3.3.5). All four eyepiece designs have a focal length of unity, have an entrance pupil diameter of $0.40F$, and a 60° FOV.

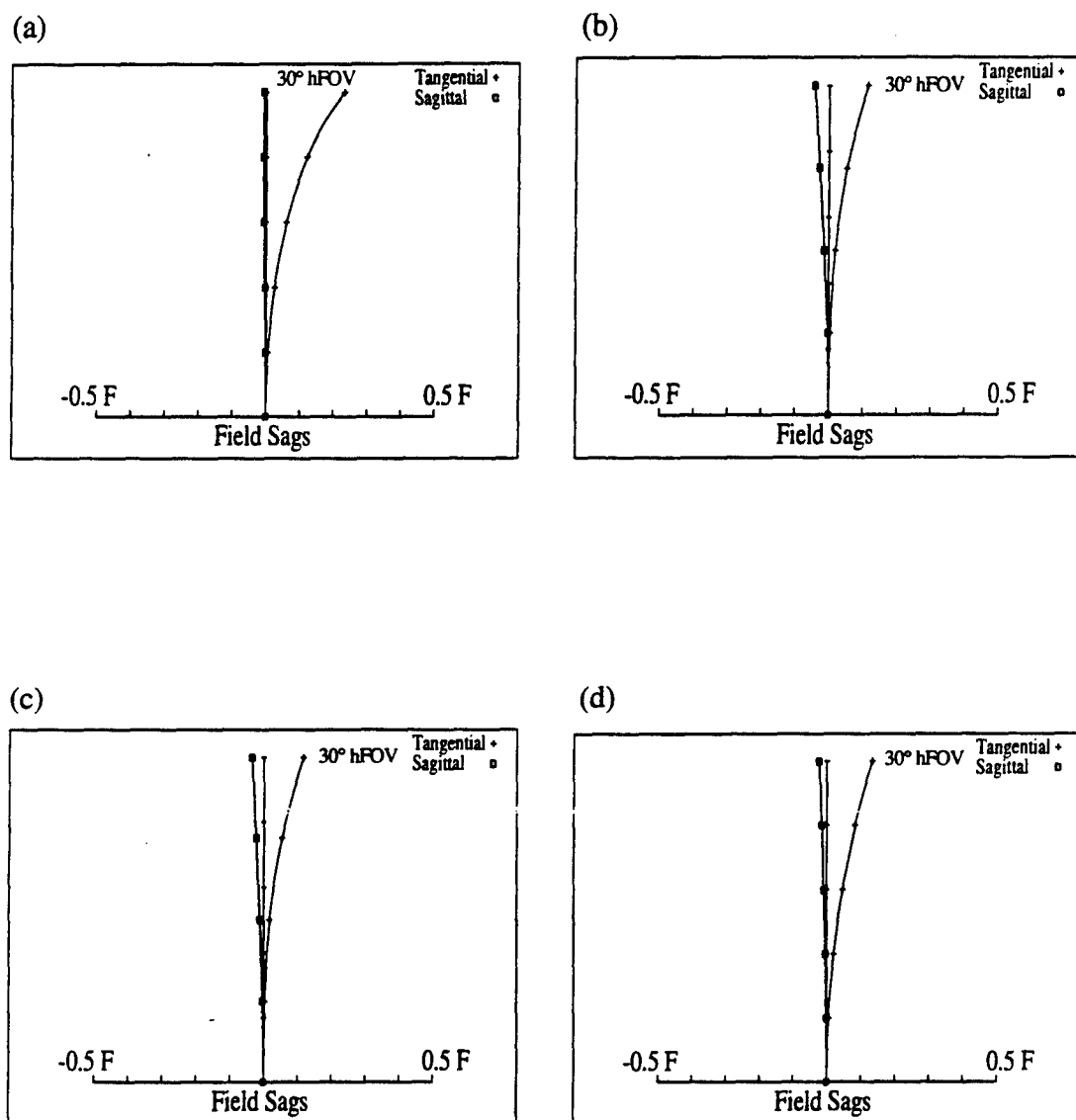


Fig. 3.3.7. Field sags plots for four eyepieces. (a) The 5-element Erfle eyepiece, (b) wide-angle hybrid diffractive-refractive eyepiece 1 (Fig. 3.3.1), (c) wide-angle hybrid diffractive-refractive eyepiece 2 (Fig. 3.3.2), (d) wide-angle hybrid diffractive-refractive eyepiece 3 (Fig. 3.3.5). All four eyepiece designs have a focal length of unity, have an entrance pupil diameter of $0.40F$, and a 60° FOV.

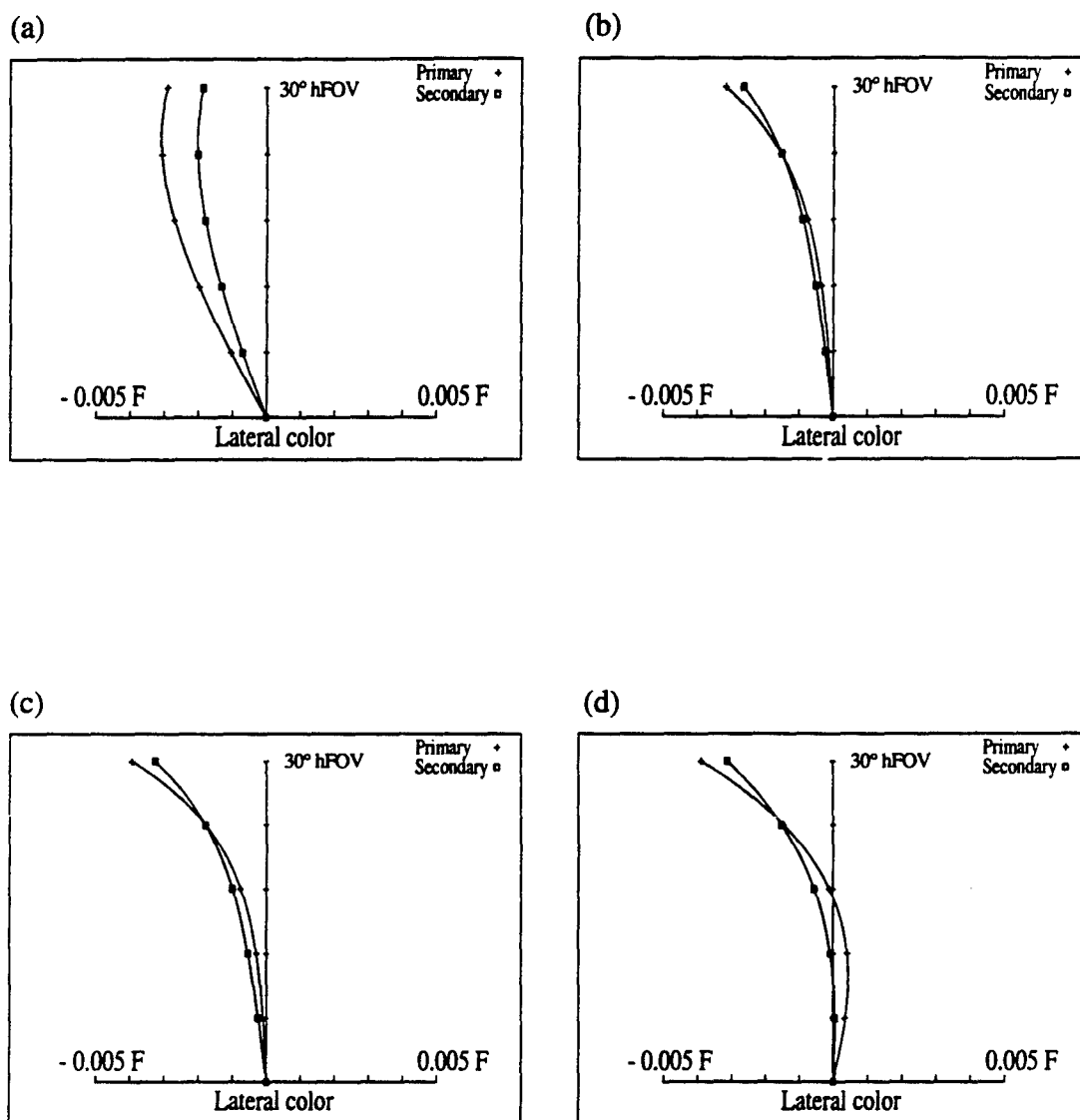


Fig. 3.3.8. Primary and secondary lateral color plots for four eyepieces. (a) The 5-element Erfle eyepiece, (b) wide-angle hybrid diffractive-refractive eyepiece 1 (Fig. 3.3.1), (c) wide-angle hybrid diffractive-refractive eyepiece 2 (Fig. 3.3.2), (d) wide-angle hybrid diffractive-refractive eyepiece 3 (Fig. 3.3.5). All four eyepiece designs have a focal length of unity, have an entrance pupil diameter of $0.40F$, and a 60° FOV.

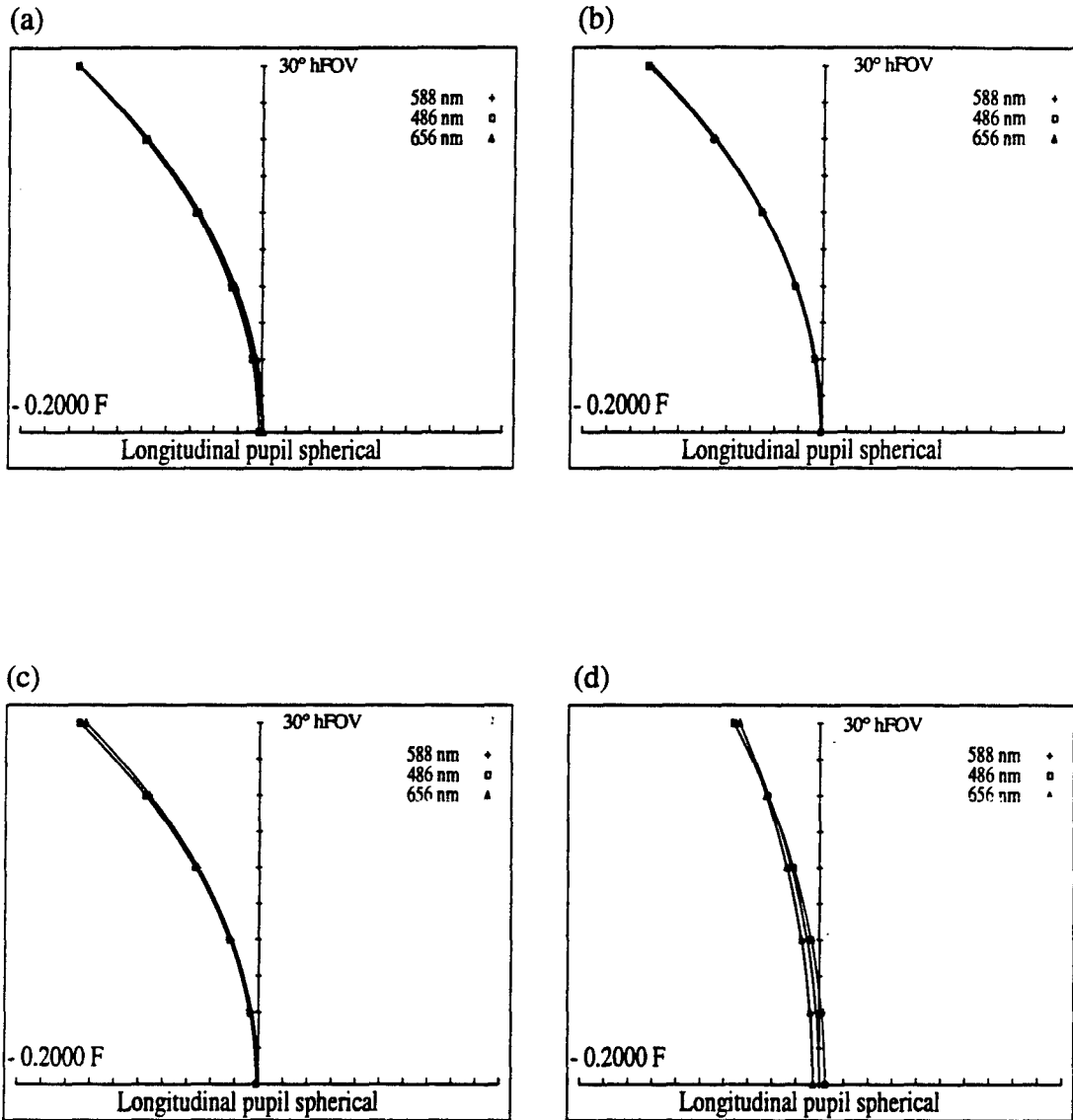


Fig. 3.3.9. Longitudinal spherical aberration of the pupil (for three wavelengths) plots for four eyepieces. (a) The 5-element Erfle eyepiece, (b) wide-angle hybrid diffractive-refractive eyepiece 1 (Fig. 3.3.1), (c) wide-angle hybrid diffractive-refractive eyepiece 2 (Fig. 3.3.2), (d) wide-angle hybrid diffractive-refractive eyepiece 3 (Fig. 3.3.5). All four eyepiece designs have a focal length of unity, have an entrance pupil diameter of $0.40F$, and a 60° FOV.

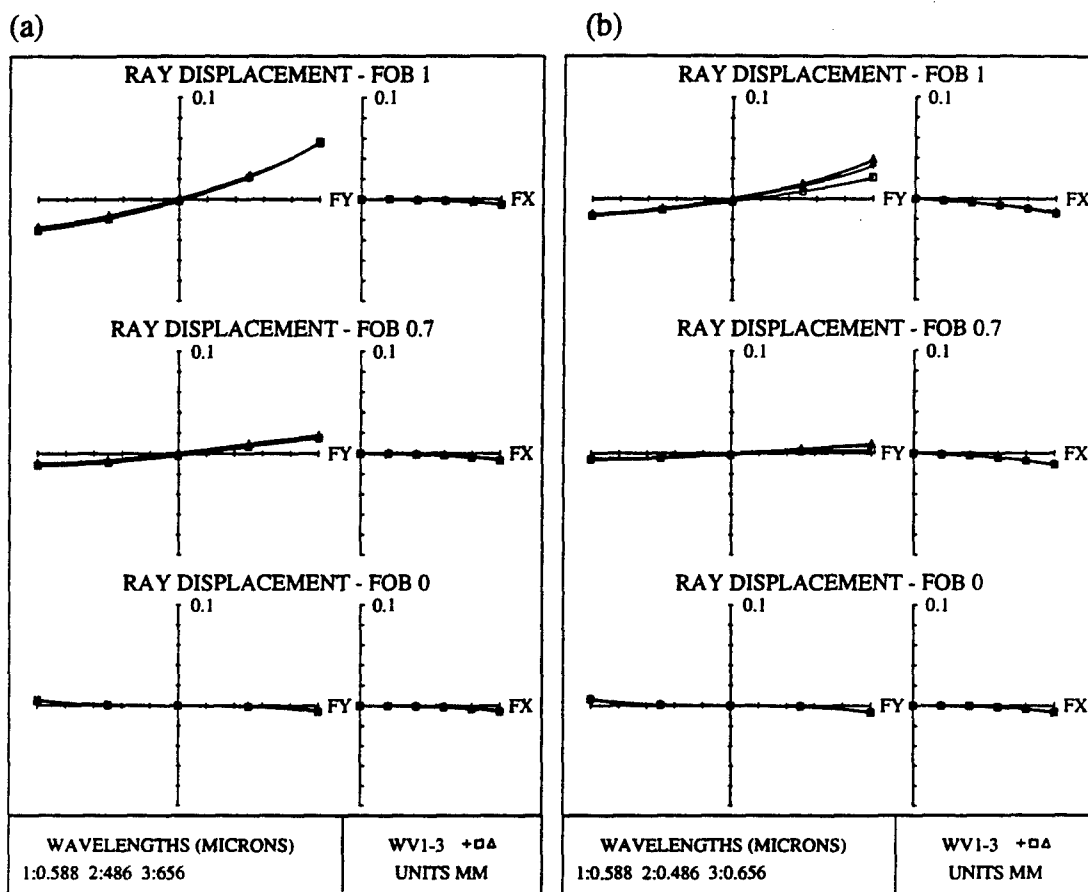


Fig. 3.3.10. Transverse ray aberration plots for two eyepieces. (a) The five-element Erfle eyepiece, (b) wide-angle hybrid diffractive-refractive eyepiece 1 (Fig. 3.3.1) Both eyepiece designs have a focal length of unity, have an entrance pupil diameter of $0.40F$, and a 60° FOV.

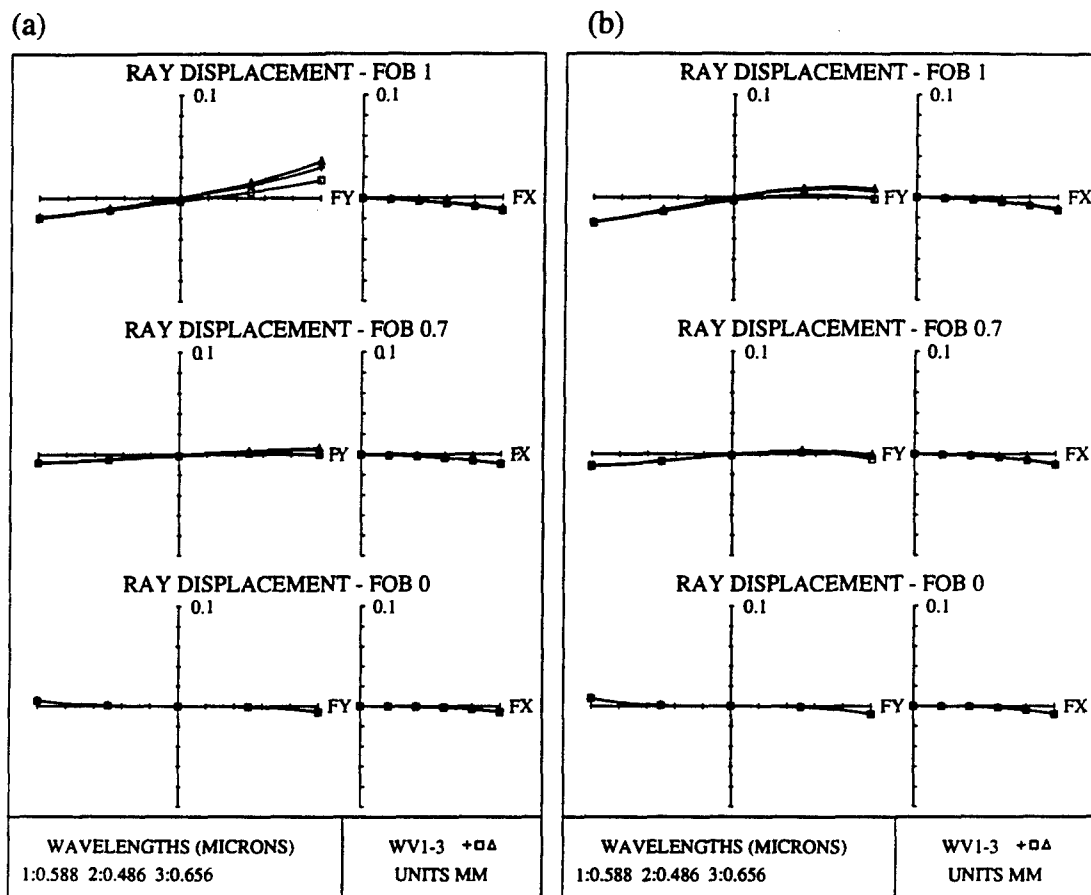


Fig. 3.3.11. Transverse ray aberration plots for two eyepieces. (a) Wide-angle hybrid diffractive-refractive eyepiece 2 (Fig. 3.3.2), (b) wide-angle hybrid diffractive-refractive eyepiece 3 (Fig. 3.3.5) Both eyepiece designs have a focal length of unity, have an entrance pupil diameter of $0.40F$, and a 60° FOV.

3.4. Summary of Chapter 3

There are many difficulties in designing wide-field eyepieces, and often as a result they become the limiting factors in the performance of visual instruments. By increasing the eye relief, while maintaining a constant field-angle, the diameters of the elements rapidly increase and aberration correction of an eyepiece can be aggravated. Also, by increasing the field-angle and maintaining the level of aberration correction, the eye relief decreases. Furthermore the lack of chief ray symmetry about the stop, which is due to the requirement for an external aperture stop, makes the correction of certain field aberrations such as distortion, lateral color, and pupil spherical aberration quite difficult. For these reasons, conventional eyepieces that are well-corrected over large field-angles are comprised of many elements and often are heavy and bulky. These physical constraints can limit their use in certain applications, and optical performance may be sacrificed to satisfy physical requirements.

Diffractive optics, when combined with refractive elements, offers new solutions for wide-field eyepieces. In Section 3.3, several hybrid, refractive-diffractive eyepieces were presented which offer performance at least equivalent to the 5-element Erfle eyepiece. These hybrid eyepieces weigh considerably less than the Erfle eyepiece, and some of the hybrid eyepieces are also considerably more compact than the Erfle design.

With an effective dispersion that is negative and many times stronger than that of ordinary glass, diffractive lenses have been used to correct the chromatic aberrations in these eyepieces while significantly reducing the weight of the entire eyepiece system. Also the index boundaries in conventional eyepieces are used to correct aberrations such as astigmatism and spherical aberration, but yield the drawback that these surfaces

also introduce chromatic variations of other aberrations such as distortion. In the hybrid eyepieces presented in Chapter 3, this index-boundary tool was not available, and therefore it does not contribute to chromatic variations of aberrations. An aspheric profile was included in the phase functions of several of the diffractive lenses in the hybrid eyepieces. Aspheric surfaces have been used in all-refractive eyepieces as a method to reduce some aberrations that are otherwise difficult to control and reduce. With a diffractive lens, adding an aspheric profile does not generally increase the difficulty of its fabrication, unlike with the fabrication of a refractive lens. The diffractive lenses containing the aspherics greatly reduce the pupil spherical aberration and distortion of the eyepieces, and these elements also aid in flattening the sagittal field.

All of the hybrid eyepiece designs comprise three refractive elements, which is two less than the Erfle. One of the designs weighed approximately 70% than the Erfle eyepiece. The reported weight reductions do not include the effects of the weight reductions due to the eyepiece mounts.

3.5. References for Chapter 3

1. R. Kingslake, *Lens Design Fundamentals* (Academic Press, New York, 1978), pp.335-343.
2. W. J. Smith, *Modern Optical Engineering Second Ed.* (McGraw-Hill, Inc., New York, 1990), pp. 403-408.
3. S. Rosin, *Applied Optics and Optical Engineering, Vol. III Optical Components*, R. Kingslake, ed. (Academic Press, Inc., New York, 1965), ch. 9, pp. 337-344.
4. W. J. Smith, *Modern Lens Design* (McGraw-Hill, Inc., New York, 1992), pp. 87-89.
5. *Optical Design-Military Standardization Handbook MIL-HDBK-141* (Defense Supply Agency, Washington, D.C., 1962), pp. 4-1 - 4-3.
6. A. Cox, *A System of Optical Design* (Focal Press , New York, 1964), pp. 443-447.
7. Ref. 6, pp.14-4 - 14-20.
8. W. C. Sweatt, "Describing holographic optical elements as lenses," J. Opt. Soc. Am. **67**, 803-808 (1977).
9. D. A. Buralli, G. M. Morris, and J. R. Rogers, "Optical performance of holographic kinoforms," Appl. Opt. **28**, 976-983 (1989).
10. W. A. Kleinhans, "Aberrations of curved zone plates and fresnel lenses," Appl. Opt. **16**, 1701-1704 (1977).
11. T. W. Stone, "Hybrid diffractive-refractive telescope," in *Practical Holography IV*, Stephen A. Benton, ed. Proc. SPIE, **1212**, 257-266 (1990).
12. S. J. Bennett, "Achromatic combinations of hologram optical elements," Appl. Opt. **15**, 542-545 (1976).
13. H. Erfle, U.S. Patent no. 1,478,704 (25 December 1923).
14. See for example Ref. 1, pp. 77 - 80.
15. D. A. Buralli, G. M. Morris, "Effects of diffraction efficiency on the modulation transfer function of diffractive lenses," Appl. Opt. **31**, 4389-4396 (1992).

4. Hybrid Diffractive-Refractive Binoculars

4.1. Introduction

A common wide-field, visual instrument is a set of binoculars. The key difference compared to monocular devices is depth perception.¹ With the use of binoculars, a user can view two or more objects within his or her field-of-view in which each object has a different convergence angle at the user's two eyes. The difference in convergence angles signals the user's brain that the objects are located at different distances. Binocular instruments have several applications including military systems, surveillance instruments, medical optics, and sports optics. In many such applications cost and weight are important factors. For example, head-mounted binocular devices and standard hand-held binoculars, which are held at the eye position for prolonged use, can cause neck or shoulder strain in the user. For these reasons, a set of binoculars was chosen as a good application and demonstration of the wide-field, diffractive-refractive eyepieces described in Chapter Three. Furthermore, binoculars are typically used in broadband illumination. Therefore, this application will yield a good test of diffractive optics in broadband usage where the human eye is the final judge of performance. This chapter discusses the application of a hybrid diffractive-refractive, wide-angle eyepiece to a pair of binoculars. Theoretical modeling, fabrication, and implementation into an existing conventional set of binoculars is presented.

In a typical set of *high-quality*, wide-field binoculars, the eyepieces may comprise a significant portion of the cost and weight of the device. Wide-field binoculars often employ a doublet objective, consisting of a crown element and a flint

element, and a five- or more- element eyepiece. The Erfle eyepiece is a common wide-field eyepiece for this type of application² and is probably the most widely used wide-field eyepiece.³ In binoculars that employ Erfle or similar multi-element eyepieces, the eyepiece can comprise 40% of the weight of the imaging optics, the other 60% of the weight in the objective. In applications where larger entrance and exit pupils are required, such as night or low-light-level use, the mass of the eyepiece is increased, and weight considerations may become critical. An off-the-shelf pair of Bausch and Lomb 8X40 Legacy Series Binoculars was chosen for usage with the hybrid diffractive-refractive eyepiece.

In Section 4.2, a description of the Bausch and Lomb Legacy 8X40 binoculars, its components, and the performance of the binoculars are presented. A "reverse-engineering" process was performed to characterize the optical system of the binoculars, since a lens prescription was not available from the manufacturer. The design of one of the previously discussed hybrid eyepieces from Section 3.3 is implemented into the Bausch and Lomb binoculars, replacing the all-refractive eyepiece. Several figures of merit are presented to describe the performance of the hybrid diffractive-refractive eyepiece as used in the binoculars. When utilizing diffractive optics in imaging systems, it is necessary to examine the effects of non-unity diffraction efficiency. A diffraction analysis is presented to account for other images resulting from light diffracted into orders other than the design order. The spectral response of the human eye is shown to have a very good match with the diffraction efficiency of a quadratic-blaze diffractive lens having a peak efficiency at $\lambda = 555$ nm, minimizing the effects of light diffracted into the zeroth and second orders. In Section 4.3 fabrication tolerance analyses and fabrication methods are presented, including the design of the opto-mechanical mount for the hybrid eyepiece.

4.2. Design and Analysis of Hybrid Binoculars

4.2.1. Bausch and Lomb Legacy Binoculars

In choosing a suitable pair of binoculars, the only available specifications and characteristics were first order properties and physical dimensions of various sets of binoculars. Obtaining more detailed data required measuring other optical quantities and performance data. The most important criterion that was used in selecting the set of binoculars for this application was the apparent field-of-view, i.e. the field-of-view in eye-space. This can be calculated by multiplying the real field-of-view with the magnifying power of the binoculars. For this reason the Bausch and Lomb 8X40 Legacy binoculars were chosen. This pair is a good compromise of a wide field-of-view instrument and a modest cost. The first order characteristics associated with these binoculars are listed in Table 4.2.1.

entrance pupil diameter	40 mm
magnifying power	8X
field-of-view (object space)	4.2°
apparent field-of-view	34°
weight	24 oz.
length	5.5"

Table 4.2.1. Specification data for the Bausch and Lomb 8X40 Legacy Binoculars.

Neither detailed specifications nor a prescription for the binoculars were available from Bausch and Lomb, therefore a "reverse engineering" procedure was performed to characterize the optical system. This involved measuring all of the physical quantities that make up its lens prescription. Laboratory measurements were

made of the airspaces between the lens elements, the center thicknesses of the individual elements, the outside diameters of the elements, the prism face dimensions, the radii of curvature of the individual lens elements, and the refractive indices of the prisms at three wavelengths with the use of a Pulfrich refractometer. In order to characterize the glass types of the lens elements, two methods were used: comparing the densities of the glasses with known densities of manufactured glasses and comparing the indices of refraction at a specific wavelength with the known indices of refraction of manufactured glasses.⁴ The density of the glass was calculated by measuring the mass of each lens element, and calculating its volume from the measured physical dimensions. The index of refraction was calculated by measuring the optical thickness of each lens component at a given wavelength and comparing it to the physical thickness of each element. The measured quantities were then inputted into an optical design program for analysis. A schematic diagram of the binoculars is shown in Fig. 4.2.1, and specifications for this set are described in the following paragraph.

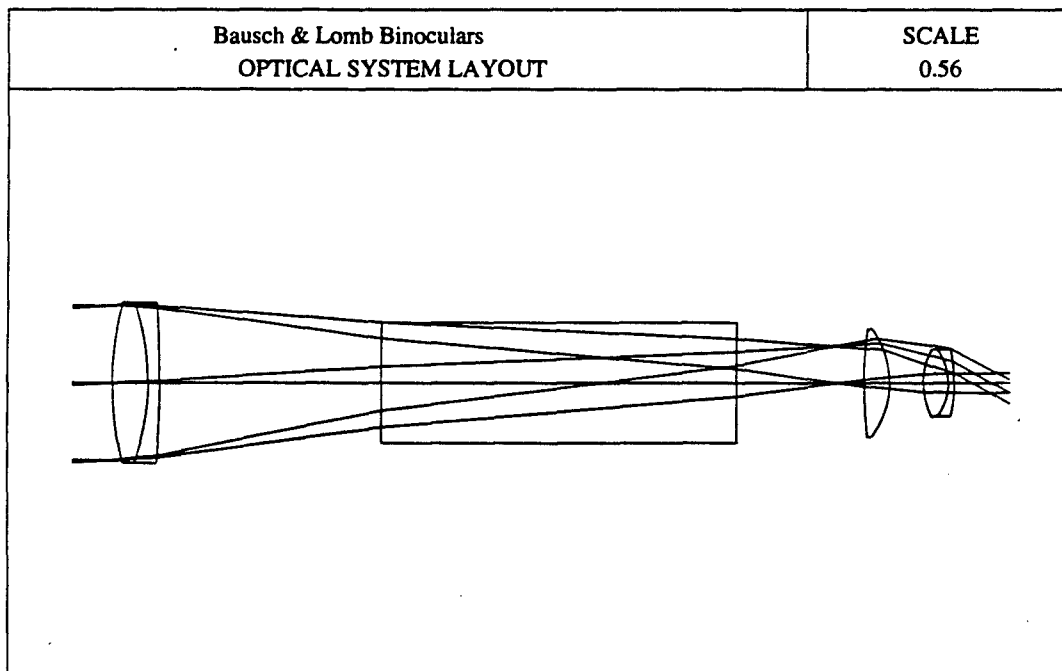


Fig. 4.2.1. The optical layout of the Bausch and Lomb 8X40 Legacy Binoculars.

The objective lens of the binoculars is a doublet comprised of a crown element and a flint element. The focal length of the objective is 150 mm and operates at $f/3.75$. The image inversion and optical folding is provided by two porro prisms made of BAK4. The unfolded optical path of the prisms is approximately 92 mm. The eyepiece is similar to a Kellner eyepiece. The focal length of the eyepiece is approximately 19 mm. Further details regarding the eyepiece are presented in the following section.

4.2.2. Binocular Eyepiece

As mentioned in the previous section, the eyepiece of the Legacy binoculars is similar to a Kellner-style eyepiece. The apparent angular field of a Kellner is approximately $\pm 20^\circ$.⁵ It is not uncommon to find binoculars fitted with Kellner eyepieces.⁶ Of course they typically are limited by a short eye relief and a narrow field-of-view. The eyepiece in the Legacy Binoculars is a modified Kellner eyepiece. It accommodates a longer eye relief and a longer back focal length compared to a standard Kellner eyepiece design.⁷ As was shown in Section 3.2.2, the Kellner is a modified two-element eyepiece where one of the elements is replaced by an achromatic doublet.

The performance characteristics of the Legacy eyepiece are shown in Figs. 4.2.2 and 4.2.3. The data are generated with a principal ray angle of 27° . This is a reasonable number based on the amount of vignetting that the Legacy eyepiece exhibits at larger angles. The percent vignetting numbers are discussed below. Most notably, the eyepiece suffers from pupil spherical aberration and lateral color. The distortion values are not atypical for wide-angle eyepieces.

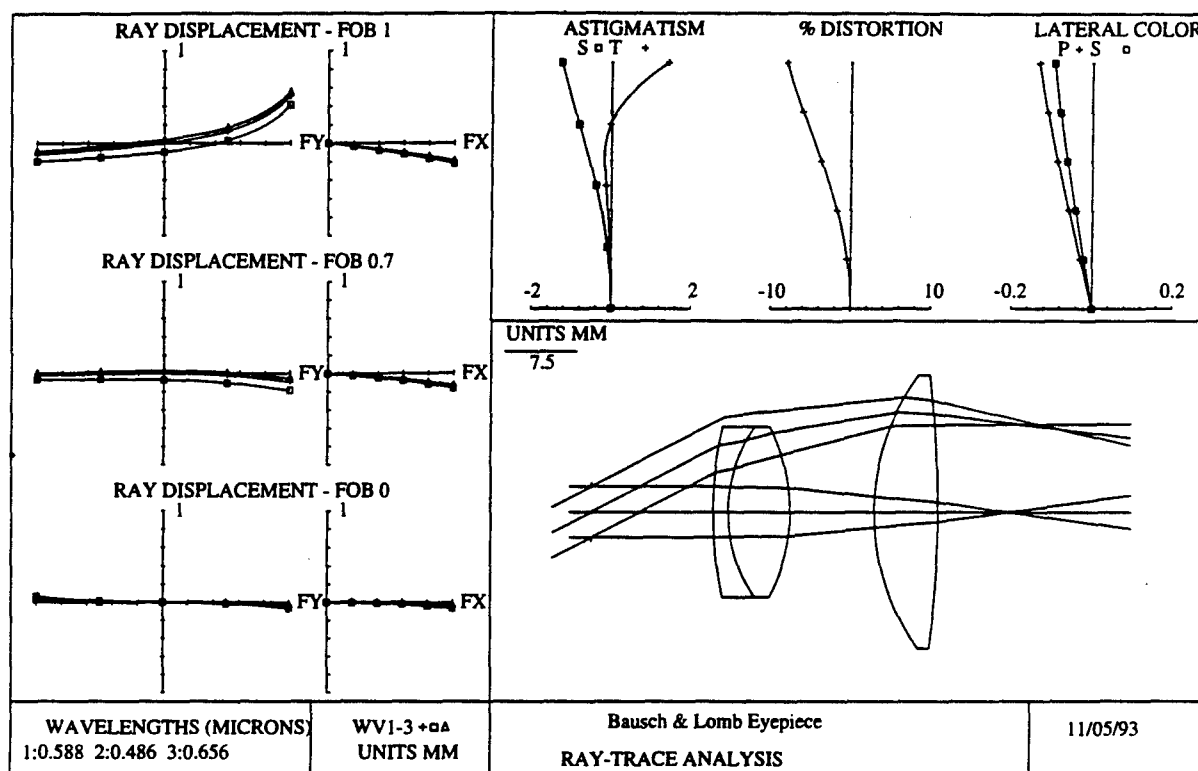


Fig. 4.2.2. The optical layout and performance evaluation curves for the eyepiece modeled from the measured quantities of the Bausch and Lomb 8X40 Legacy Binoculars. Included are transverse ray plots for three field positions, 0.0, 0.7, and 1.0 (where 1.0 refers to 27° hFOV); percent distortion; field curves; and lateral color.

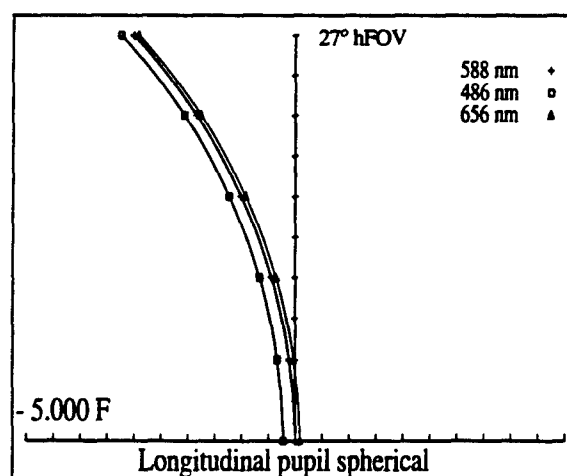


Fig. 4.2.3. Longitudinal pupil spherical aberration of the eyepiece modeled from the measured quantities of the Bausch and Lomb 8X40 Legacy Binoculars. The edge of the field corresponds to 27° hFOV.

Just as the Kellner eyepiece is not designed for wide-angles, the eyepiece shown in Fig. 4.2.1 exhibits significant vignetting at increased field angles. (Note that this eyepiece design is modeled from experimental data of the Bausch and Lomb Legacy 8X40 Binoculars and is not based upon the actual prescription.) For example, the binoculars are specified as being able to accept field angles up to 34° , yet this eyepiece exhibits the following vignetting data:

hFOV	Percent Vignetted
22.5°	0%
25.0°	20%
30.0°	30%
32.7°	35%

Table 4.2.2. Vignetting data for the eyepiece modeled from the measured quantities of the Bausch and Lomb 8X40 Legacy Binoculars.

The Kellner eyepiece is a relatively simple, three-element design. As was discussed in Section 3.2.2 (Fig. 3.2.4), the eyepiece works well out to a half field-of-view of approximately 20° . Beyond that angle, field aberrations become more significant and the performance decreases. Some figures of merit in evaluating the eyepiece are listed in Table 4.2.3 along with the same quantities for a typical Kellner at the same field-of-view. The visual field of the Kellner eyepiece is extremely vignetted at this field angle and was not intended for use at this angle; the data in Table 4.2.3 is reported only for comparison.

Relevant first order quantities	B&L Legacy Eyepiece	Typical Kellner Eyepiece
eye relief	0.66F	0.28F
back focal length	0.4F	0.21F
overall length	1.21F	1.50F
Aberration quantities		
distortion (@ d-line, 588nm)	8%	<5%
paraxial lateral color	-0.168mm	-0.087mm
chromatic variation of paraxial pupil position (486nm - 656 nm)	0.3mm	0.25 mm
longitudinal pupil spherical (d-line)	4.0 mm	3.0 mm

Table 4.2.3. Optical performance data for the eyepiece modeled from the measured quantities of the Bausch and Lomb 8X40 Legacy Binoculars with comparisons to a standard Kellner eyepiece*. Overall length is measured from the first physical surface to the last; F is the total eyepiece focal length. For comparison, the first order constructional parameters of the Kellner were scaled appropriately, i.e. focal length = 19.28mm, f -number = 3.73, FOV=30°.

As can be seen from the table, the optical performance of the Legacy eyepiece is much different than that of a typical Kellner eyepiece. The Legacy eyepiece offers a much longer eye relief and back focal length, while yielding lesser quality optical performance in terms of color correction, distortion, and pupil spherical aberration.

* Note that it is standard practice when evaluating eyepieces that rays are traced from the side of the pupil through the lens system, except in the case when evaluating the pupil aberrations.

The center of the visual field is perhaps the most important area of the visual field since the eye is generally centered there and naturally returns to that point after viewing off-axis objects. To show the on-axis performance, Fig.4.2.4 is a transverse ray error plot for the modeled eyepiece from the Bausch and Lomb 8X40 Binoculars. The plot shows the errors of rays traced from an axial point. The eyepiece exhibits considerable spherochromatism, i.e. chromatic variation of spherical aberration.

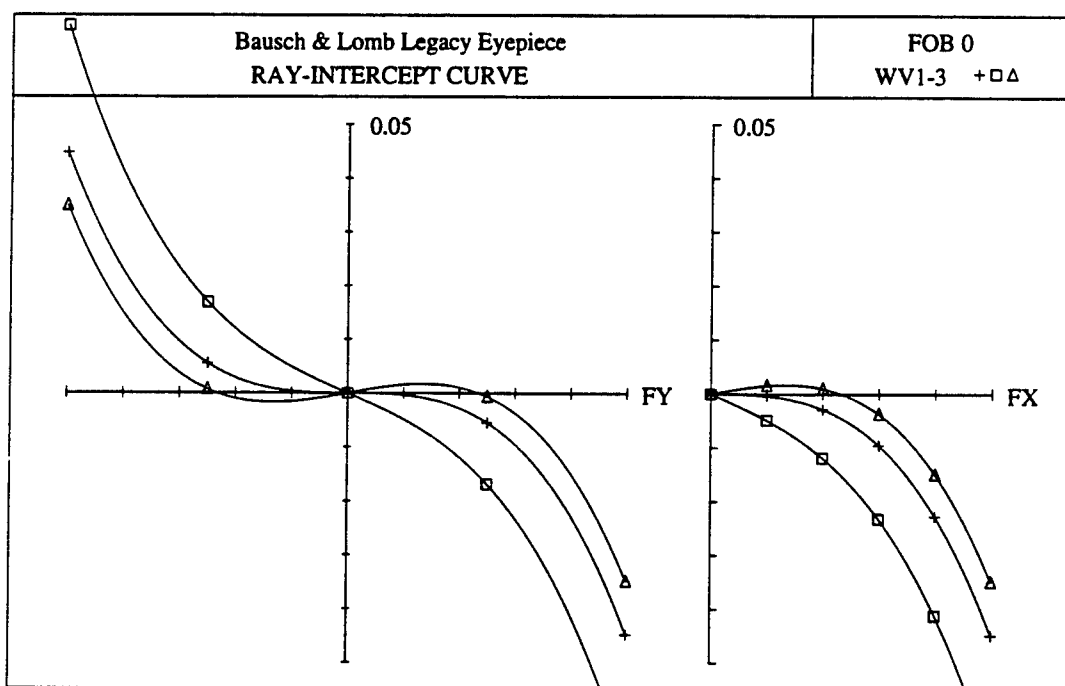


Fig. 4.2.4. On-axis transverse ray plots for the tangential and sagittal fields of the eyepiece from the Bausch and Lomb 8X40 Legacy Binoculars.

4.2.3. Diffractive-Refractive Eyepiece Design For The Binoculars

From Section 3.3.3 there are several wide-angle, hybrid eyepiece designs that can be used in these binoculars. The hybrid eyepieces have overall excellent optical performance, but each has unique advantages over the others. For the binocular application, the design shown in Fig. 3.3.3, referred to as wide-angle, hybrid diffractive-refractive eyepiece No.3, was chosen. This eyepiece employs only one diffractive element. In terms of overall light transmission, this eyepiece is better than eyepiece designs employing two diffractive elements. A single-diffractive-element system provides a higher system throughput of light in the first diffracted order. The diffraction efficiency of the combination of elements is equal to the product of the diffraction efficiencies of the separate elements as given by

$$\eta_T = \eta_1 \times \eta_2, \quad (4.2.1)$$

where $\eta_{1,2}$ refer to the diffraction efficiencies of the first and second diffractive elements, respectively, and η_T refers to the overall diffraction efficiency of the combined elements. Furthermore, the diffractive element in this eyepiece is internal to the binoculars, which is desirable in this case since it is environmentally protected.

As was described in Section 3.3.4, the hybrid wide-FOV eyepieces offer performance equivalent to or better than a typical Erfle eyepiece. From the eyepiece examples in Section 3.2.2, the Erfle eyepiece was shown to offer much better performance than a Kellner eyepiece. Therefore the hybrid eyepiece in this application is expected to have significantly better performance than the Bausch and Lomb eyepiece. This application of the hybrid eyepiece is not intended to be a comparison with a Kellner eyepiece, but rather it is intended to be a demonstration of the hybrid

eyepiece in a common, wide-angle, visual application. Just as an Erfle eyepiece would improve this set of binoculars, so will the hybrid eyepiece. For completeness, the advantages of the hybrid eyepiece in these binoculars are a reduction of approximately 70% in longitudinal pupil spherical aberration, a reduction of more than 35% in distortion, and a reduction of 60% in primary lateral color at 27° half FOV.

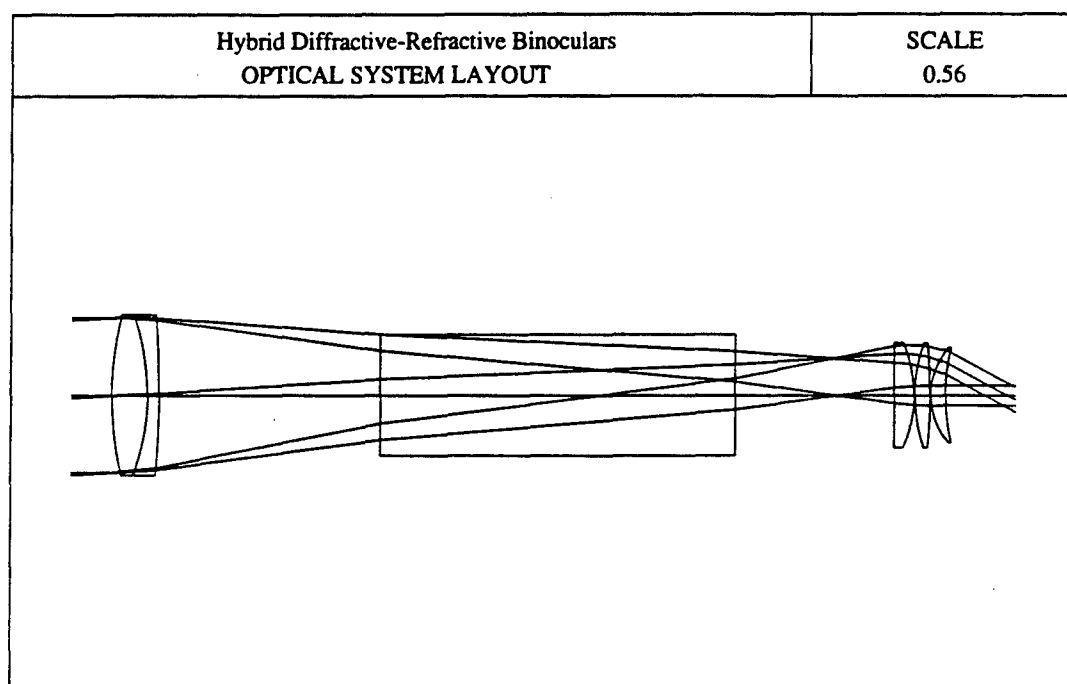


Fig. 4.2.5. The optical layout of the hybrid eyepiece implemented into the Bausch and Lomb Legacy Binoculars.

The first step in incorporating the diffractive-refractive eyepiece into the binoculars was to scale the first order properties of the eyepiece design to fit the requirements of the binoculars. The scaled hybrid eyepiece design was then inserted into the binoculars design for analysis (Fig. 4.2.5). The focal length of the hybrid was scaled to 19.3 mm and the entrance pupil was opened to a radius of 2.6mm. The vignetting data for the hybrid eyepiece are as follows:

hFOV	Percent Vignetted
22.5°	0%
25.0°	0%
30.0°	10%
32.7°	30%

Table 4.2.4. Vignetting data for the wide-angle, hybrid diffractive-refractive eyepiece implemented into the binoculars.

It appears, by examining Tables 4.2.2 and 4.2.4, that the off-axis images will appear much brighter through the hybrid binoculars than the all-refractive pair.

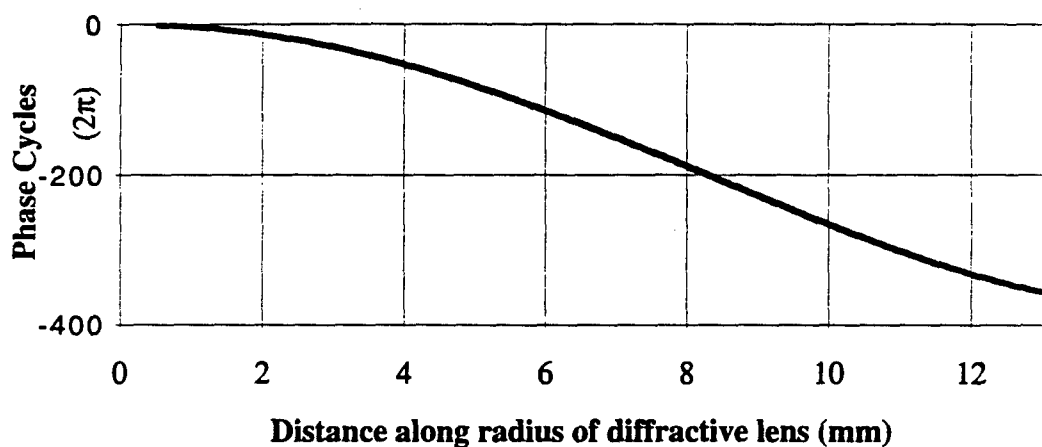


Fig. 4.2.6. The phase function of the diffractive lens in the eyepiece for the hybrid binoculars.

The phase function of the diffractive element has the profile shown in Fig. 4.2.6. The aspheric terms added to the diffractive lens "smoothes" out the phase profile of the lens. This feature reduces the zone spacing at the edge of the lens. The minimum zone spacing according to Eq. (3.3.3) is about 11 microns. The actual minimum zone spacing is approximately 25 microns, which actually occurs at about

70% of the aperture. As a result, the fabrication process is eased and the tolerance limits can be loosened as well.

4.2.4. Diffraction Efficiency of the Hybrid Binoculars

With the use of diffractive optical elements in any system, it is necessary to calculate the effects of non-unity diffraction efficiency. For example the diffraction efficiency is a function dependent upon many quantities including wavelength. Even if the diffractive element is fabricated as a quadratic-blaze profile lens with no manufacturing errors, when used in polychromatic illumination, light will be diffracted into orders other than the design order (Section 2.2.2). Typically most of the light which is not diffracted into the first order is distributed between the zeroth and second diffracted orders. There is relatively very little light diffracted into other orders as discussed in Chapter Two. As a consequence, the light in the zeroth and second diffracted orders must be accounted for.

In the case of binoculars, the visual effect of diffracted light in other orders will vary from user to user and will also depend upon the object location. The reasons for this is that with focusing-binoculars the user may adjust the final image location to accommodate his/her own eye's characteristics. To demonstrate the effects of the diffracted light in other orders, two examples are demonstrated in Table 4.2.5. Both cases are for an object at infinity; the first case is for 0 D (diopters) of refocusing of the eyepiece, and the second case is for -1 D of refocusing of the eyepiece. The relaxed eye seeing an empty field tends to focus not at infinity, but at about 1 meter in front of the eye, i.e. -1 D.⁸

m=1 image at infinity (0.0 D)	m=1 image at -1.00 D
m=2 image at + 2.70 D	m=2 image at +1.56 D
m=0 image at - 2.36 D	m=0 image at - 3.23 D

Table 4.2.5. Data for the locations of images produced by the zeroth and second diffracted orders of the diffractive lens in the binoculars.

In both cases above, the second order image lies behind the users eye. Note that a negative dioptric setting refers to an image location in front of the eye; for example, 0 D is at infinity, -1 D is 1 meter in front of the eye, etc. Only a hyperopic (or far-sighted) eye can focus light which is converging at the eye, or in other words an image that is formed behind the eye. Neither a "good" eye nor a near-sighted eye can possibly accommodate light focusing beyond the eye.⁸

In both cases, the zeroth order light (undiffracted) forms an image which is much closer to the eye than the first order image. The undiffracted light forms images at approximately sixteen and twelve inches in front of the eye, in the two cases respectively. In each case, the distance is significantly far away from the first order image. The amount of light in these separate orders must be considered.

Figure 2.2.2 in Chapter 2 showed the amount of light diffracted into the zeroth, second, and first orders (based on scalar theory) versus wavelength for a quadratic-blaze profile lens neglecting Fresnel reflection losses. More importantly it is necessary to examine the spectral characteristics of the light diffracted in these orders in comparison to the spectral response of the human eye. In Fig. 4.2.7, the diffraction efficiency for a quadratic-blaze profile lens with center wavelength of 0.555 μm is

plotted on the same graph as the standard relative luminosity for the eye in photopic conditions.⁹

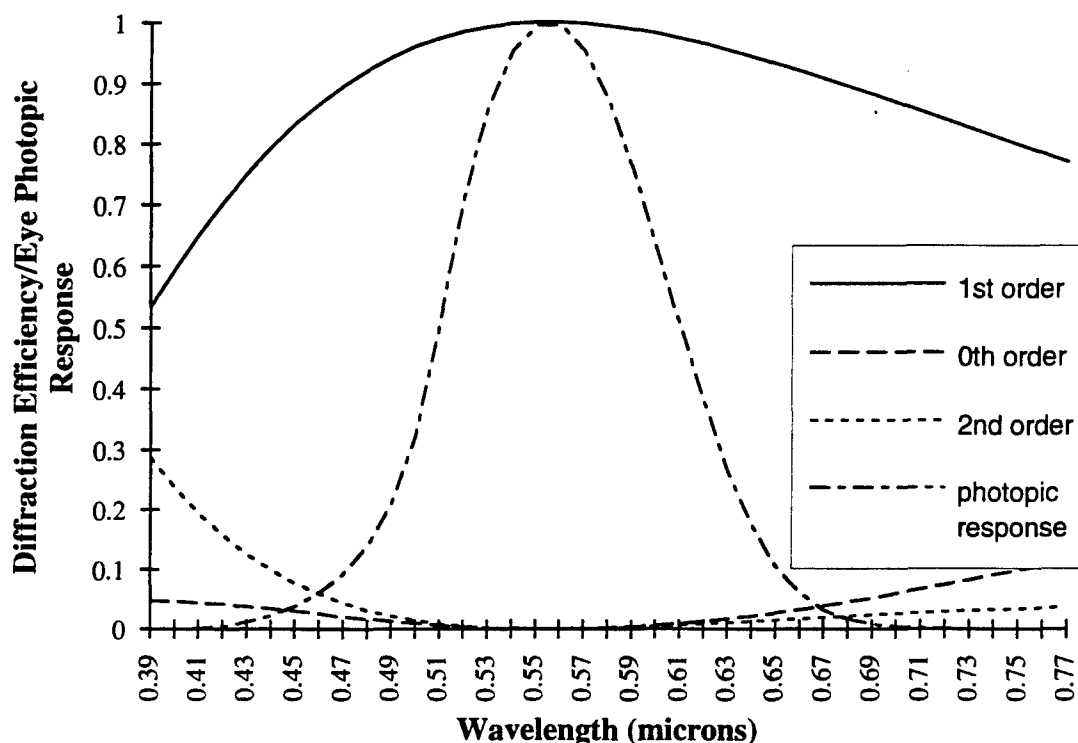


Fig. 4.2.7. The diffraction efficiency of a diffractive lens with a quadratic-blaze profile with $\lambda_0 = 0.555 \mu\text{m}$ and the relative spectral response of the human eye for photopic conditions.

Note that at the point where the visual sensitivity drops to about 25% ($\lambda = 0.630 \mu\text{m}$), the combined light in the 0th and 2nd orders amounts to about 2.5%. The polychromatic integrated efficiency as defined in Chapter Two [Eq. (2.2.27)] has a value of 92% over the visible spectrum ($0.4 \mu\text{m} - 0.7 \mu\text{m}$). For this reason, not only will the background light in the zeroth and second orders be severely out of focus, but also the human eye is relatively insensitive to the light at which the images in these orders will appear.

4.3. Fabrication

4.3.1. Fabrication Tolerances

To fabricate the hybrid eyepiece discussed in the previous sections, fabrication errors, which can effect deviations from the nominal design performance, must be calculated and analyzed to determine fabrication tolerance specifications. To establish the tolerance limits for the eyepiece, the constructional parameters are varied until a predetermined decrease in optical performance is reached and then the value of the constructional parameter is stored. From this data a worst case limit and a standard deviation can be calculated. The tolerances that are relevant to the refractive element are errors in surface power, surface irregularity, surface tilt or element wedge, thickness, index of refraction, and airspace.

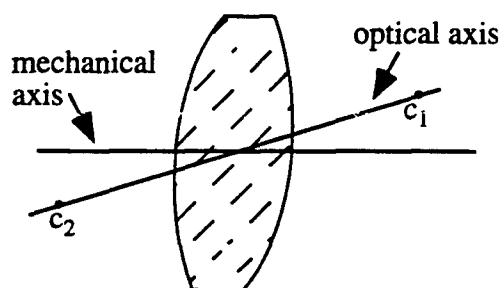


Fig. 4.3.1. Refractive element with tilt. The optical axis of the lens is defined by the line containing the centers of curvature of the two elements; the mechanical axis is defined by the edge of the lens.

The tolerances relevant to the diffractive element are errors in blaze height, decenter, and tilt. Errors of decenter in a hybrid doublet and of blaze height in a diffractive lens are depicted in Figs. 4.3.2 and 4.3.3.

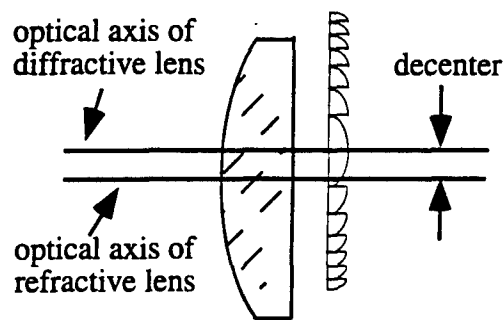


Fig. 4.3.2. Decenter between the axes of the refractive element and the diffractive element.

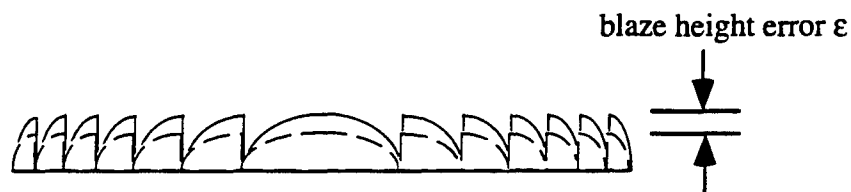


Fig. 4.3.3. Error in the blaze height of a diffractive lens.

An iterative tolerance analysis was performed, as described above, to determine the tolerance budget for the eyepiece fabrication. Some tolerances strictly affect either the refractive elements fabrication, the eyepiece mount fabrication, or the replication of the diffractive element onto the refractive element. The merit used to determine the tolerances was the root mean square of the on-axis spot size. The tolerance budget is listed below in Table 4.3.1.

The worst case performance for the eyepiece, i.e. the performance if the elements are fabricated with an error in each construction parameter equal to its maximum tolerance value, is a 2% change from nominal performance with a 0.29% standard deviation. It is assumed that the errors in fabrication are equally like to occur anywhere within the tolerance limits. In other words, there is a 68% probability that the performance will be within 0.29% of the nominal design, and there is a 95%

probability that the performance will be within 0.58% of the nominal design.¹⁰ Tolerances such as decenter and tilt in the hybrid doublet and in the individual refractive elements will mainly affect the fabrication of the mount, as will be described later.

Refractive element fabrication tolerances	Tolerance Limits	Effect on RMS spot size
curvature	5 fringes	0.1365 %
surface regularity	1 fringe	0.6782 %
center thickness	0.100 mm	0.3719 %
refractive index	0.001	0.2521 %
tilt	0.05730°	0.0060 %
decenter	0.050 mm	0.1839 %
airspace	0.100 mm	0.3158 %
Diffraction element fabrication tolerances		
tilt	0.05730°	0.00046 %
decenter	0.050 mm	0.0163 %
Hybrid doublet tolerances		
tilt	0.05730°	0.0017 %
decenter	0.050 mm	0.0103 %

Table 4.3.1. The tolerance budget for the hybrid diffractive-refractive eyepiece for use in the binoculars. Listed also are the percent deviations from nominal for the various errors in the design. The optical merit used to describe the deviation from the nominal performance is the root mean square spot size for the on-axis case (the fringe wavelength is 546.1 nm).

In fabricating the diffractive element, an error in blaze height must also be accounted for. Since the zone spacings of a diffractive lens solely affect the power and aberration correction of a diffractive lens, a blaze height error effects only a change in the diffraction efficiency of the lens.¹¹ By altering the blaze height of the diffractive lens, the 2π phase height no longer corresponds to the center wavelength, but to some new wavelength. The efficiency profile shown in Fig. 2.2.2 is essentially unchanged, but the peak efficiency is shifted to another spectral location as given by Eq. (4.3.1).¹²

$$d = (1 + \epsilon) \frac{\lambda_o}{n(\lambda_o) - 1}, \quad (4.3.1)$$

where d is the maximum height of the diffractive lens, ϵ is the normalized blaze height error, λ_o is the design wavelength, and $n(\lambda_o)$ is the material index at the design wavelength. Typical cumulative tolerances in the master fabrication and replication processes are ± 50 nm. For a diffractive lens with a design center wavelength of 555 nm, the spectral location of the peak efficiency has a wavelength change equal to about ± 28 nm. The net effect of the change in diffraction efficiency can be compared to the visual response of the human eye – as was done in Section 4.2 – to establish tolerance limits for this error. For example, the effects of a ± 5 % blaze height error on the lens described above are shown in Table. 4.3.2.

Visual Response	Wavelength	Diffraction Efficiency in the 1st Order with a + 5 % error	Diffraction Efficiency in the 1st Order with a - 5 % error
100 %	$\lambda = 555 \text{ nm}$	99.5 %	99.5 %
50 %	$\lambda = 510 \text{ nm}$	94 %	99.6 %
	$\lambda = 610 \text{ nm}$	99 %	94 %
10 %	$\lambda = 470 \text{ nm}$	82 %	95 %
10 %	$\lambda = 650 \text{ nm}$	97 %	89 %

Table 4.3.2. Comparison of diffraction efficiency versus photopic visual sensitivity for blaze height fabrication errors of $\pm 5 \%$ in a diffractive lens with a nominal peak diffraction efficiency at 555 nm.

4.3.2. Fabrication and Replication of the Diffractive Element

The diffractive element was placed directly onto the refractive substrate – the BK-7 plano-convex element, using a cast and cure method. In order to replicate the diffractive element, a master element and a replication tool were first made. The master element was fabricated by exposing the diffractive pattern into photoresist via a laserwriter pattern generator.¹³ Once the photoresist was developed, a replication tool was made from the photoresist diffractive pattern. The replication tool has a shape that is inverse that of the final diffractive lens. This replication tool was then used to stamp the diffractive pattern into a UV resin, which is subsequently cured by ultraviolet light. Similar processes have been used to replicate mirrors, aspheric surfaces, and diffractive elements,¹⁴⁻²⁰ and similar methods have been used to generate master elements.²¹⁻²² The process is described in greater detail below.

Photoresist is evenly spun onto a clean, flat substrate. A laser writer is then used to 'write' the diffractive pattern into the photoresist. The exposure of the focused

laser beam is varied across the surface to achieve the proper blaze shape and depth. The exposure time versus photoresist depth must first be characterized in order to construct the proper blaze profile. By using a laser writer, much higher resolution in the diffractive lens profile can be achieved compared to a multi-level, photolithographic process in which 4, 8, and 16 level diffractive lenses are more common.²³ The blaze of each zone is not approximated by a few discrete steps, but is limited only by the spot size of the laser. Since the laser writer works on an x-y coordinate system, radially symmetric as well as anamorphic patterns can be generated.

The photoresist is then developed, leaving the diffractive pattern remaining on the refractive substrate. This pattern is then used to create a replication tool that is used to produce replicas. Once this tool is made, the tool is assembled in an alignment system to cast numerous replicas of the master element. Figure 4.3.4 shows this process.

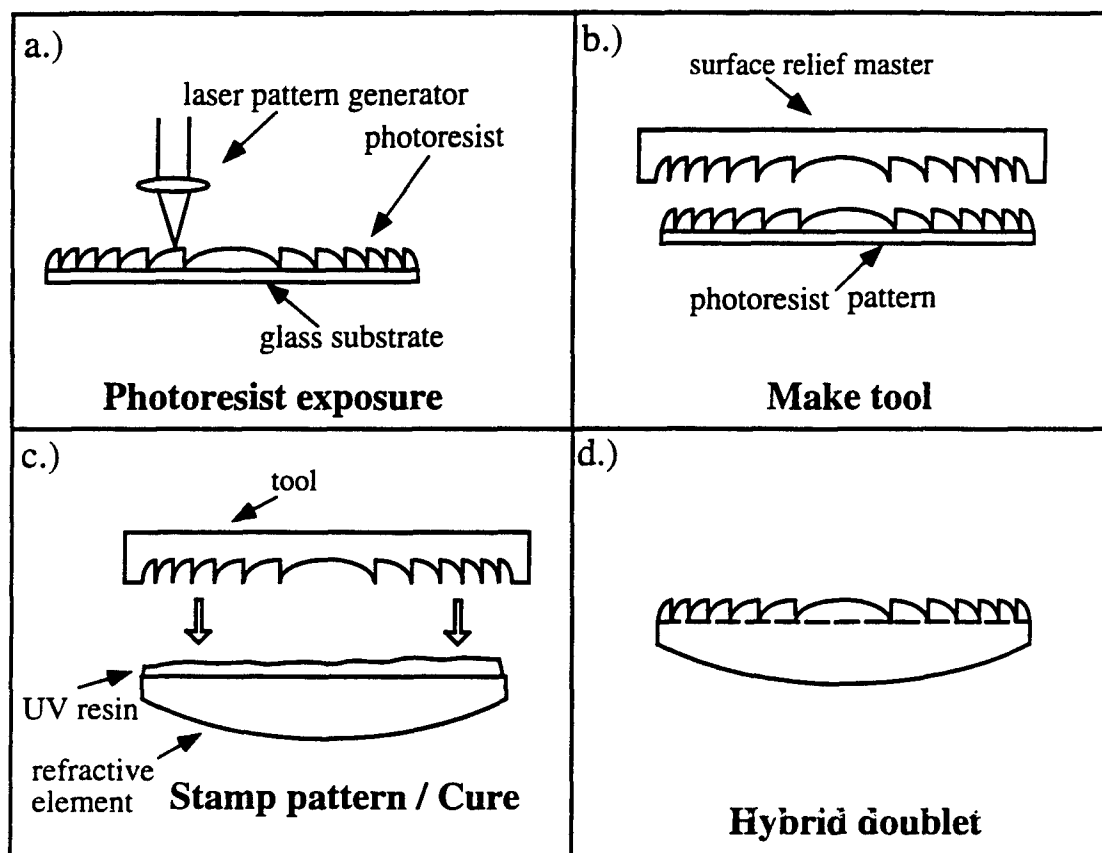


Fig. 4.3.4. Fabrication process for diffractive elements. a.) Writing the diffractive pattern into photoresist to create master, b.) making the tool from the master, c.) casting the pattern into UV resin on a plano-convex refractive element, d.) the resulting hybrid diffractive-refractive doublet after the UV curing step.

The alignment process is a critical step in replicating diffractive lenses. In aligning the diffractive pattern tool with the refractive element, it is important that the optical axes of the two components be matched up with a high degree of precision and

known repeatability. To accomplish this task the alignment system shown in Fig. 4.3.5 was used.*

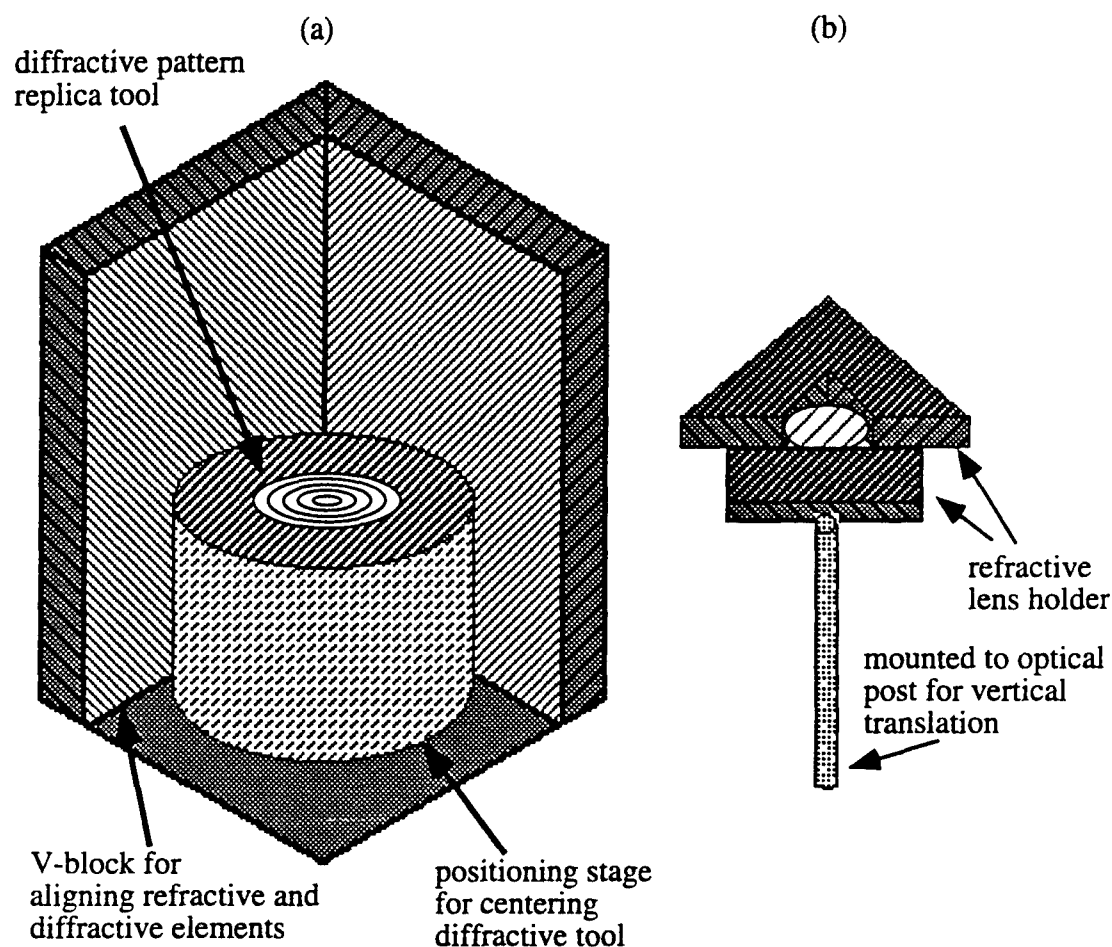


Fig. 4.3.5. Alignment and replication assembly for fabricating diffractive-refractive doublet lenses. (a) Cylinder stage with x- and y-translation and θ rotation for centering the diffractive lens, and the V-block assembly for aligning the diffractive and refractive elements, (b) refractive lens mount with spring-loaded rod for pressure against V-block.

The diffractive element tool is aligned by centering it with respect to the cylindrical stage in which it is mounted. This centering is accomplished by means of determining the location of the replication tool with respect to the edge of the cylinder

* This system was designed and developed by a visiting scientist to the Institute of Optics at the University of Rochester, Yasuhiro Yoshitake from Hitachi Corp., Japan, 1992.

along a given chord of the cylinder. The midpoint of the chord is found, and the tool is subsequently moved to that position. The stage is then rotated ninety degrees and the process is repeated. The alignment process of the diffractive lens tool with respect to the cylinder stage is then complete. The standard deviation of the errors in aligning a diffractive lens using this set-up has been measured to be 13 μm in each of the two alignment steps, i.e. the x and y directions.

The refractive element is then placed in the lens mount in Fig. 4.3.5. Tilt in the refractive element can be removed by adjusting the lens position, while the holder and lens are viewed through an auto-collimator instrument. The planar side of the refractive lens is used to retro-reflect the light in the autocollimator. The lens holder has a spring-loaded rod, perpendicular to the optical axis of the refractive lens, which is mounted to a pole that allows for vertical displacement of the refractive element down onto the diffractive lens tool. The lens holder is then placed into the V-block assembly, to which the diffractive lens is mounted, and the spring-loaded rod ensures that the lens mount is securely fixed in the V-lock assembly for accurate replication. A layer of ultraviolet epoxy is then applied to either the replication tool or the refractive element. The refractive element is subsequently lowered down to the diffractive tool for the replication casting. Ultraviolet light is then used to cure the photosensitive resin. When the photopolymer is adequately hardened, the tool is separated from the resin, and a hybrid doublet is completed.

Several tests were performed to determine the centering accuracy and repeatability of the alignment system. A glass reticle was used as a test refractive substrate in a simulated replication process. The tests consisted of placing and centering a diffractive lens tool in the cylinder stage of the alignment setup described above. A reticle was mounted into the refractive lens holder, which was subsequently placed into the V-block assembly shown in Fig. 4.3.5. The lens holder securing the

reticle was then lowered down onto the diffractive lens tool. A CCD camera was then used to examine the alignment of the two elements.

The reticle was a simple round, planar, glass element with a crosshair pattern placed on one side. The reticle had a diameter equal to the diameter of the refractive element in the hybrid eyepiece discussed in this chapter, i.e. 27 mm. The thickness of the reticle was 2.28 mm; the width of the crosshair lines was approximately 20 μm . The accuracy of the diameter of the reticles was specified and measured to be ± 0.05 mm. The accuracy of the placement of the crosshair with the outside diameter of the reticle had to be measured for each reticle, since the alignment of the system is determined by the outside diameter of the refractive element. For each replication test the detected alignment between the two elements was measured and the difference between the outside diameter of the reticle and the location of the center of the crosshair was taken into account. Three separate reticles were used in the various tests. A variety of rotations of the reticle was used in several tests. Also, some tests involved the removal and remounting of the reticle in the refractive lens holder, while others simply used the same mounted reticle to determine the repeatability of the replication accuracy. The data for both cases were relatively indistinguishable. In each set of tests, the average alignment error was 72.3 μm ; the standard deviation of the errors was 27 μm . The number of test samples was 10.

4.3.3. Eyepiece Mount

There are two basic requirements that had to be satisfied by the eyepiece mount. These were that the eyepiece was required to be fitted into the existing binocular housing and that the mount constrained the individual elements in their proper locations within certain tolerances in order to meet the specified optical performance. As a result, a stack-mounting assembly was chosen. A stack-mounted assembly is the type of lens mount in which the individual lens elements are inserted into either a cell or lens barrel sequentially, with spacers in between the elements, and a single retainer ring holding all the elements in place.²⁴ This method is easy to assemble and also assures precision alignment. Each of the lens elements is contacted on a polished spherical surface either by a seat-cut in the barrel or by a spacer. This element mounting technique is used for elements requiring maximum decentrations of 0.075 to 0.025 mm.²⁵ By contacting the lens element on an optically polished, spherical surface – as opposed to contacting the lens on its edge, high-precision centering can be achieved, similar to the action of truing bells in edge-grinding a lens. When lens elements are edge-centered, the edge of the outside diameter is the contact surface for mounting the lens, and errors in fabricating the lens result in centering errors as well. This is not the case when elements are contacted on spherical surfaces. For example, a common error which can occur if the lens is edge-mounted is tilt of the element. If the lens is not edged properly and the optical axis does not properly line up with the mechanical axis of the lens, then mounting the lens by its edge will introduce misalignment in the image. Two errors in edging the lens can result in these defects, a wedged lens and a decentered lens. In Figs. 4.3.6-4.3.7 a comparison of edge mounting and spherical-contact mounting is demonstrated.

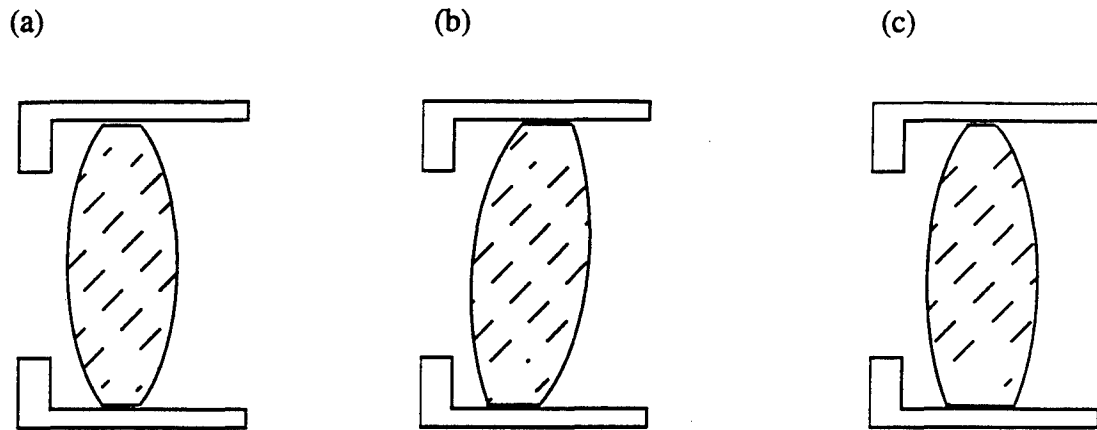


Fig. 4.3.6. Edge mounting a lens. (a) A perfect lens in a perfect cell, (b) a tilted lens in a perfect cell, (c) a decentered lens in a perfect cell.

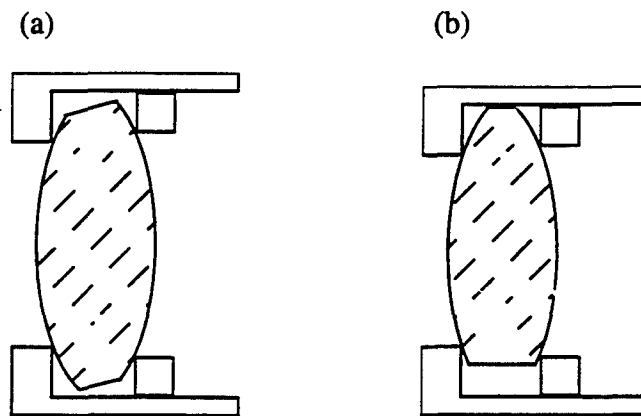


Fig. 4.3.7. Mounting a lens by contacting the lens on a polished, optical spherical surface; errors in edging the lens do not result in mounting errors. (a) a tilted lens in a cell, (b) a decentered lens in a cell.

Edge mounting has the inherent uncertainty of the placement of the lens.²⁶ Furthermore, with the use of edge-mounting, the edges of the lens elements must be perfectly perpendicular to the optical axis in order to maintain proper alignment with the spacers and retainer ring. If the mounting surfaces are not perpendicular to the optical

axis, then the lens elements can contact the spacers at a single point, and as a result strain can be induced into the mount spacers and retainer ring. Naturally when using the type of mounts in Fig. 4.3.7, the tolerances on tilt and decenter in the fabrication of the lens elements can be kept much looser.

The design for the eyepiece mount assembly is shown in Fig. 4.3.8. Note that all of the elements are contacted on a polished spherical surface either by the barrel or a spacer.

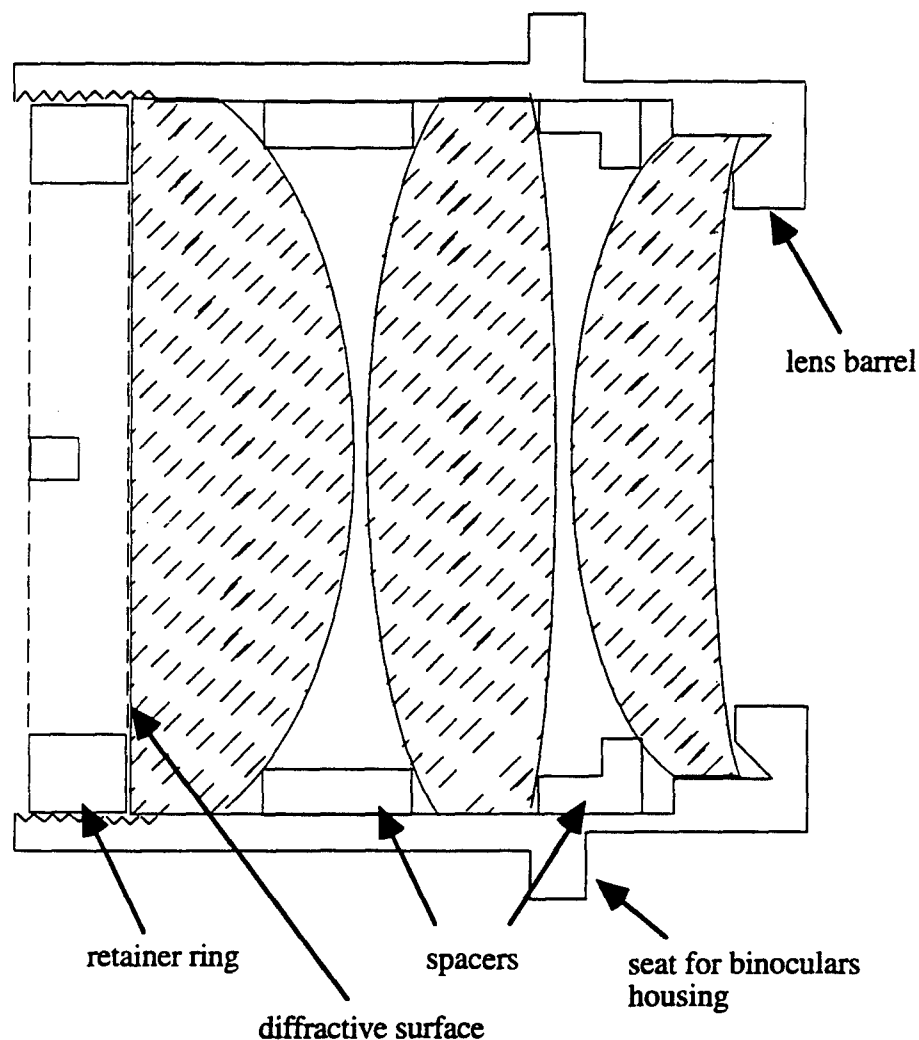


Fig. 4.3.8. Mount for hybrid diffractive-refractive eyepiece.

4.4. References for Chapter 4

1. H. E. Rosenberger, *Optics Source Book*, S. Parker, ed. (McGraw-Hill, Inc., New York, 1988), ch. 2, p. 67.
2. *Optical Design-Military Standardization Handbook MIL-HDBK-141* (Defense Supply Agency, Washington, D.C., 1962), pp. 14-14 – 14-15.
3. W. J. Smith, *Modern Optical Engineering Second Ed.* (McGraw-Hill, Inc., New York, 1990), pp. 403-408.
4. *Schott Optical Glass Catalog No. 3111, 1986 edition* (Schott Glass Technologies, Duryea, Pennsylvania, 1986).
5. Ref. 2, pp. 14-6 – 14-7.
6. R. Kingslake, *Optical System Design* (Academic Press, Inc., Orlando, 1983) pp. 208-210.
7. Ref. 2, pp. 14-6 – 14-7.
8. Ref. 2, pp. 4-3 – 4-10.
9. Ref. 3, pp. 122 - 128.
10. See for example, R. N. Goldman, J. S. Weinberg, *Statistics An Introduction* (Prentice-Hall, Inc., Englewood Cliffs, 1985), pp. 213-226.
11. J. A. Cox, T. Werner, J. Lee, S. Nelson, B. Fritz, J. Bergstrom, "Diffraction efficiency of binary optical elements," in *Computer and Optically Formed Holographic Optics*, Sing H. Lee, ed. Proc. SPIE, **1211**, 116-124 (1990).
12. G. J. Swanson, "Binary Optics Technology : The Theory and Design of Multi-Level Diffractive Optical Elements," Tech. Rep. 854 (Lincoln Laboratory, MIT, Lexington, Mass., 1989).
13. J. Bowen, C. G. Blough, and V. Wong, "Fabrication of optical surfaces by laser pattern generation," in Optical Fabrication and Testing Workshop, Vol. 13, 1994 OSA Technical Digest Series (Optical Society of America, Washington, D.C., 1994), pp. 153-156.
14. W. E. Asher, "Epoxy replication - advantages and limitations," in *Replication and Molding of Optical Components*, M. Reidl, ed. Proc. SPIE, **896**, 2-5 (1988).
15. H. Howden, J. A. Clarke, "Refracting replica aspheric optics," *Opt. Eng.* **15**, 197-201 (1976).

16. S. D. Fantone, "Replicating optical surfaces using UV curing cements : a method," *Appl. Opt.* **22**, 764 (1983).
17. R. J. M. Zwiers, G. C. M. Dortant, "Aspherical lenses produced by a fast high-precision replication process using UV-curable coatings," *Appl. Opt.* **24**, 4483-4488 (1985).
18. G. B. A. Hut., J. W. Versluis, "Replicated aspheres meet optical memory needs," *Laser Focus World* **25**, 105-113 (1989).
19. M. Tanigami, S. Ogata, T. Yamashita, K. Imanaka, "Low-wavefront aberration and high-temperature stability molded micro fresnel lens," *IEEE Photonics Technology Letters*, **1**, 384-385 (1989).
20. J. Jahns, K. H. Brenner, W. Däschner, C. Doubrava, T. Merklein, "Replication of diffractive microoptical elements using a PMMA molding technique," *Optik* **89**, 98-100 (1992).
21. M. T. Gale, M. Rossi, H. Schütz, P. Ehbets, H. P. Herzig, and D. Prongué, "Continous-relief diffractive optical elements for two-dimensional array generation," *Appl. Opt.* **32**, 2526-2533 (1993)
22. M. T. Gale, M. Rossi, and H. Schütz, "Fabrication and replication of continuos-relief DOEs," in *Fourth International Conference on Holographic Systems, Components, and Applications*, IEE Proc., **379**, 66-70 (1993)
23. See for example, G. J. Swanson and W. B. Veldkamp, "Diffractive optical elements for use in infrared systems," *Opt. Eng.* **28**, 605-608 (1989).
24. P. R. Yoder, Jr., *Opto-Mechanical Systems Design Second Ed.* (Marcel Dekker, Inc., New York, 1993), pp.207-270.
25. Ref. 19, pp. 155-176.
26. R. E. Hopkins, "Optical element mounting and alignment technique," in *Geometrical Optics*, Robert E. Fischer, William H. Price, Warren J. Smith, eds., *Proc. SPIE*, **531**, 187-195 (1985).

5. Experimental Results

5.1. Introduction

For experimental characterization of the wide-field, hybrid diffractive-refractive eyepiece previously described in Chapters Three (Fig. 3.3.5) and Four, three tests have been performed. These include a test of the modulation transfer function (MTF) and two imaging tests. The MTF of a lens gives a measure of the resolving power of the lens at a given set of testing conditions. The experimental results for the hybrid eyepiece are compared with the predicted theoretical data. Additionally a commercially produced, 6-element Erfle-type eyepiece was also tested on the MTF bench for comparison.

The two imaging experiments test the eyepiece in two possible configurations in which an eyepiece can be used. The first imaging test uses the eyepiece as a magnifier lens; the second imaging experiment examines the image formed by the hybrid eyepiece as part of a set of binoculars, as described in Chapter 4. In the first imaging experiment, the Erfle eyepiece was also tested for a comparison with the hybrid eyepiece. In the second imaging experiment, the all-refractive set of Bausch and Lomb binoculars was tested for comparison with the same type of binoculars equipped with the hybrid eyepiece.

5.2. Modulation Transfer Function

5.2.1. Theory and Experiment

The modulation transfer function (MTF) of a lens gives a measure of the resolving power of a lens as a function of the spatial frequency of an image. While it is an important index of the performance of a lens, the specific test conditions directly influence the results. For example, in testing an eyepiece at infinite conjugates on an MTF bench, pupil spherical aberration of the exit pupil can not be determined. Furthermore, when testing or specifying the MTF of a lens, the exact test parameters must be known and stated. Resolution tests under a specific set of conditions do not necessarily guarantee similar performance under a different set of test conditions. These specifications include the conjugates of the object and image (magnification), the lens aperture, the wavelength of the source illumination, the field angle of the object, and the spatial frequencies of the test. The MTF of a lens is typically expressed as a function of the spatial frequency of the image, v . The MTF can be a very important evaluation to be used as a comparison for several lenses.

Modulation in the object and image can be expressed as:¹

$$M = \frac{I_{\max} - I_{\min}}{I_{\max} + I_{\min}}, \quad (5.2.1)$$

where: $I_{\max, \min}$ are the maximum and minimum intensities of the scene, respectively.

The MTF of a lens can be expressed as a ratio of the modulation in the image to the modulation in the object:

$$\text{MTF}(v) = \frac{M_i(v)}{M_o(v)}. \quad (5.2.2)$$

The output image intensity for an incoherently illuminated object of an optical system is a convolution of the object intensity with the incoherent point spread function (PSF),²

$$I_i(x', y') = \{pp^*\} \otimes I_o(x, y), \quad (5.2.3)$$

where, the subscripts *i* and *o* refer to the image and object, respectively. The incoherent PSF can be found by multiplying the coherent impulse response *p* by its complex conjugate *p*^{*}.³ The impulse response is the Fourier transform of the pupil function:

$$p(r, s) = \mathfrak{F} \{P(u, v)\}. \quad (5.2.4)$$

The incoherent OTF, of which the modulus is the MTF, of a lens is the Fourier transform of the incoherent point spread function (PSF). Equivalently, this is the normalized autocorrelation of the pupil function:²

$$\text{MTF}(f_x, f_y) = \left| \frac{P \otimes P}{P^2} \right|. \quad (5.2.5)$$

Since an eyepiece is typically a subsystem of a more complex optical system, the MTF of the eyepiece does not reveal the whole story. While MTFs of a set of cascaded components can usually be multiplied together to determine the overall system

MTF, often one part of an optical system is used to compensate for another, and therefore their individual MTFs cannot be combined so simply. Nevertheless, as a comparison between the theoretical and experimental performance of the hybrid eyepiece and as a comparison between two similar eyepieces (i.e. same FL and f -number), the MTF provides a good measure.

An Ealing Solid State EROS MTF bench, as shown in Fig. 5.2.1, was used to perform the MTF evaluations. The bench consists of a tungsten-halogen lamp source with a spectral filter assembly, an array of slits with a variety of widths, a collimating lens for infinite conjugate tests, a relay lens assembly, and a photodiode detector array, and a computer. The source, slit, and collimator group provide a slit source at an infinity. The lens under test then images a line spread function (LSF). The relay lens system images the LSF onto a detector. The computer then calculates the MTF of the lens by computing the Fourier transform of the LSF; a similar process is described by Bruning.⁴ The computer calculates a one-dimensional MTF along a single axis, since the LSF is essentially a one-dimensional PSF.

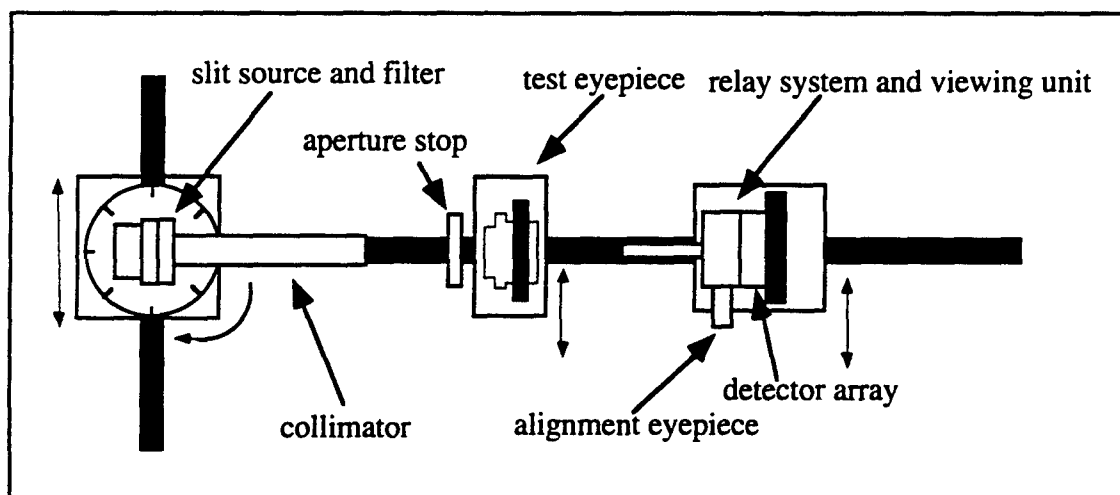


Fig. 5.2.1. MTF bench used to test the eyepieces described in this section.

5.2.2. Diffraction Efficiency – Experimental

To accurately report the MTF data for the hybrid eyepieces, the diffraction efficiency must be measured and used for scaling the data. In the Ealing MTF equipment, the background light is suppressed in the calculation. Therefore, the measured values of the MTF must be appropriately scaled by the integrated diffraction efficiency. To calculate the efficiency of the lens at specific radial positions, the power of the light in the first diffracted order was divided by the measured power transmitted through a portion of the substrate that was coated with the diffractive lens material. This method automatically accounts for reflection and absorption losses due to the material's properties. The efficiency was measured at three wavelengths for MTF scaling purposes (efficiencies at other wavelengths were measured to more fully characterize the lens' spectral characteristics), $\lambda = 543.5$ nm, $\lambda = 488$ nm, and $\lambda = 632.8$ nm. The sources used in the testing were a green helium neon laser, an argon-ion laser, and a red helium neon laser. The diffraction efficiencies of the lens for several radial positions at the said laser lines are listed Tables 5.2.1 - 5.2.3.

Radial position	Diffraction Efficiency, η
0-3 mm	90.0%
4-5 mm	89.7%
6-7 mm	80.3%
8-9 mm	80.0%
10-11 mm	78.8%
12-13 mm	81.1%

Table 5.2.1. Measured diffraction efficiency for specific radial positions of the diffractive lens for $\lambda = 543.5$ nm.

Radial position	Diffraction Efficiency, η
0-3 mm	87.0%
4-5 mm	86.3%
6-7 mm	79.5%
8-9 mm	78.4%
10-11 mm	81.8%
12-13 mm	80.5%

Table 5.2.2. Measured diffraction efficiency for specific radial positions of the diffractive lens for $\lambda = 488.0$ nm.

Radial position	Diffraction Efficiency, η
0-3 mm	77.1%
4-5 mm	70.9%
6-7 mm	69.1%
8-9 mm	62.1%
10-11 mm	66.8%
12-13 mm	72.3%

Table 5.2.3. Measured diffraction efficiency for specific radial positions of the diffractive lens for $\lambda = 632.8$ nm.

From the measured diffraction efficiencies of the lens at specific radial positions and wavelengths, values for the integrated efficiency can be calculated. This is done by summing the weighted diffraction efficiencies of the specific annular regions and normalizing the quantity by the total area of the lens. The diffraction efficiency for a given region is weighted by its annular area. The integrated efficiency of the diffractive lens in this case is $\eta_{\text{int}}=81.5\%$ for $\lambda = 543.5$ nm, $\eta_{\text{int}}=81.2\%$ for $\lambda = 488$ nm, and $\eta_{\text{int}}=69.8\%$ for $\lambda = 632.8$ nm.

The diffraction efficiency of the diffractive lens varies considerably with the radial position of the measurement (this is actually a simplification, since the diffraction efficiency actually varies with the general position of the lens aperture). This is due to the method of generation of the master element, which is accomplished by a laser point generation machine.

To generate the master, a laser beam is focused down onto a photoresist-covered substrate, and the desired surface profile is exposed into the photoresist. The machine that is used to generate the diffractive surface controls the exposure system on an x-y coordinate system. Conversely, the diffractive lens is a rotationally symmetric element. The pattern generator is optimized for non-rotationally symmetric elements, such that the types of optics that can be handled by the machine can be kept somewhat general, i.e. anamorphic lenses and gratings can therefore be fabricated. Certain fabrication errors are almost inevitable as a result. For instance, x-y raster scan lines can actually be written into the element if the element is generated without sufficient information coded into the element. This error was unavoidable in this element due to the excessively long generation times required for its fabrication. As a result of these errors, the diffraction efficiency significantly decreases as the zone spacing gets smaller. As evidence of the fact that the efficiency decreases as the zone spacings decrease, note that due to the asphericity in the profile of the lens element, the zone

spacing decreases as the radius increases out to about 70% of the aperture, at which point the spacing begins to increase slightly as the edge of the lens is approached. Both sets of the efficiency measurements show an increase in diffraction efficiency at the edge of the lens as compared to the second or third outermost regions of the lens. In the future the vendor of these elements plans to use an r - θ machine, i.e. one that is rotationally symmetric. This will greatly alleviate these types of fabrication errors. Diffraction efficiencies similar to those measured on-axis are expected to be obtained across the entire lens.

The off-axis diffraction efficiency deviated significantly from the on-axis efficiency; additionally, the on-axis efficiency was not as high as expected at the center wavelength. There is a blaze height error in the lens that causes a spectral shift in the location of the peak diffraction efficiency. This error can typically be corrected with about five to six iterations and optimizations in the master generation process. In this instance, the necessarily lengthy element-generation times were too long to resolve this issue.

The blaze height for the on-axis zones was measured with a surface profilometer, and a typical profile scan of the second and third zones of the diffractive lens is shown in Fig. 5.2.2.

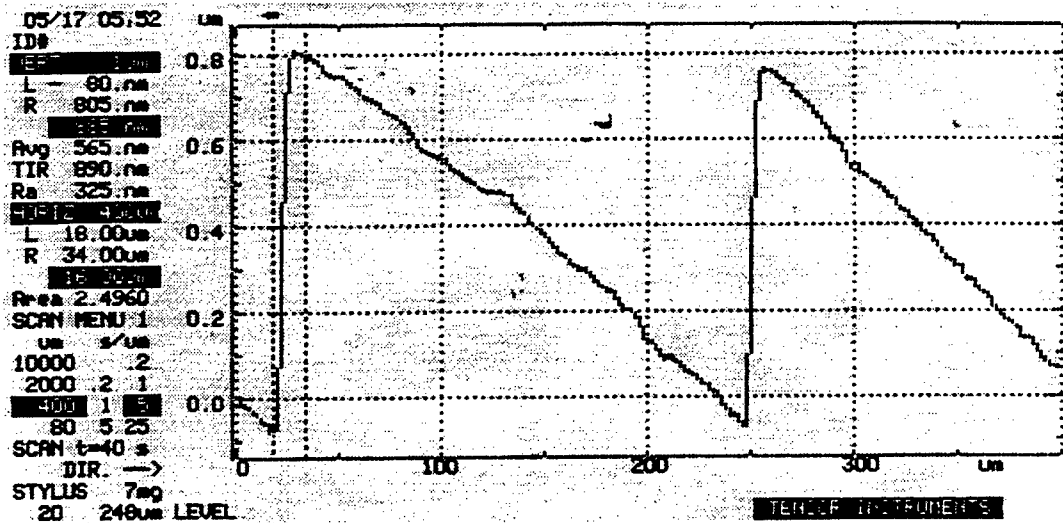


Fig. 5.2.2. Surface profilometer measurement of diffractive lens. The blaze height of the lens is measured to be $0.885 \mu\text{m}$.

From the profilometer measurement, the blaze height of the diffractive surface profile is approximately $0.885 \mu\text{m}$. The surface profile tool used in this measurement has a radius equal to $12.5 \mu\text{m}$. The result of the finite radius on the tool is that a true measurement of the depth cannot necessarily be made, since the tool may not be able to get deep enough into the groove. With possible errors in the profile measurement due to the tool size, the actual peak efficiency wavelength is likely to be longer than the calculated wavelength (using the measured depth to estimate the peak wavelength).

Given the maximum surface height of the diffractive element and the refractive index for the diffractive lens material, the wavelength at which the peak diffraction efficiency occurs can be located with the use of Eq. (2.2.8). The refractive index of the material used to construct the diffractive lens is approximately 1.56. With the given index of refraction and the surface profile measurement ($0.885 \mu\text{m}$), the wavelength at which maximum diffraction efficiency for the design order ($m=1$) occurs is $\lambda = 496 \text{ nm}$.

The on-axis (actually 3 mm radial position) diffraction efficiency of the diffractive lens was measured at several wavelengths ($\lambda = 477$ nm, $\lambda = 488$ nm, $\lambda = 497$ nm, $\lambda = 515$ nm, $\lambda = 543.5$ nm, $\lambda = 632.8$ nm) to help characterize the spectral properties of the lens and to identify the spectral location of the maximum efficiency (Fig. 5.2.3). From the measured height of the diffractive lens, the peak efficiency should occur at $\lambda = 496$ nm, although based on the efficiency measurements, it appears that the diffractive lens has a peak efficiency between $\lambda = 515$ nm and $\lambda = 543.5$ nm.

The graph in Fig. 5.2.3 shows two plots for the theoretical scalar diffraction efficiencies of a diffractive lens with peak efficiencies at $\lambda = 555$ nm and $\lambda = 530$ nm and several points of the measured on-axis diffraction efficiency for the fabricated diffracted lens at various wavelengths listed in the previous paragraph. With the assumption that the actual peak efficiency does occur at $\lambda = 530$ nm, the measured efficiencies of the lens are all approximately 9-13% below the theoretical efficiencies, based on the scalar diffraction model, although the measured efficiencies do follow the shape of the theoretical curve.

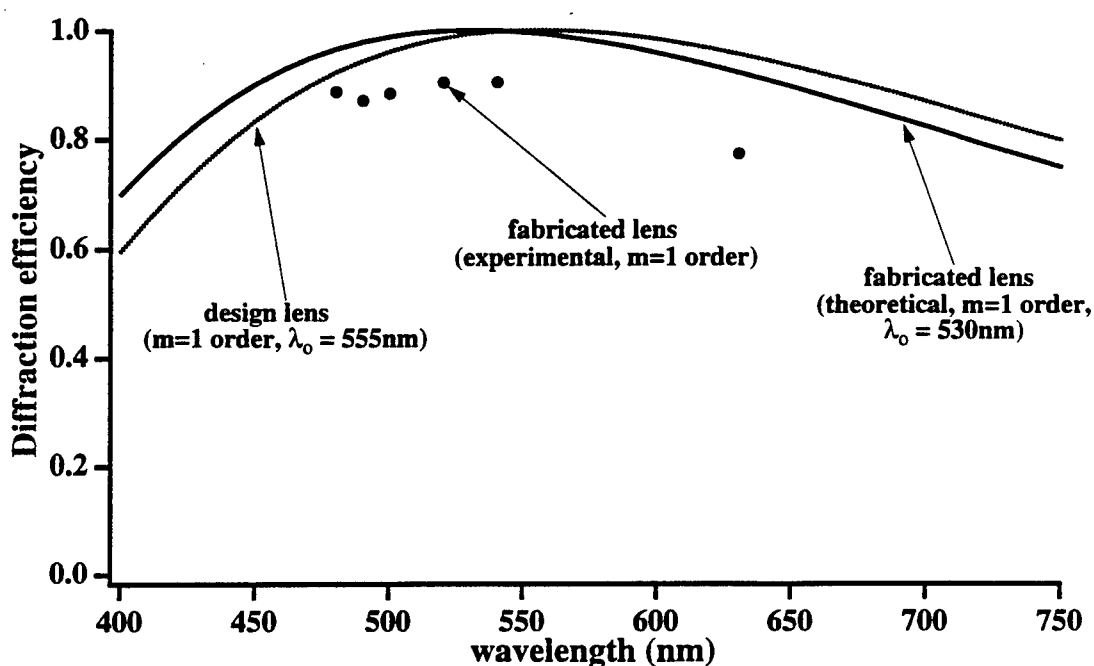


Fig. 5.2.3. Theoretical scalar diffraction efficiencies for a diffractive lens designed with a peak wavelength at $\lambda_0 = 555$ nm and for a diffractive lens fabricated with a blaze height error such that the peak wavelength occurs at $\lambda_0 = 530$ nm; individual points plotted for measured on-axis diffraction efficiency of fabricated lens.

5.2.3. Experimental MTF Results

The hybrid eyepieces were experimentally tested and compared to a 20-mm FL Erfle eyepiece using an Ealing MTF test bench (as shown in Fig. 5.2.1). An infinite conjugate configuration on the eye side of the eyepiece was used. In the test set-up, a 5-mm aperture stop was placed at the exit pupil location of each eyepiece so that the eyepieces were tested at $f/4$. The conventional, refractive eyepiece used in the testing was a 6-element Erfle eyepiece from Edmund Scientific Inc., in which the patented design is modified by the replacement of the center element with a doublet. The additional lens in this commercial, Erfle-type eyepiece was added to improve the lateral color correction over that of the patented 5-element design.

The first experiment was an on-axis measurement of the MTF at $\lambda = 555$ nm. The on-axis experimental results and theoretical predictions for the hybrid eyepiece are shown in Fig. 5.2.4. Both data groups are scaled by the measured integrated diffraction efficiency of the lens for the portion of the lens sampled. Light from specific regions of an object sample sub-aperture portions of the diffractive lens; therefore the efficiency values can be different for various fields-of-view. The measured, on-axis efficiency of the lens is 90% for $\lambda = 555$ nm. For ease of comparison, the experimental on-axis MTF results for the 6-element Erfle eyepiece and for the hybrid eyepiece are shown plotted on the same graph in Fig. 5.2.5.

For off-axis MTF performance testing, the eyepieces were tested at 30° full FOV at $\lambda = 555$ nm. Again the experimental and theoretical results for the hybrid eyepiece are compared in Fig. 5.2.6. The data are similarly scaled by the measured integrated diffraction efficiency of the sampled portion of the lens, which was 83%. Note that the diffractive element in the eyepiece was a prototype lens; further optimization of the blaze profile is expected to improve the integrated diffraction efficiency of the lens to a value approaching 95%; this will directly raise the MTF curves by the increase in the efficiency. For ease of comparison, the experimental off-axis MTF results for the Erfle eyepiece and for the hybrid eyepiece are shown on the same graph in Fig. 5.2.7.

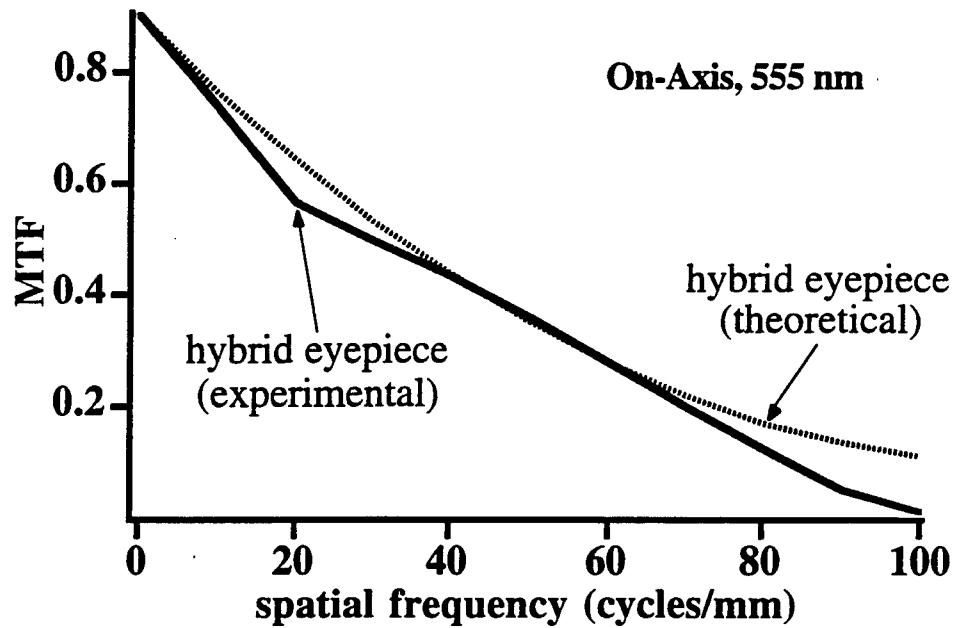


Fig. 5.2.4. Experimental and theoretical on-axis MTF data for hybrid eyepiece with $\lambda = 555$ nm.

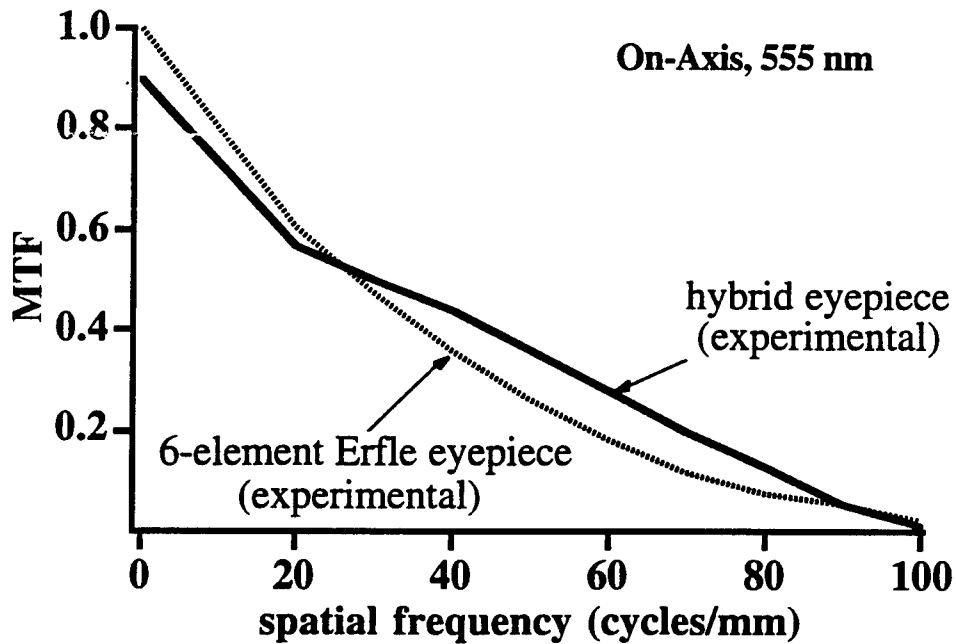


Fig. 5.2.5. Experimental on-axis MTF data for six-element Erfle eyepiece and hybrid eyepiece with $\lambda = 555$ nm.

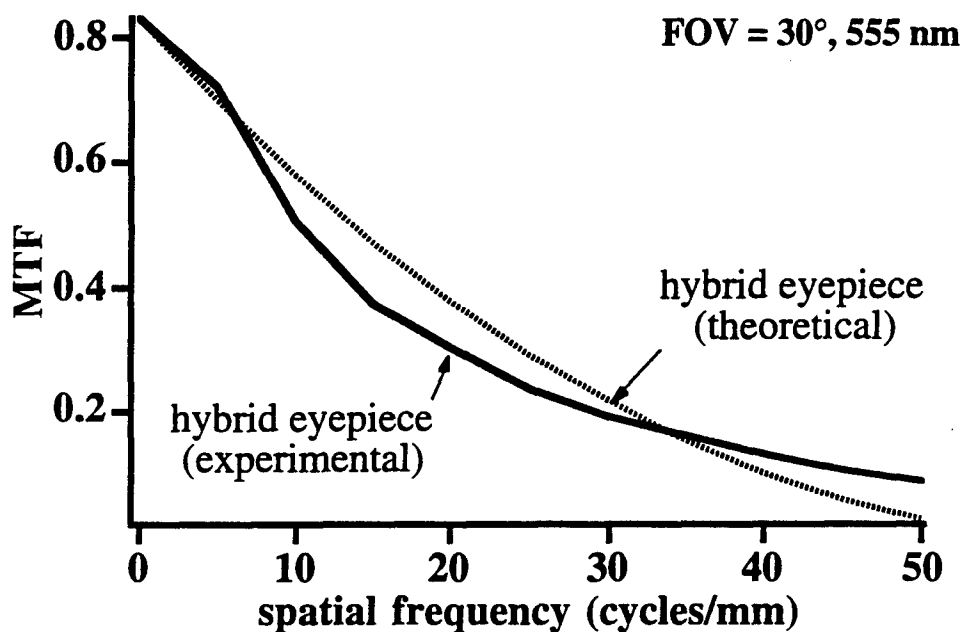


Fig. 5.2.6. Experimental and theoretical 30° full field-of-view (FOV) MTF data for hybrid eyepiece with $\lambda = 555$ nm.

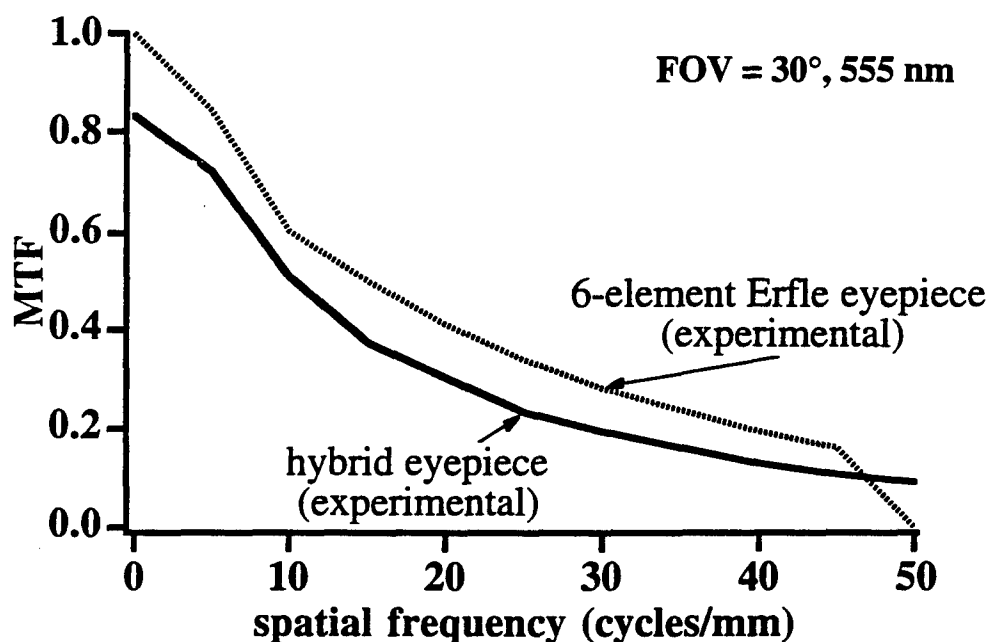


Fig. 5.2.7. Experimental 30° FOV MTF for six-element Erfle eyepiece and hybrid eyepiece with $\lambda = 555$ nm.

The same MTF tests that were performed for the eyepieces at $\lambda = 555\text{nm}$ were performed at the F-line ($\lambda = 486\text{ nm}$) and C-line ($\lambda = 656\text{ nm}$) as well. The experimental resolution performance of the hybrid eyepiece at both $\lambda = 486\text{ nm}$ and $\lambda = 656\text{ nm}$ also matches well with the theoretical predictions. The format for the presentation of the experimental and theoretical MTF data for the on-axis and 30° full FOV cases at $\lambda = 486\text{ nm}$ and $\lambda = 656\text{ nm}$ are the same as that for the $\lambda = 555\text{ nm}$ plots and are plotted in Figs. 5.2.8-5.2.15. These data are also scaled by the measured, integrated diffraction efficiencies. For $\lambda = 486\text{ nm}$, the on-axis efficiency is 87.0%, while the off-axis efficiency is 82.2% (for the sampled area); and for $\lambda = 656\text{ nm}$ the on-axis efficiency is 77.1%, while the off-axis efficiency is 69.8% (for the sampled area). The integrated efficiency used to scale the $\lambda = 656\text{ nm}$ MTF data was actually measured at $\lambda = 632.8\text{ nm}$.

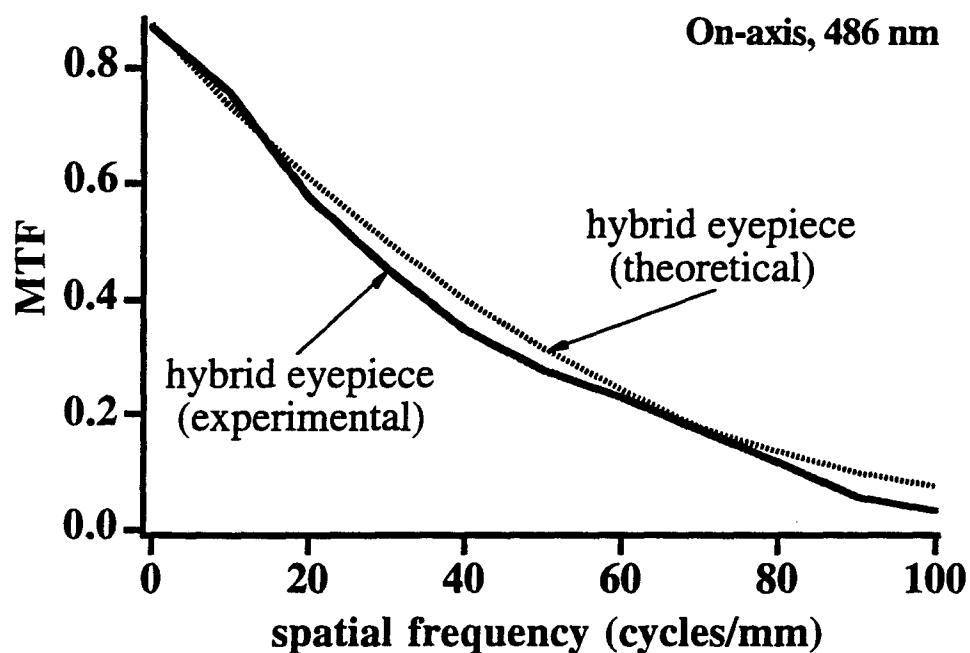


Fig. 5.2.8. Experimental and theoretical on-axis MTF for hybrid eyepiece with $\lambda = 486$ nm.

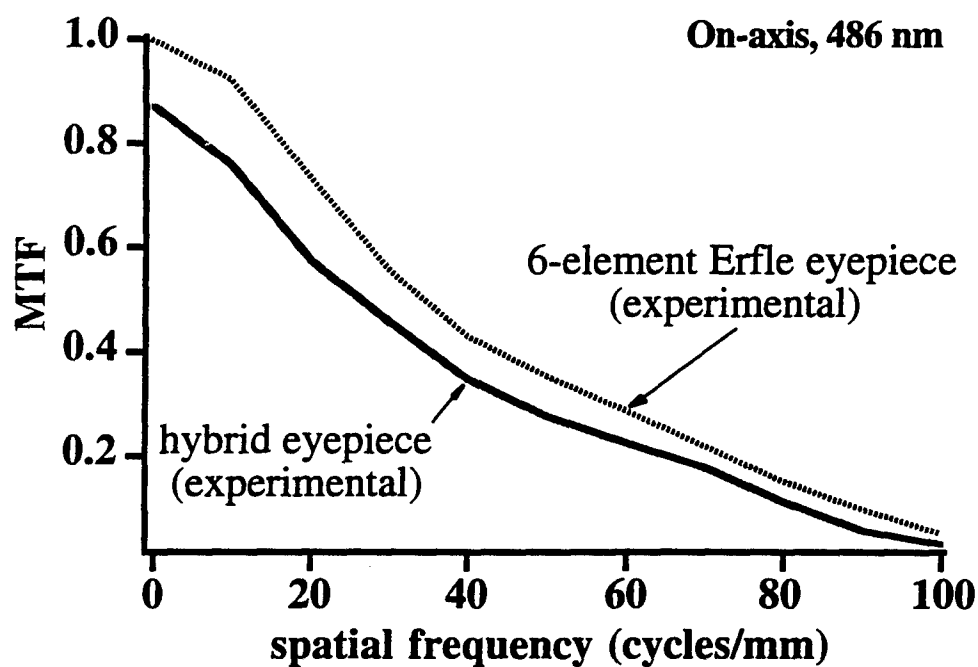


Fig. 5.2.9. Experimental on-axis MTF data for six-element Erfle eyepiece and hybrid eyepiece with $\lambda = 486$ nm.

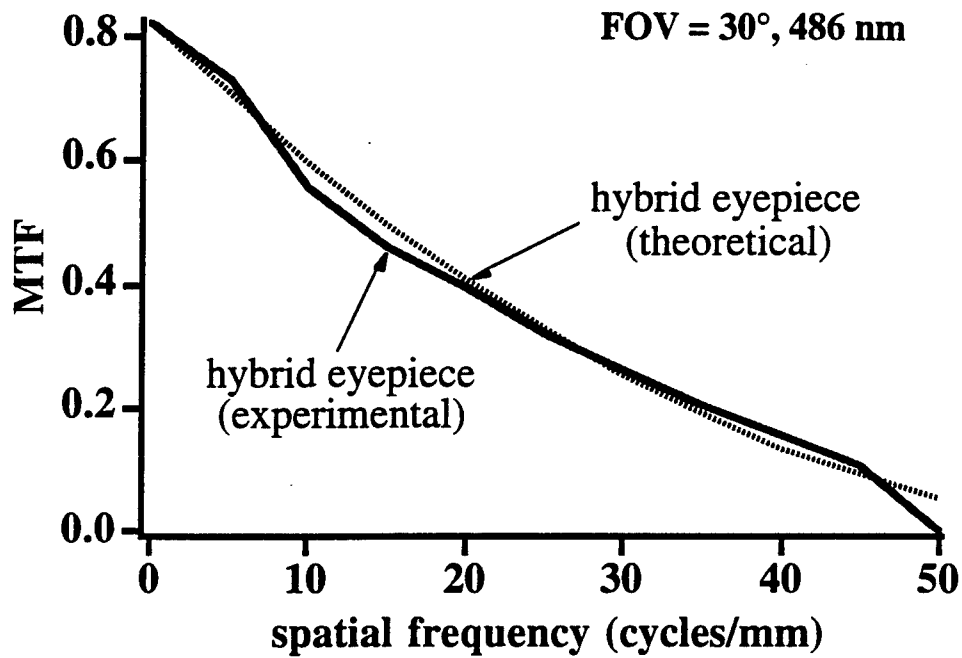


Fig. 5.2.10. Experimental and theoretical 30° FOV MTF for hybrid eyepiece with $\lambda = 486$ nm.

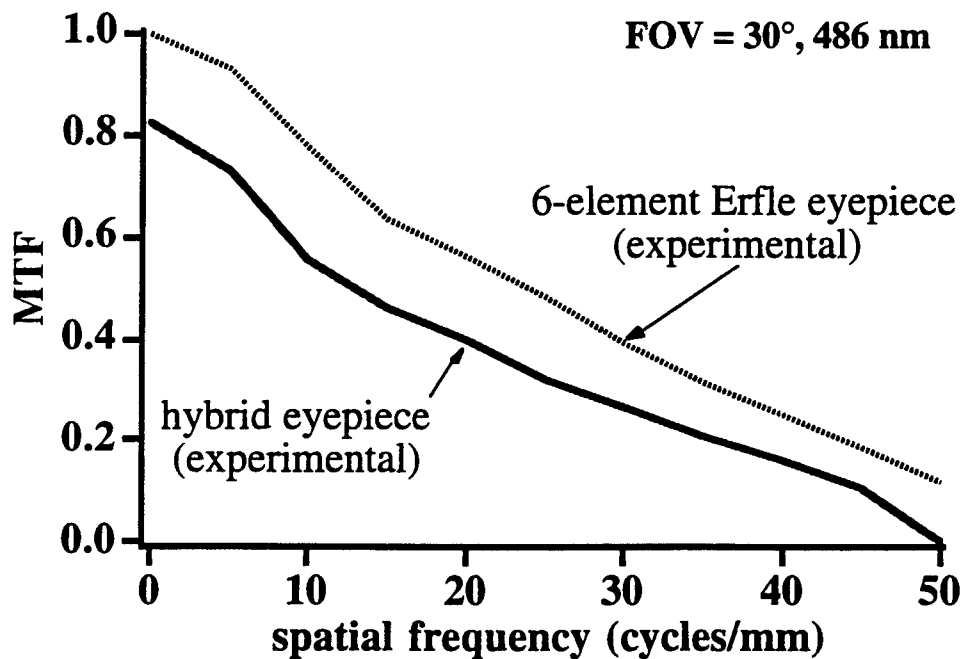


Fig. 5.2.11. Experimental 30° FOV MTF for six-element Erfle eyepiece and hybrid eyepiece with $\lambda = 486$ nm.

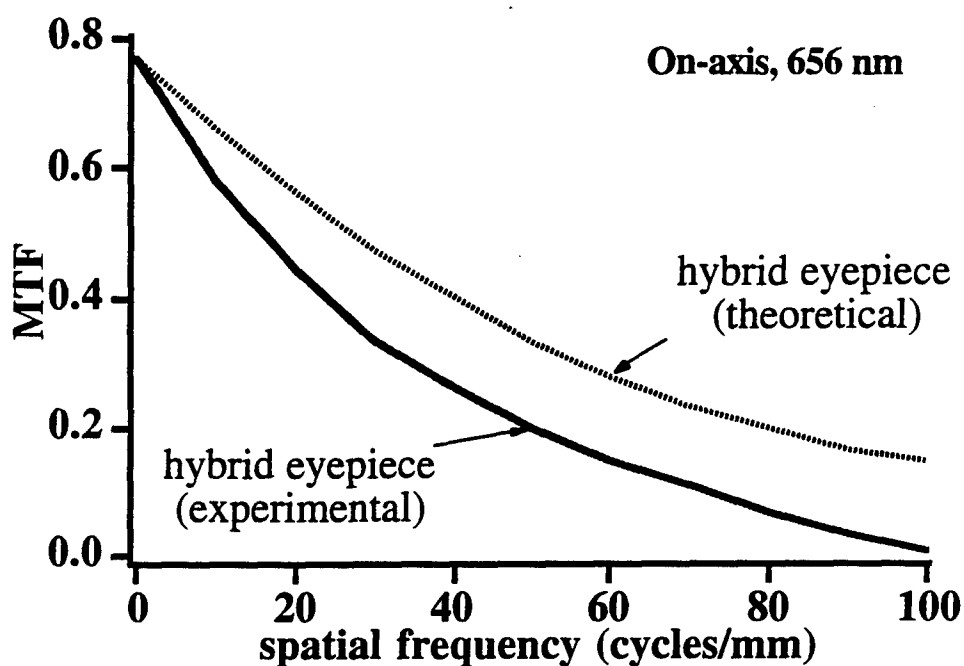


Fig. 5.2.12. Experimental and theoretical on-axis MTF for hybrid eyepiece with $\lambda = 656$ nm.

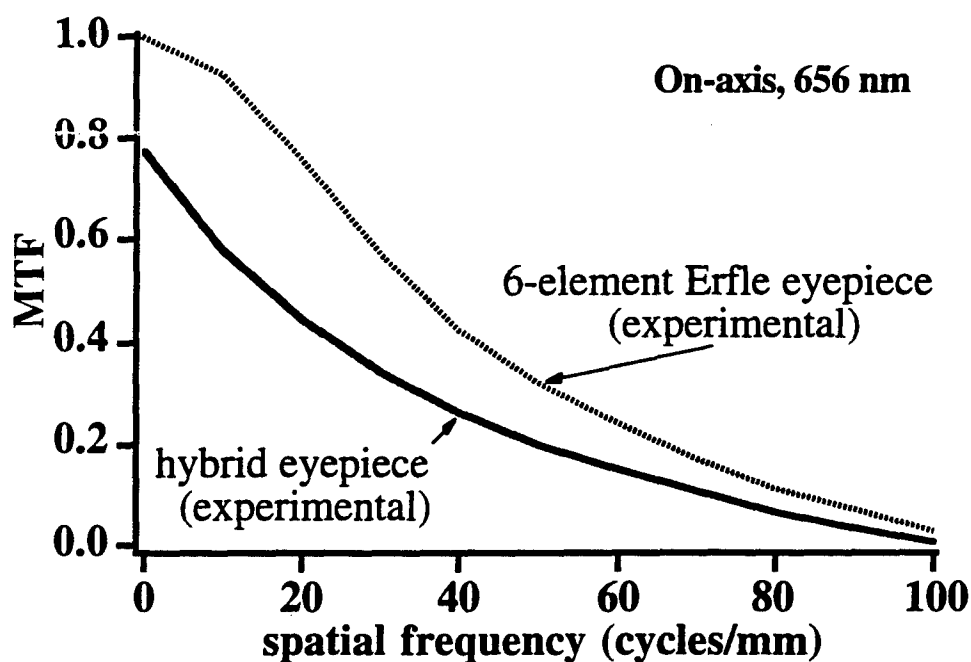


Fig. 5.2.13. Experimental on-axis MTF data for six-element Erfle eyepiece and hybrid eyepiece with $\lambda = 656$ nm.

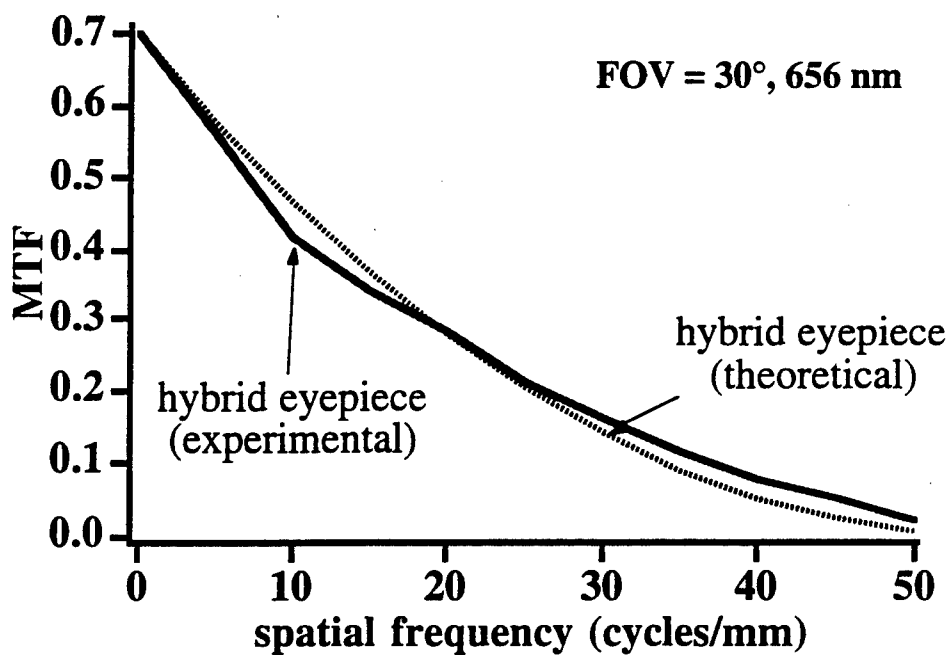


Fig. 5.2.14. Experimental and theoretical 30° FOV MTF for hybrid eyepiece with $\lambda = 656$ nm.

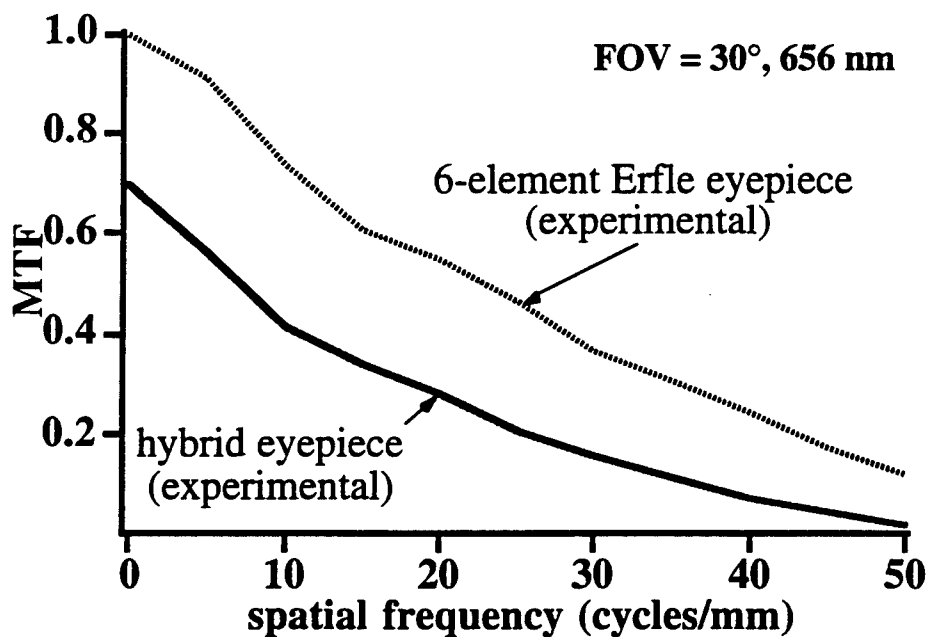


Fig. 5.2.15. Experimental 30° FOV MTF for six-element Erfle eyepiece and hybrid eyepiece with $\lambda = 656$ nm.

The experimental results are in excellent agreement with the theoretical predictions. Further improvements in the MTFs can be gained by improving the diffraction efficiency of the lens. Using a rotationally-symmetric pattern generator to fabricate the master element, diffraction efficiencies across the aperture are expected to approach the on-axis value, which is expected to approach a value of 95% at the design wavelength. Note that these increases in efficiencies will directly raise the MTF curves by the increase in the respective efficiencies, and thus make them very nearly equal to the Erfle MTF data in all cases.

5.3. Imaging Experiment - Eyepiece as a Magnifier

An eyepiece may be used as a magnifier, and in many applications, such as helmet mounted displays (HMDs), that is precisely its function : to magnify a small screen or display. The similarities and differences between eyepieces and magnifiers were discussed in Chapter 1. Key differences of this type of use (incoherently-coupled devices) from coherently-coupled systems (such as telescopes and binoculars), are that there is no pupil imaging, source illumination is often not broadband, and the lens systems tend to have considerably larger focal ratios. As this is the case, magnifiers generally can not be used as eyepieces, but several eyepiece designs have been used as magnifiers.

This experiment tests the eyepieces with an actual image at the real image plane, not at the infinite conjugate test as was the case for the MTF testing. For this reason this imaging test simulates the function of the eyepiece fairly accurately. Quantitatively, the imaging quality of the eyepiece can be measured. For example distortion, field curvature, and lateral color can easily be seen. More importantly, the effects of these aberrations on the image quality can directly be seen. Therefore, testing eyepieces as magnifiers in an imaging setup is a good visual demonstration of their imaging quality, although it lacks information about the pupil imaging quality such as spherical aberration of the exit pupil.

The test conditions for these experiments were the following: a white light source was used for illumination and a 2.5 cm X 2.5 cm square image was used as the object scene. A Sony CCD video camera (XC-999) and a Sony video graphic printer (UP-860) were used to capture and record the images. The experimental test set-up is depicted in Fig. 5.3.1.

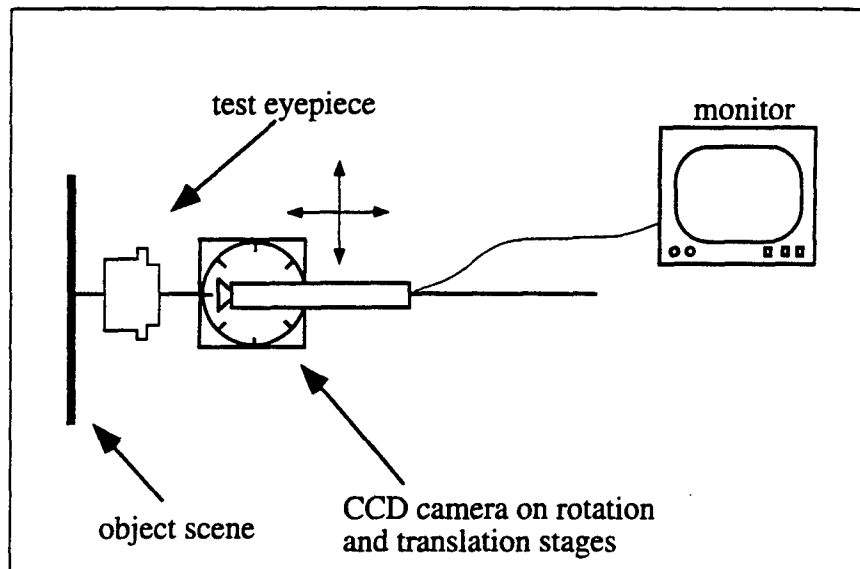


Fig. 5.3.1. Imaging experiment using an eyepiece as a magnifier.

During the experiment the eyepiece and image scene maintain a fixed position, while the camera is rotated manually to capture every portion of the field-of-view. Translation stages are used to maintain the camera lens position in the exit pupil of the eyepiece to reduce vignetting as best as possible. The arrows above the stage of the camera (in Fig. 5.3.1) indicate the directions of translation.

Figure 5.3.2 shows the on-axis image comparison of the 6-element Erfle eyepiece and the hybrid eyepiece. The image used is a slide of the capitol building in Washington, D.C. The on-axis performance of the two eyepieces is nearly similar. The diffraction efficiency for the on-axis case is very high, therefore it can be expected that the optical performance of the hybrid eyepiece ought to be very similar to the Erfle eyepiece.

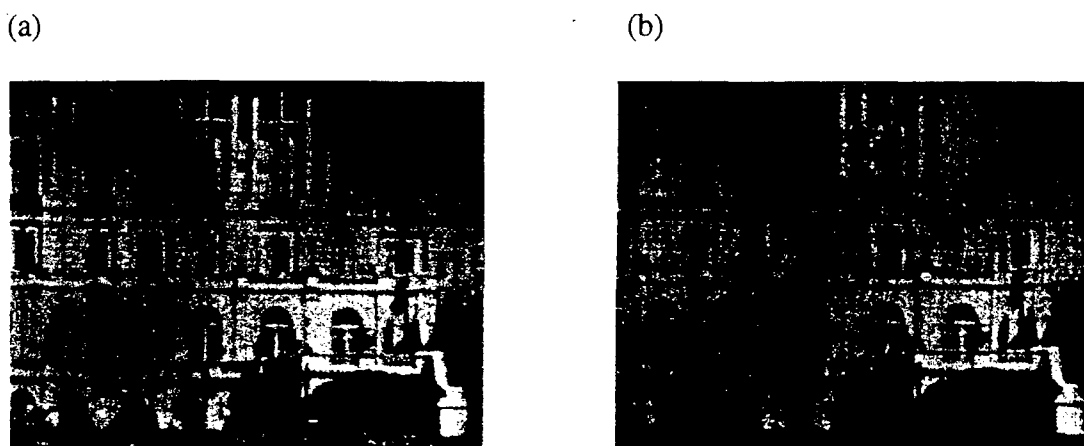


Fig. 5.3.2. On-axis imaging performance of (a) a 6-element Erfle eyepiece and (b) the hybrid eyepiece.

Shown in Fig. 5.3.3 is the 20° hFOV off-axis comparison of the 6-element Erfle eyepiece, and the hybrid eyepiece. In the off-axis case, note that the hybrid eyepiece exhibits blurring due to the presence of non-design diffraction orders. Due to the significant measured decreases in diffraction efficiency off-axis, it is expected that the off-axis image quality will be reduced. This result also agrees with the MTF experiments. Optimization of the blaze profile of the diffraction element will help this situation. Also the Erfle eyepiece shows considerable vignetting at this field angle.

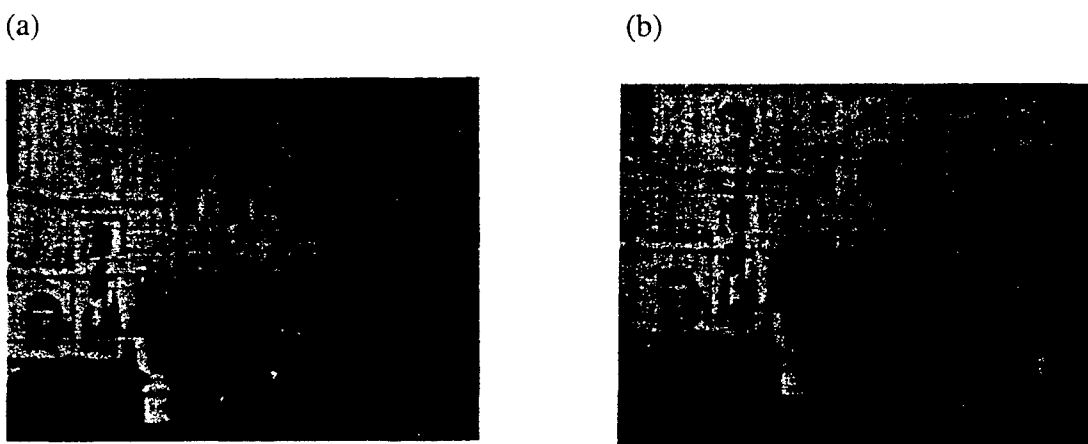


Fig. 5.3.3. Off-axis (20° hFOV) imaging performance of (a) a 6-element Erfle eyepiece and (b) the hybrid eyepiece.

5.4. Binoculars - Imaging Experiment

The image from a pair of binoculars can be captured by a camera as a method to examine the imaging quality of the instrument. The benefits in comparing the images from the two sets of binoculars (all-refractive and hybrid) are similar to those for the magnifier imaging experiment, with the differences that the internal image is formed by the objective lens and that the experiment is actually testing the instrument as a whole.

The setup depicted in Fig. 5.4.1 was used to capture the images. The same camera and printer used in the previous magnifier experiments were also used in this test. The lens of the camera was set to focus at infinity since the binoculars are afocal. The camera replaces the eye as the image-collecting device. In this experiment a distant scene, located at a distance of approximately 200 meters, was used as a test object. The illumination conditions consisted of those during a typical Rochester August morning (overcast and hazy).

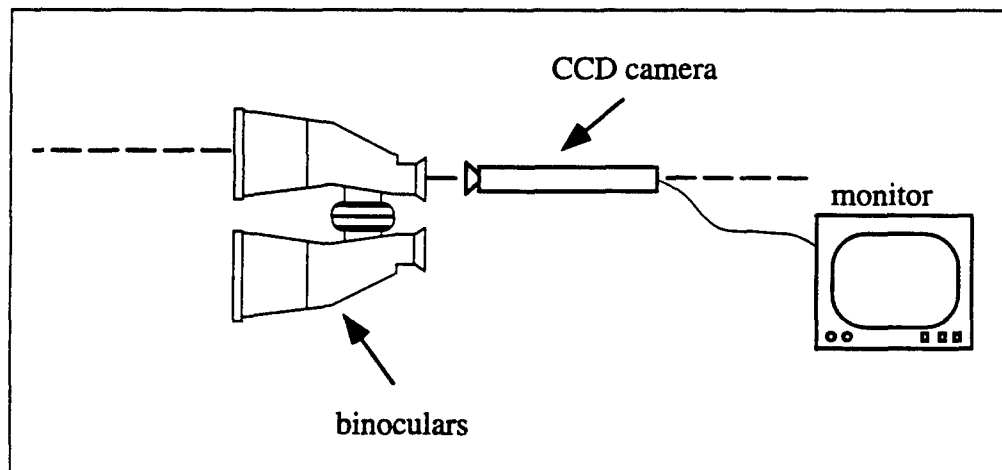
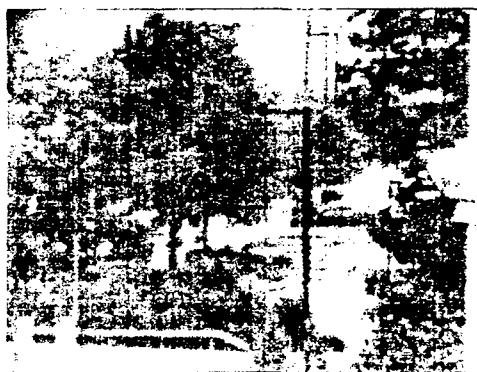


Fig. 5.4.1. Imaging experiment capturing an image through binoculars.

The camera was positioned directly against the eyepiece of the binoculars in order to minimize the amount of vignetting; this corresponds to the typical position of a human eye viewing through the binoculars. For this reason, the camera could not be tilted off-axis to view objects at larger field angles. In Fig. 5.4.2 the images taken from the two sets of binoculars are shown. Figure 5.4.2 (a) is the image from the all-refractive set. Figure 5.4.2 (b) shows the image taken from the binoculars equipped with a hybrid eyepiece. The imaging of the two sets is very similar. As a result of the undiffracted light in the hybrid pair, some haziness can be seen around marginal portions of the image. The diffraction efficiency effects (already discussed in the previous section) cause these blurring results, and improvements in the fabrication process will raise the efficiency thus increasing the image quality.

(a)



(b)



Fig. 5.4.2. Image captured via video camera through the Bausch and Lomb binoculars equipped with (a) the standard all-refractive eyepiece and (b) the hybrid diffractive-refractive eyepiece.

5.5. References for Chapter 5

1. W. J. Smith, *Modern Optical Engineering Second Ed.* (McGraw-Hill, Inc., New York, 1990), pp. 508-510.
2. J. W. Goodman, *Introduction to Fourier Optics* (McGraw-Hill, New York, 1968) pp. 101-140.
3. J. D. Gaskill, *Linear Systems, Fourier Transforms, and Optics* (John Wiley and Sons, New York, 1978) pp. 449-520.
4. J. H. Bruning, *Optical Shop Testing*, D. Malacara, ed. (John Wiley and Sons, New York, 1978), ch. 13, pp. 430-432.

6. Summary and Conclusions

6.1. Review of Thesis

The objective of this thesis was to investigate the use of diffractive optics in eyepiece design. In Chapter Two, the theory and design of diffractive lenses was discussed. The calculations for scalar diffraction efficiency for a blazed diffractive lens and a stepped-profile lens with paraxial zone spacings were presented. The effects of non-unity diffraction efficiency on the optical performance of a lens system containing diffractive lenses were shown. Lens design models for diffractive lenses were also presented, with the calculation of several first order parameters such as the power of a diffractive lens, the transmission function for a diffractive lens, and the effective dispersion of a diffractive lens. A method was described to convert a designed diffractive lens into fabrication specifications.

Eyepiece design was discussed in Chapter Three. A presentation of general eyepiece design was given, as well as all-refractive examples. The general design of hybrid eyepieces was presented, with specific examples for the wide-field case. Eyepieces, which employed one and two diffractive lenses, offering comparable or better optical performance with reduced weight and size (compared to the all-refractive, 5-element Erfle eyepiece) were designed. In one case, the refractive components of the hybrid eyepiece were designed using all BK-7 glass.

In Chapter Four, an application of one of the wide-field, hybrid eyepieces to a pair of all-refractive binoculars was investigated. A reverse-engineering procedure was used to characterize and model the design prescription of a commercial set of wide-angle binoculars. The existing all-refractive eyepiece of the binoculars was replaced by

the wide-field, hybrid eyepiece in the design of a pair of hybrid binoculars. An analysis of the hybrid optical performance was performed, including a diffraction analysis to identify the effects of light diffracted into diffraction orders other than the design order. The hybrid eyepiece was fabricated to the specifications of the hybrid design for the binoculars. To fabricate the components and mount, a tolerance analysis was performed.

The experimental testing of the hybrid eyepiece was presented in Chapter Five. A modulation transfer function (MTF) test and two imaging tests were performed to measure the performance of the lens. The MTF of a lens gives a specific index of the resolving power of a lens at a given spatial frequency under a given set of test conditions. The experimental data were in excellent agreement with the theoretical predictions. The first imaging test of the eyepiece was to capture images formed by the hybrid eyepiece when used as a magnifier, and the second test was to capture images through a pair of binoculars that were equipped with a hybrid diffractive-refractive eyepiece, which was presented in Chapter Four. Comparisons with an all-refractive, six-element Erfle eyepiece of a similar focal length and a conventional all-refractive set of binoculars were presented. The imaging performance of the hybrid eyepiece was similar to the all-refractive, conventional eyepiece in each case, except where the effects of non-unity diffraction efficiency were very strong. These effects were primarily due to a non-ideal diffractive element fabrication process. Additional optimization in the diffractive surface profile is expected to ameliorate this problem.

6.2. The Role of Diffractive Optics in Eyepiece Design

Eyepieces present a difficult design problem due to a wide field-of-view requirement, an external aperture stop, and standards for high-performance. With the

use of only conventional optics, eyepiece designs often take on complex, multi-element forms sometimes employing exotic glasses. Optical performance may therefore be sacrificed to maintain other critical parameters such as weight, overall size, cost, or number of glass elements. As a result diffractive optics can play an important role in visual systems in which such sacrifices cannot be made. Diffractive optics makes an excellent match with the design difficulties of eyepieces. This is in part due to many of the design difficulties imposed by conventional optics to the eyepiece design problem, and also is due to the powerful variables offered by diffractive optics.

In conventional, wide-angle eyepieces, correcting lateral color often requires the use of strong, negatively-powered, color-correcting elements. The use of these elements often results in adding more difficulties to correcting other field aberrations, since the curvatures of the other elements are increased thus aggravating other monochromatic field aberrations. Conversely, the inherent strong, negative dispersion of diffractive lenses is a strong tool used to reduce the large amount of lateral color found in wide-angle eyepieces while only employing positive elements.

As part of my research I also investigated the monochromatic correction of wide-field eyepieces using only three refractive elements. By eliminating the requirement for chromatic aberration correction, the curvatures of an all-refractive design are significantly reduced, and consequently fewer variables are required to reduce the residual aberrations. In fact, the three-element, all-refractive eyepieces all performed well, with a few exceptions. They suffered from under-corrected astigmatism, and some residual distortion and pupil spherical aberration. Additionally, in each case at least one surface had a zero or nearly zero curvature; which makes a good location for a diffractive lens. (It has been suggested that the requirement for a plane surface in hybrid diffractive-refractive lens designs eliminates/counteracts the advantages added by the diffractive element.) This exercise justified that the use of a

diffractive element to correct color would also significantly reduce the monochromatic aberrations, which could be further reduced by an aspheric phase profile in the diffractive element. In the hybrid eyepieces detailed in this thesis, the diffractive elements simultaneously correct for color and weaken the other surface curvatures and thus inherently induce less aberrations. The aspheric terms are used to correct the residual field aberrations, particularly distortion and pupil spherical aberration, which are difficult to control using only conventional, spherical optics. A strong design limitation in these hybrid diffractive-refractive eyepieces is the elimination of glass-index boundaries; the change in refractive index across surface boundaries in conventional designs is used to help add overcorrected astigmatism.

This thesis has addressed several issues important to determining the applicability of diffractive optics in eyepiece designs. Diffractive-refractive eyepieces have been designed and fabricated that offer equivalent performance to all-refractive systems (Erflé eyepiece), while simultaneously reducing the size, weight, and number of elements in the system. Additionally, common, inexpensive glasses may be used in the hybrid eyepieces for all of the elements. One can determine the usefulness of these eyepieces in his or her application based on the theoretical and experimental comparisons presented with the Erflé eyepiece, since the Erflé eyepiece has often been used as a benchmark for other systems. The Erflé eyepiece is the most widely-used large field-angle eyepiece today. These eyepieces have been fabricated and exhibit excellent agreement with the theoretical predictions.

6.3. Future Work

Hybrid diffractive-refractive eyepieces have been shown here to have excellent performance compared to all-refractive eyepieces. New types of hybrid eyepiece designs can be explored. These types can include the use of plastic elements in place of the BK-7 elements. Some plastics, such as methyl methacrylate, have similar optical (but not necessarily thermal and mechanical) properties as BK-7 glass. A hybrid diffractive-refractive, plastic eyepiece can offer even further weight reductions than those designs described in this thesis. Additionally, other hybrid designs can be investigated, i.e. those with a buried surface (cemented doublet) to further reduce astigmatism, those with field flattening elements to reduce field curvature, or designs with very high refractive index materials. These types violated the initial constraints put on the designs in this thesis.

As indicated in Chapter 5, the diffractive elements fabricated in this thesis have been fabricated using equipment that is optimized for anamorphic elements. The lens can be fabricated much more efficiently, and very likely with higher fidelity, with the use of a rotationally symmetric pattern generator. With this type of master element, higher efficiencies can be obtained across the aperture of the lens. This will directly increase the MTF of the eyepiece, and therefore improve its visual performance.

With the improved diffractive element in the hybrid eyepiece, subjective tests could be performed with human observers viewing a variety of scenes through two sets of visual instruments (binoculars, for instance), one equipped with all-refractive eyepieces, the other with the hybrid eyepiece. A qualitative assessment can then be performed to determine the usefulness of the systems. Additionally, the use of bandpass filters can be used to reduce the spectrum to improve the polychromatic

integrated diffraction efficiencies of the lenses. In sport binoculars, for instance, often yellow filters are used to improve the resolution of the lenses. Also in night vision goggles, the internal displays typically have a 50 nm, greenish, spectrum. These situations can not only improve the overall efficiency, but also they relax the stringent broadband color correction.

Further explorations in specific applications with these types of hybrid diffractive-refractive eyepieces can be investigated. Such applications include head mounted displays (HMDs), astronomical devices, and other lightweight binocular applications.